Phil. Trans. R. Soc. Lond. A **304**, 327–364 (1982) [327]
Printed in Great Britain

HOMOGENEOUS SOLID STATE TRANSFORMATIONS IN NIOBIUM OXIDES

BY E. SIAN CRAWFORD AND J. S. ANDERSON, F.R.S.†
Edward Davies Chemical Laboratory, University College of Wales, Aberystwyth, Dyfed SY23 1NE, U.K.

(*Received* 13 *April* 1981)

[Plates 1–14]

CONTENTS

† Present address: Research School of Chemistry, Australian National University, Canberra, A.C.T., Australia.

In homogeneous solid state reactions, transformation takes place within the crystals, and structural continuity is preserved; reactant and product structures are coherently intergrown. If the transformation starts independently at numerous loci, the incompletely reacted state of the crystals is inherently disordered. Crystallographic methods that average the structure over the whole crystal cannot fully characterize the actual, real-space structure, as it evolves during reaction, but that structure can, in favourable cases, be sampled by high resolution electron microscopy. Homogeneous reactions in the niobium oxide 'block structure' type crystals lend themselves to this technique.

This study relates to the oxidation of the lower niobium oxides, $Nb_{22}O_{54}$, $Nb_{25}O_{62}$ and $Nb_{53}O_{132}$, to niobium pentoxide. In each case, complete oxidation takes place at very low temperatures; the first products are reported to differ little in structure from the parent oxides, and to transform continuously into the stable polymorphic form, H–Nb_2O_5, over a wide temperature range and via several intermediate structures. By using lattice imaging methods, the structure elements present at each stage in the reactions have been identified, and their rearrangement has been followed.

The initial oxidation step is completely non-reconstructive, and produces cation-deficient modifications of the original structures; all subsequent changes take place at constant composition, Nb_2O_5. In oxidized $Nb_{22}O_{54}$, a drastic rearrangement sets in at 350–400 °C, involving (*a*) an exchange of places and an apparent diffusion of the columnar structure elements (or blocks) and (*b*) a disproportionation that creates blocks of different cross sections. By a suitable mapping method, it is possible to infer exactly where, and how many, niobium atoms have undergone displacement into new sites, and to show that a single mechanism, proposed by Andersson and Wadsley, effects the observed changes of structure. Only a few atoms at a time, at the edge of one block, need to shift. Passing through a highly disordered state, blocks (3×3) octahedra in cross section are progressively segregated into microdomains of a new polymorphic structure of Nb_2O_5, $Nb_{10}O_{25}$, while blocks (5×3) octahedra in cross section are formed by disproportionation and built into microdomains of H–Nb_2O_5. These changes are initiated at random centres, 8–10 nm apart, starting at the edge of a single block; the displacements are propagated rapidly up the crystal *b*-axis and relatively slowly from block to block along rows and up files of blocks. Extended defects and compromise structures are formed where effects spreading from different initiating centres impinge; these faults serve as sinks for eliminating cation vacancies. The final result, stable up to 950 °C, is a domain structure, with nearly continuous walls of $Nb_{10}O_{25}$ enclosing slabs of H–Nb_2O_5 structure, and intersected by nearly continuous walls of fault structure. In oxidized $Nb_{25}O_{62}$, the first stage detected is the formation of triangular nuclei; one side of the triangle is formed of H–Nb_2O_5 structure, the other side of $Nb_{10}O_{25}$ structure, with an abrupt boundary to unchanged $Nb_{25}O_{62}$ in each case. As these nuclei expand, by propagation of atom row displacements along rows and files of blocks, they merge to create relatively extensive domains of H–Nb_2O_5 structure, separated by narrow walls of $Nb_{10}O_{25}$ and linked by faults. Transformation of oxidized $Nb_{53}O_{132}$ is similar.

Long annealing of all the oxides at 900 °C gives products with essentially similar domain structures, but differing in the relative proportions of H–Nb_2O_5 and $Nb_{10}O_{25}$ domains. They are stable up to 950 °C; at higher temperatures, transformation into H–Nb_2O_5 appears to be a catastrophic, and probably a heterogeneous process, for after heating at 950–1100 °C, any one crystal is either fully transformed into recrystallized H–Nb_2O_5 or retains its domain structure with no significant change. There is some evidence that the domain structure is mobile at high temperatures.

1. Introduction

Homogeneous reactions in crystals of simple structure can be fairly well understood. The same processes of place exchange between atoms that underlie diffusion and self-diffusion provide a mechanism for superlattice ordering, order–disorder transformations, the segregation of new

phases etc. in metallic alloy structures. There is an extensive theoretical framework, built up by Hillert (1961), Cahn (1961, 1962*a*, *b*) and others, that interprets at least the kinetic aspects of how local fluctuations form, and are propagated, to produce large-scale transformations of crystal structure.

Homogeneous reactions, including both ordering processes and structural rearrangements, can also take place in crystals of more complex structure and strongly polar character, and the mechanism of these processes is less evident. McConnell (1974, 1978) has gone some way in interpreting such processes as the development of modulated structures in the plagioclase felspars in terms of the generalized theories of ordering reactions. There is an essential difference between the metallic alloy structures, based on simple packing, and the silicates, other oxide structures and polar compounds generally; the latter class can be viewed as networks of linked coordination polyhedra, and the appropriate coordination environment must be preserved, for each species of atom, in all structural transformations. This condition imposes some restrictions on the topochemistry of such processes. In this paper we describe how some homogeneous transformations take place in a group of materials – the niobium oxide structures – based on networks of linked coordination polyhedra.

In any homogeneous solid state reaction, all processes must take place *within* the reacting crystals, without loss of structural continuity. This is in contrast with the more familiar heterogeneous reactions, in which the locus of reaction is an *interface*, which moves through the crystal as reaction proceeds. Preservation of structural continuity implies that the product should be intergrown coherently in the reactant crystal; this, in turn, requires that the initial and final structures should be closely related and topologically compatible, if not identical (as they are, for example, in order–disorder processes, or such clustering processes as the spinodal unmixing of TiO_2–SnO_2 solid solutions). Provided that the condition of topological compatibility can be fulfilled, homogeneous reactions can impose a change of crystal structure, and such processes are or particular interest. Their initial step can be visualized as some purely localized fluctuation of structure, which is then propagated through the crystal from each initiating centre. If this happens, more or less randomly, throughout the bulk of a reacting crystal, the first result is necessarily to create a disordered structure. On this disordered structure there must subsequently operate some longer range, correlating process, which rearranges it into the final, crystallized product. To understand the reaction, evidence is needed about the primary act, how the process is propagated, and how long-range order is finally established.

Although it is possible to derive much structural information about imperfectly ordered crystals, by fully exploiting the diffuse scattering of X-rays and neutrons (see, for example, Chen *et al.* 1979), that information is essentially statistical, averaged over the entire crystal. It can furnish only limited evidence about how structural changes take place. The possibility of directly observing the local structure within imperfectly ordered crystals is provided, however, by high resolution, structure imaging, electron microscopy, and the niobium oxide family of structures lends itself particularly to this approach. A serious limitation is that the method can only sample, rather arbitrarily, the structures traversed during the reaction process. Nevertheless, by sampling many crystals at different stages of transformation, it is possible to accumulate sufficient evidence to build up a fairly detailed, phenomenological description of the process.

2. Structure and chemistry of the system

All the niobium oxide family of compounds – niobium pentoxide, the mixed valence niobium oxides and numerous double oxides – have crystal structures derived from the DO_9 (ReO_3) type structure, according to a common plan. The ReO_3 structure is a network of $[MO_6]$ coordination octahedra, linked through the oxygen atoms at their vertices. This is collapsed, so as to eliminate anion sites, by two sets of crystallographic shear planes (c.s. planes) which, being necessarily atomically stepped, demarcate a set of rectangular blocks or columns. Internally, each block has the ReO_3 structure, but adjacent blocks are joined across a c.s. interface, where the octahedra share edges. This necessarily requires that the niobium atoms in adjacent blocks should lie at different levels (at $y = 0$ or $y = \frac{1}{2}$) along the unique crystallographic axis. The cross section of the blocks is uniquely determined by the orientation and spacing of the recurrent c.s. planes; every regular, resultant configuration represents a definite (ideal) stoichiometry. This principle not only enables small differences in stoichiometry to be accommodated by regular structures, but also provides wide scope for coherent intergrowth between structure elements that correspond to different compositions or different polymorphic forms, and hence

Table 1. Structures of the niobium oxides

oxide		block sizes and connectivity
$Nb_{12}O_{29}$	phase B	$(4\times3)_\infty$
$Nb_{22}O_{54}$	phase C	$(4\times3)_\infty+(3\times3)_1$
$Nb_{47}O_{116}$	phase D	$\{(4\times3)_\infty+(3\times3)_1\}+(4\times3)_2$
$Nb_{25}O_{62}$	phase E	$(4\times3)_2$
$Nb_{53}O_{132}$	phase F	$\{(5\times3)_\infty+(4\times3)_1\}+(4\times3)_2$
$Nb_{28}O_{70}$	H–Nb_2O_5	$(5\times3)_\infty+(4\times3)_1$

for disorder or non-stoichiometry. Within each block, the niobium atom positions (about 0.39 nm apart) should be resolvable by electron microscopy; at the c.s. interfaces, the niobium atom spacing, projected on (010) of the monoclinic structures, is little more than 0.2 nm, so that those atoms cannot be resolved in an n-beam structure image at 0.35 nm resolution. What is explicitly displayed is the cross section and connectivity of each block, which represents an individually recognizable structure element, with a definite composition. Homogeneous reactions in this versatile family of structures include both polymorphic transformations and reactions that impose a change of composition. In the latter, long-range atom transport processes must be involved, as well as the truly homogeneous, local structural reorganization (cf. Obayashi & Anderson 1976). In every reaction, the cross section and the connectivity of the columnar structure elements has to be altered through purely local atom movements.

We have examined how the lower, mixed valence oxides $Nb_{22}O_{54}$ ($NbO_{2.454}$) and $Nb_{25}O_{62}$ ($NbO_{2.480}$) undergo rearrangement when they are homogeneously oxidized and transformed into the stable polymorph of niobium pentoxide, H–Nb_2O_5 (crystallographic formula $Nb_{28}O_{70}$). How extensive that ultimate rearrangement must be, can be judged from table 1, which sets out the cross sections of the component blocks, and how they are linked, in the structure of this family of oxides.

H–Nb_2O_5 (figure 1*a*) is the stable, high temperature structure, into which all the polymorphs are transformed above about 950 °C. The lower oxides $Nb_{12}O_{29}$, $Nb_{22}O_{54}$ (figure 1*b*), $Nb_{25}O_{62}$ (figure 1*c*), $Nb_{47}O_{116}$ (a 1:1 intergrowth of $Nb_{22}O_{54}$ and $Nb_{25}O_{62}$) and $Nb_{53}O_{132}$ (a 1:1 inter-

growth of $Nb_{25}O_{62}$ and $Nb_{28}O_{70}$) (figure 1*d*) all oxidize to niobium pentoxide with extreme ease: detectably at 150 °C, rapidly at 300 °C. Each oxide thereby forms its own new, unstable form of Nb_2O_5, with a structure that is almost indistinguishable from that of the starting material (Schäfer *et al.* 1966). A mechanism for the low temperature oxidation of $Nb_{12}O_{29}$ was postulated, on electron microscope evidence, by Browne & Anderson (1974, 1976) and Iijima (1975), who found that some more profound rearrangement sets in above about 400 °C. It has now been possible to trace almost the complete sequence of events during the initial oxidation and subsequent structural reorganization, for $Nb_{22}O_{54}$ and $Nb_{25}O_{62}$.

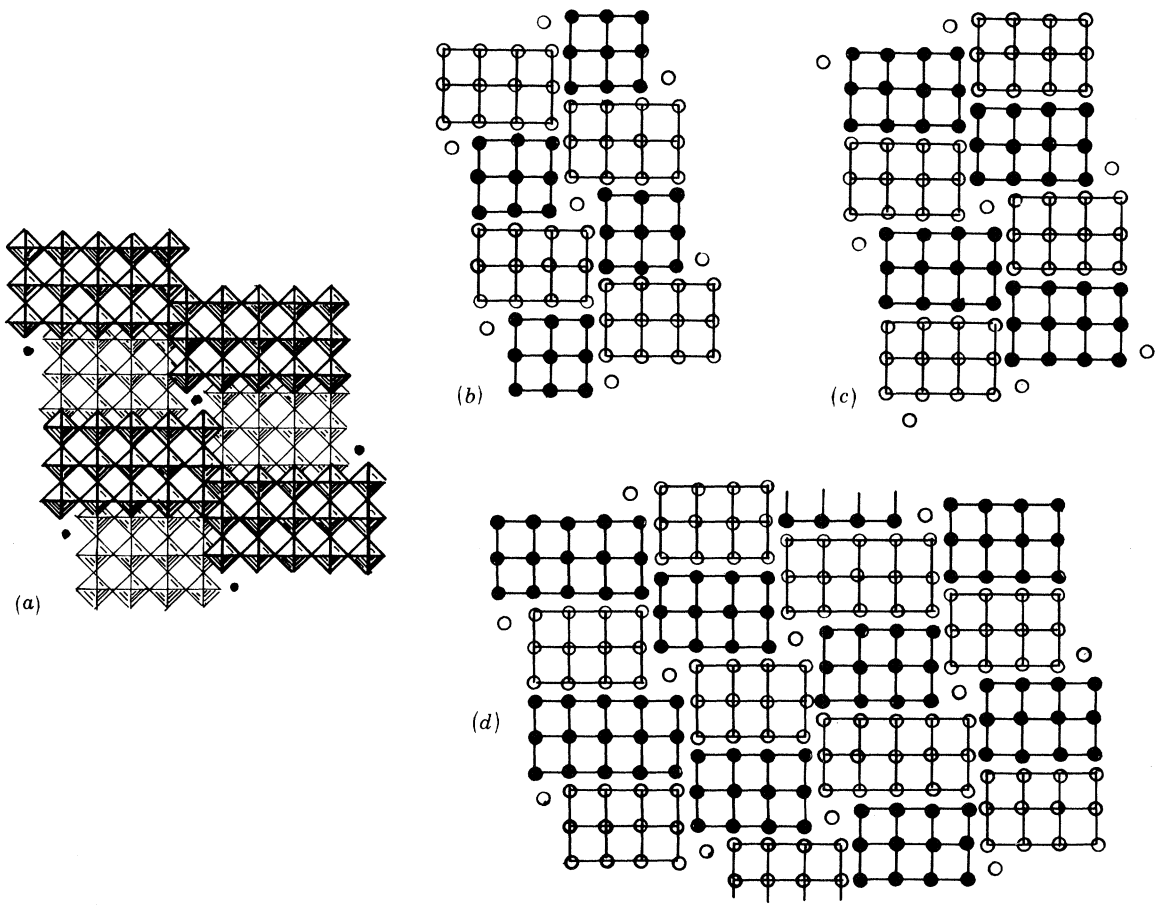

FIGURE 1. (*a*) The structure of *H*–Nb_2O_5 ($Nb_{28}O_{70}$) projected on (010). (*b*)–(*d*) Cross sections of blocks, and cation positions, in the structures of (*b*) $Nb_{22}O_{54}$, (*c*) $Nb_{25}O_{62}$ and (*d*) $Nb_{53}O_{132}$.

A recent, careful re-examination of these oxidation processes by Hibst & Gruehn (1978), using X-ray diffraction methods, led to the view that, in each case, the ultimate conversion into *H*–Nb_2O_5 proceeded through several ill defined steps (table 2). Oxidation is already complete in the first step; subsequent processes represent structural changes at constant composition. The reactions appear to be homogeneous and, as already stated, are likely to involve some imperfectly ordered structures. It is this feature that makes the X-ray evidence ambiguous.

Electron microscopy of these materials makes it evident that their oxidation and subsequent transformation follow a common pattern, comprising:

(*a*) The oxidation reaction proper, a completely non-reconstructive process (§4).

(*b*) Localized reconstruction of the resulting, unstable Nb_2O_5 polymorphs, in which blocks of different cross sections are rearranged, and blocks with new cross sections are created. This is a transient stage, with an inherently disordered structure (§ 5).

(*c*) Partial ordering, in which the structure elements of the disordered state are segregated into a quasi-regular domain structure. In this, two different crystal structures of identical stoichiometry (i.e. Nb_2O_5), one stable and one metastable, are coherently intergrown (§ 6).

(*d*) Conversion of the metastable domain structure into the thermodynamically stable *H*-Nb_2O_5 structure. This final step may be a heterogeneous process (§ 7).

TABLE 2. OXIDATION OF LOWER NIOBIUM OXIDES: PRODUCT PHASES (AFTER HIBST & GRUEHN 1978)

starting material	reaction temperature / °C	product phase
$Nb_{12}O_{29}$ (monoclinic) phase BI	100–390	OX1BI
	400–700	OX2BI
	700	*H*-Nb_2O_5
$Nb_{12}O_{29}$ (orthorhombic) phase BII	100–400	OX1BII
	500–700	OX2BII
	700	*H*-Nb_2O_5
$Nb_{22}O_{54}$ phase C	250	OX1C
	300–450	OX2C
	450–700	OX3C
	700–950	OX4C
	950	*H*-Nb_2O_5
$Nb_{25}O_{62}$ phase E	250–430	OX1E
	430–900	OX2E
	950	*H*-Nb_2O_5
$Nb_{53}O_{132}$ phase F	300–900	OXF
	950	*H*-Nb_2O_5

The transformations (*a*) → (*b*) → (*c*) can be described in terms of a single, localized reaction mechanism, which serves to displace the c.s. interfaces between adjacent blocks. Up to the completion of stage (*c*), the number of blocks, and of c.s. interfaces between them, remains constant; only the final step (*d*) is non-conservative.

3. EXPERIMENTAL

(*a*) *Materials*

Starting materials were well defined samples of the lower oxides, prepared at 1300 °C under equilibrium conditions (Kimura 1973), kindly given to us by Dr S. Kimura. They had been characterized as single-phase $Nb_{22}O_{54}$, $Nb_{25}O_{62}$ and $Nb_{53}O_{132}$ by both analysis and X-ray diffraction. Electron microscopy confirmed their homogeneity. Intergrown Wadsley defects were rarely found, but some crystals of $Nb_{25}O_{62}$ contained domains of $Nb_{53}O_{132}$, and the behaviour of such crystals showed that the intergrowth phases followed the same reaction pattern as the individual block structures.

(*b*) *Oxidation*

A preliminary thermogravimetric survey showed that $Nb_{22}O_{54}$ and $Nb_{25}O_{62}$ differ from $Nb_{12}O_{29}$. For $Nb_{12}O_{29}$, the oxidation kinetics approximate to those of a diffusion-controlled process, as is compatible with the mechanism proposed earlier (Browne & Anderson 1974). With $Nb_{22}O_{54}$ and $Nb_{25}O_{62}$, the initial rate is proportional to time, and the kinetics resemble those of the 'contracting sphere' model, indicating that some interfacial reaction is rate-controlling. In the light of later evidence, this is probably the reaction of molecular oxygen at the crystal surface. The kinetic difference may be associated with a difference in structure: in $Nb_{22}O_{54}$, $Nb_{25}O_{62}$ and the intergrowth structures, the corners of blocks enclose channels, which accommodate cations in tetrahedral coordination (figure 1), but there are no tetrahedral sites in $Nb_{12}O_{29}$. A consequence of this difference is that no site-creating displacement of cations can be formulated analogous to that which provides the primary reaction step in the oxidation of $Nb_{12}O_{29}$.

For the main electron microscope study, a series of materials were oxidized and annealed under conditions very close to those found by Hibst & Gruehn to yield the several defined stages listed in table 2. The finely ground oxides were heated, in silica or platinum containers, in an oven or tube furnace, according to the temperature required. In subsequent series of experiments, and as an adjunct to tracing the detailed course of transformation, materials that had been brought to some defined stage were heated for short times above the next Hibst & Gruehn 'transformation temperature'. Small samples, in a silica or platinum boat of small heat capacity, were plunged into a tube furnace set to the required temperature; they were withdrawn after controlled times and air quenched within a few seconds, to freeze in the transformation at a very incomplete stage.

It is convenient, in the subsequent sections, to retain the symbols used by Hibst & Gruehn to denote the different materials. The thermogravimetric results, and the white colour of the products, showed that oxidation to stoichiometric $NbO_{2.500}$ was already complete at the stages designated OX1C (from $Nb_{22}O_{54}$, phase C), OX1E (from $Nb_{25}O_{62}$, phase E) and OXF (from $Nb_{53}O_{132}$, phase F).

(*c*) *Characterization: X-ray diffraction*

X-ray diffraction patterns were taken, by using a Guinier camera and monochromated Cu $K\alpha_1$ radiation; we are indebted to Dr R. J. D. Tilley for these. Figure 2 shows microphotometer traces of patterns from $Nb_{22}O_{54}$ and the series OX1C to OX4C. These agree well with those published by Hibst & Gruehn. The diffraction pattern from OX1C (figure 2*b*) agrees closely with that from the parent $Nb_{22}O_{54}$ (figure 2*a*), except that the *h*0*l* lines corresponding to the longer spacings are weak or absent, and there is some line broadening and a more intense diffuse background. In OX2C, OX3C and OX4C (figure 2*c*, *d*, *e*) there are significant changes in the groups of lines at $11° < \theta < 16°$, which display characteristic differences between the similar diffraction patterns of all the block structures. There are also changes in the relative intensity and in the splitting of closely spaced lines. The pattern sharpens, and the diffuse background diminishes, at the OX4C stage. The progressive changes are real, but subtle, and strong similarities persist. It is impossible to index the patterns on any consistent basis and, in the light of later evidence, they emphasize that X-ray diffraction from disordered structures can be subject to severe limitations. They show that $Nb_{22}O_{54}$ and its immediate oxidation product are very closely related, and that the OX2C stage introduces some real structural change.

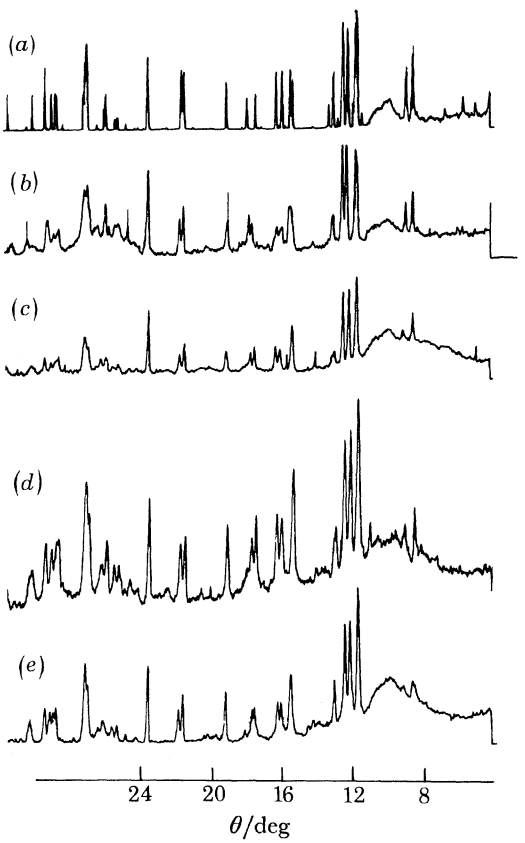

FIGURE 2. Microphotometer traces from X-ray diffraction patterns of (*a*) $Nb_{22}O_{54}$, (*b*) OX1C, (*c*) OX2C, (*d*) OX3C and (*e*) OX4C.

(*d*) *Characterization: electron diffraction*

Selected area electron diffraction patterns were routinely recorded, corresponding to the areas imaged by high resolution microscopy. Figure 3 (plate 1) shows representative patterns at various stages in the transformation OX1C → OX4C. Streaking and spreading of spots show that these patterns come from imperfectly ordered structures; the disorder is, in fact, on a scale that could result in significantly different diffraction patterns from crystals of the same material. The diffraction pattern of OX1C (figure 3*a*, *b*) was virtually identical with that of $Nb_{22}O_{54}$, except for the variable intensity or occasional absence of certain diffraction spots. There was usually streaking along [001], with some evidence for a doubled *c*-axis, although no evidence for any superlattice could be seen in the structure images projected down [010]. However, if a doubled *c*-axis arose from correlation between partially occupied tetrahedral sites, both within any one channel and between adjacent channels (see below), it would not necessarily be detectable in the structure images. Marked changes in the diffraction pattern accompany the onset of transformation to OX2C and the subsequent evolution of that structure (figure 3*c*, *d*). The diffraction spots break up, with close satellites, and streaking develops along [100]. The prominent quadrilateral of spots (which corresponds to the unit cell for $Nb_{22}O_{54}$ first chosen by Norin *et al.* (1966)) loses its centering, and the angles may vary from one crystal to another. At the defined OX2C stage (figure 3*e*,*f*) it has become almost rectangular, it is uncentred and the spots are strongly spiked; other diffraction spots are replaced by streaks along a direction

close to [10$\bar{2}$] of the original structure. The corresponding structure images show that this pattern comes from a structure with no long-range order, dominated by the dimensions of (4×3) blocks. There is no longer any true unit cell, and the c.s. interfaces between rows of blocks are no longer planar; their average orientation and average spacing both vary from one region to another. Little further change in the diffraction pattern marks the transformation to OX3C and OX4C (figure 3*g*, *h*), except that, as annealing is prolonged, another weak diffraction pattern is superimposed. This is identifiable as that of H–Nb_2O_5.

As is discussed below, the structure images provide an interpretation of these diffraction patterns. Disorder first sets in along the [100]-direction, thus virtually halving the *a*-axis. A domain structure is formed, in which (4×3) blocks largely determine the spacing of c.s. interfaces. There are, indeed, small domains of at least three different block structures, from which certain diffraction spots almost coincide; it is this that leads to the spiking of the stronger diffraction patterns.

(*e*) *Characterization: electron microscopy*

Standard procedures for *n*-beam structure imaging were followed, by using a Siemens 102 electron microscope with a double tilt and lift stage. Crushed crystal flakes were dispersed on reticular carbon support films, and micrographs were taken, usually at 300 K to 500 K magnification and at 70–90 nm underfocus, from thin fracture flakes or edges, in a projection exactly normal to the *h*0*l* reciprocal lattice net. Under these conditions, and for the block structures in particular, there is a wealth of evidence that image contrast approximates closely to the projected charge density distribution. Local structures can confidently be read directly from the micrographs.

It has been necessary, in this work, to determine the real space structure of the largest possible regions of crystal. Problems arise in the high resolution electron microscopy of large object fields, through the flexibility of very thin crystals, which militates against accurate zone axis orientation over the whole field, from the variation in defocus across a tilted crystal, and from the dynamic effects due to variations in thickness. However, as was found by Fejes *et al.* (1973), the relative amplitudes of all diffracted beams can, in certain circumstances, be the same for a thick crystal (about 100 nm) as for a thin crystal (< 10 nm). A good structure image can then be obtained, with a resolution little inferior to that obtained in the thin crystal régime. This possibility has been exploited. It has also been possible to cover adjacent areas at optimum resolution by overlapping micrographs. By these means, very extensive areas of crystal have been mapped at a resolution (certainly better than 0.5 nm) adequate for the unambiguous identification of their component structure elements. A very large number of crystals has been examined in the course of this work, and the micrographs reproduced are adequately representative of the structures found.

A high resolution structure image of the kind required for this study presents information at two distinct levels: (*a*) making the highest demands on resolution, the detailed information implicit in image contrast, about atomic positions, detectable atom displacements, defects etc; and (*b*) less demanding on resolution, the nature and dimensions of the blocks that form the structure, how they are mutually connected across c.s. interfaces and how they are distributed within the coherent, but disordered, structure of the crystals.

For analysing how a crystal with a modulated or jig-saw puzzle structure is organized, a micrograph in black and white contains a surfeit of information; the pattern in which component structure elements are distributed can be obscured and is not immediately assimilated. We have found it essential to display that distribution pattern more clearly, by colour mapping.

Enlarged prints (two–ten million total magnification) were tinted with transparent colours, each indicative of a particular principal structure element (block size). The underlying high resolution detail was not obscured, and the detailed local analysis of structure could be viewed against the surrounding structure at the next level of organization. A minimum of three colours are usually needed to display the information of such a micrograph fully and clearly; in the accompanying half-tone plates, certain sets of structure elements have been tonally enhanced, but some clarity of information is thereby lost.

This technique largely obviated the need for detailed mapping of real space structure, but mapping is needed to disclose the presence of dislocations or dimensional mismatch between structure elements. We discuss later the use of mapping methods in such a way as to show the displacement of individual atom rows and the propagation of such displacement processes through the crystal.

4. The non-reconstructive low temperature oxidation

High resolution micrographs showed that the structure images of $Nb_{22}O_{54}$ and OX1C were identical, except for two frequent, but not invariable, features (figure 4, plate 1). The structure is that of a regular alternation of (4×3) and (3×3) blocks, but in a few places (e.g. at X, figure 4) these units have exchanged places. The extent to which this occurred varied widely from one crystal to another and, especially, from one preparation to another. In some regions imaged, almost half the blocks had been interchanged, bringing one half of the structure randomly into anti-phase to the rest, thereby effectively halving the *a*-axis. The c.s. planes that define the structure are no longer straight; their averaged orientation results in small, but variable, distortions of the average unit cell. Differences between the diffraction patterns of OX1C and the perfect $Nb_{22}O_{54}$ structure are thereby explained. As is considered in § 5, the initial stages of the transformation of the OX1C structure involve an exchange of places between the blocks, and we suspect that the variable, localized incidence of that process during the oxidation reaction may arise fortuitously, for example from local self-heating during the exothermic reaction. The second peculiarity of OX1C images, found only occasionally, is that the image contrast at some of the sites of tetrahedral cations is abnormally light. Image contrast computations (Skarnulis *et al.* 1976) have shown, however, that this contrast is very sensitive to the exact imaging conditions, and it is uncertain whether any weight can be attached to the observations.

Similar considerations apply to the oxidation of $Nb_{25}O_{62}$ to OX1E (figure 5, plate 1): their structure images are identical, except that, in OX1E, a pair of (4×3) blocks is here and there replaced by one (5×3) and one (3×3) block; these may or may not be contiguous. No such faults have been observed in $Nb_{25}O_{62}$ itself, nor has any interchange of blocks been seen in

---

Description of plate 1

Figure 3. Selected area electron diffraction patterns at successive stages in the oxidation and transformation of $Nb_{22}O_{54}$ to OX4C.

Figure 4. Structure image of oxidized $Nb_{22}O_{54}$, OX1C. Places where the positions of blocks have been interchanged are marked by arrows.

Figure 5. Structure image of oxidized $Nb_{25}O_{62}$, OX1E. Places where blocks have undergone disproportionation are marked by arrows.

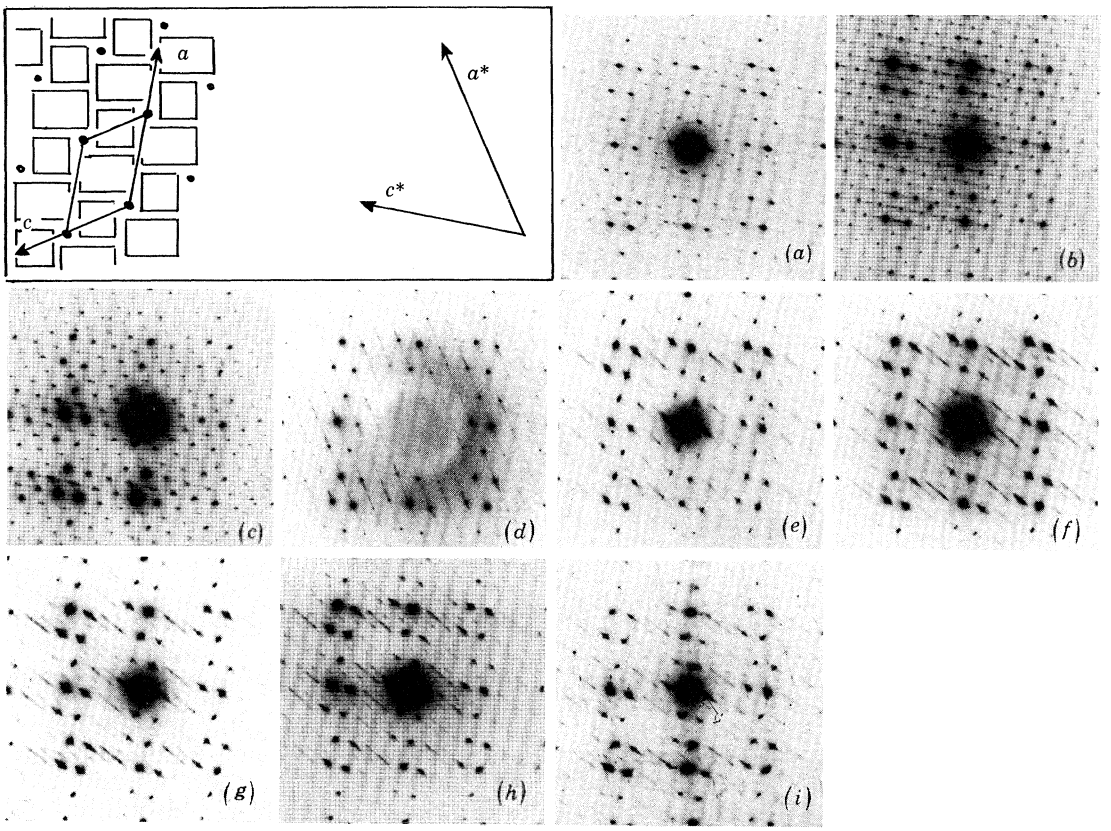

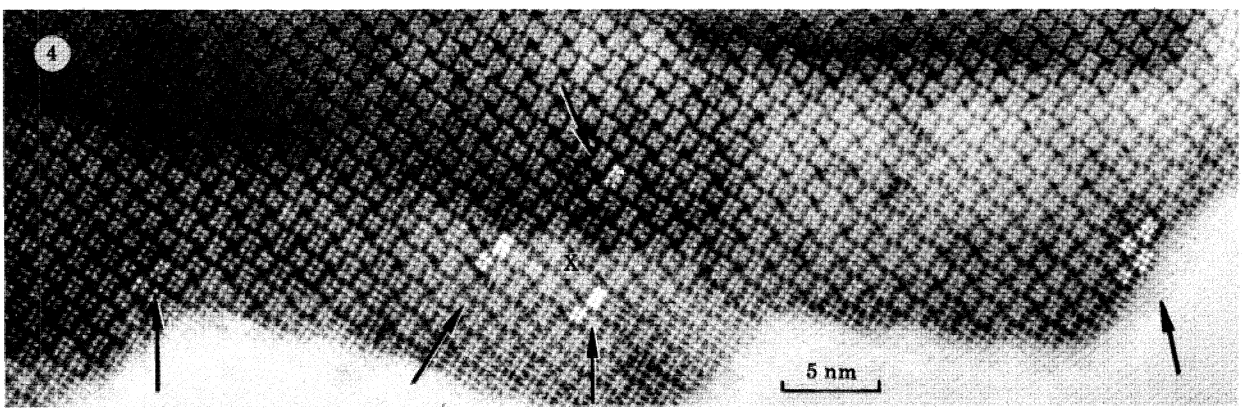

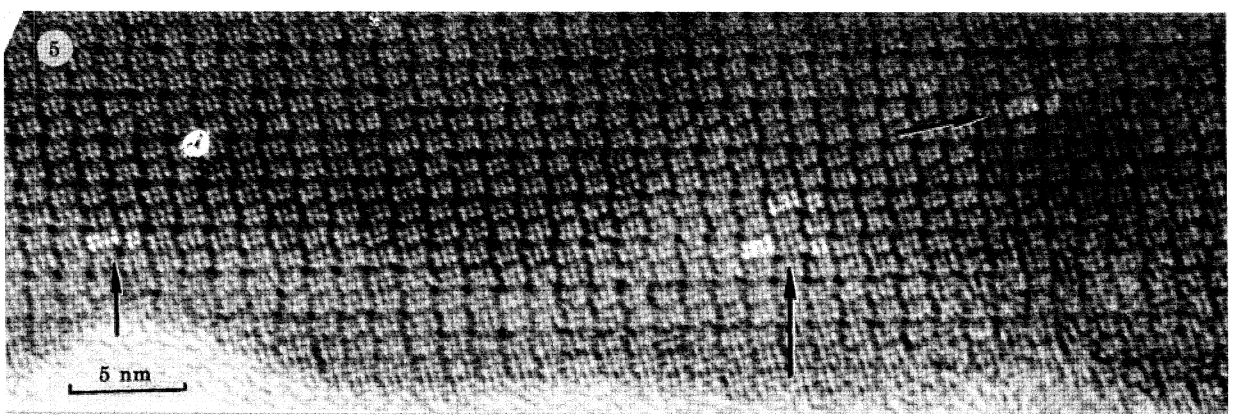

FIGURES 3–5. For description see opposite.

(*Facing p.* 336)

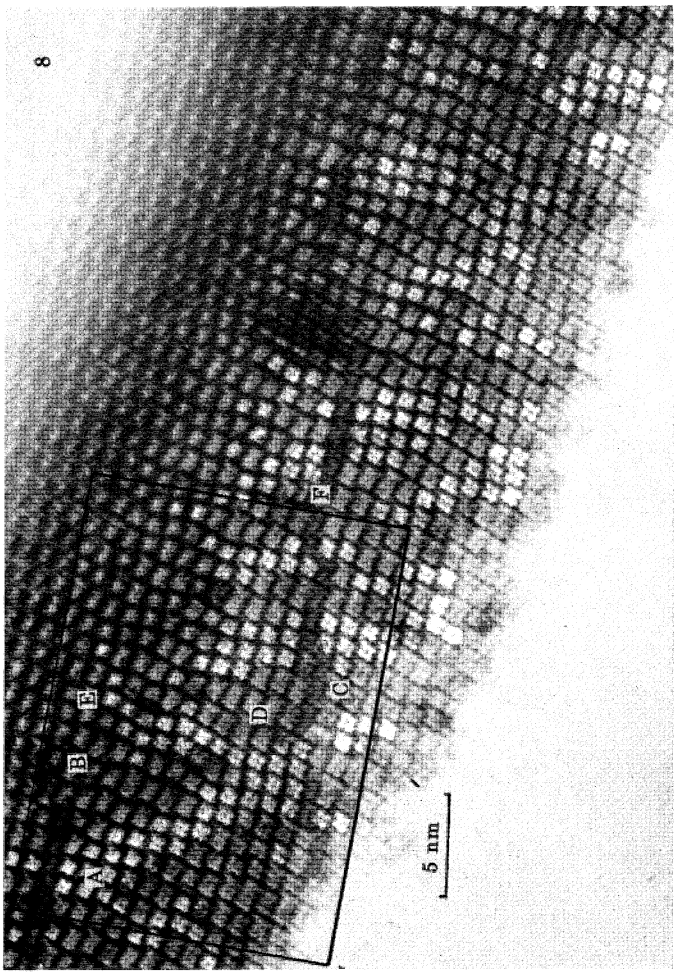
8
A
B
E
D
C
F
5 nm

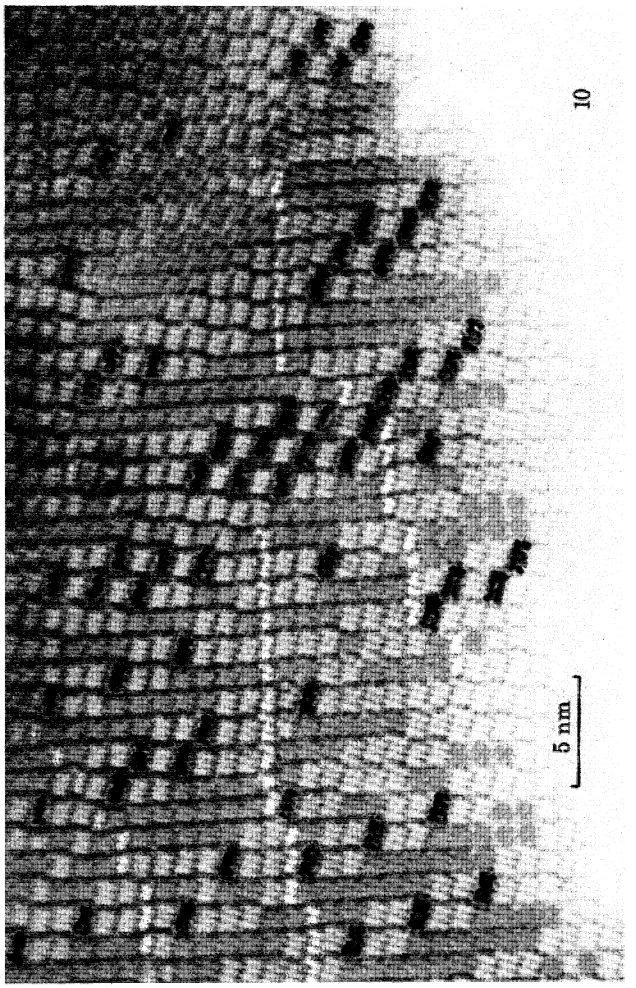
10
5 nm

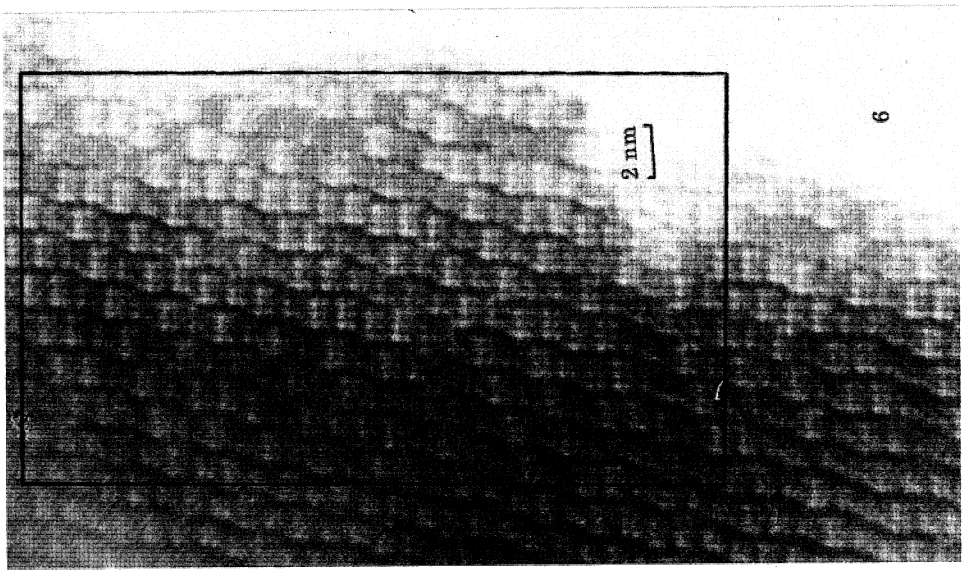
6
2 nm

$Nb_{22}O_{54}$; they occur only in the oxidized materials. Long annealing experiments afforded no evidence for any kind of superstructure ordering in the plane of projection.

It must be inferred from the structure images that the niobium atom positions and the whole network of linked blocks in OX1C and OX1E remain virtually unaltered from those of $Nb_{22}O_{54}$ and $Nb_{25}O_{62}$. After oxidation, both have the composition $NbO_{2.500}$, whereas their structures correspond to the compositions $NbO_{2.454}$ and $NbO_{2.480}$ respectively. It follows that either (*a*) oxygen atoms must have been so incorporated in the structure as to give unit cell compositions $Nb_{22}O_{55}$ and $Nb_{50}O_{125}$, without affecting image contrast in any way, or (*b*) stoichiometric balance has been achieved by a partial emptying of niobium atom sites within an otherwise unchanged network, to give unit cell compositions $Nb_{21.6}O_{54}$ and $Nb_{24.8}O_{62}$ respectively. There is no site in either structure at which an extra oxygen atom could be inserted, to give appropriate coordination, reasonable interatomic distances and local charge balance. Neither can new anion sites be created by the sort of individual cation shifts that occur in the oxidation of $Nb_{12}O_{29}$. Any occurrence of cation displacements within the blocks is ruled out by the identity of the structure images of parent oxide and oxidation product. The inference is that these latter have cation-deficient structures, and that the essence of the oxidation reaction is a migration of niobium atoms to the crystal surface, where they react to form new layers of oxide. It is uncertain which sites are left with partial occupancy. If they were completely random, every column of atoms viewed in projection would have about 2 % of vacancies, and no effect would be expected in the image contrast distribution. It may be significant, however, that this mode of reaction applies to those structures in which there are channels with tetrahedral sites. It is known that metal-excess non-stoichiometry in block structures is due to over-filling of those channels (Anderson *et al.* 1975), and it is not unlikely that cation vacancies should be preferentially located at the tetrahedral sites in metal-deficient structures. Support for that hypothesis comes from electron diffraction patterns of OX1C. Those that display the b^*-axis usually, although not invariably, show a very weak streaking between the layer lines; this is sometimes broken up into faint, but discrete, diffraction spots. It corresponds to a doubled *b*-axis, but with very poor medium- and long-range ordering of the feature that constitutes the superlattice. This would be explicable if, in some channels of tetrahedral sites, exactly half the sites were occupied in an ordered fashion, but that adjacent channels were only weakly correlated. Within any one channel, the site occupancy might well switch from an ordered 50 % to 100 %, in different segments, provided that 80 % of the total channel length in any crystal of OX1C, or 40 % in OX1E, was half filled. Localized, short-range, purely one-dimensional ordering of that kind would have no distinctive effect on the image contrast around the tetrahedral sites.

If heating promotes an exchange of places between blocks, it is important to ascertain whether the observed effects could, at least in part, be artefacts produced by beam heating in the act of imaging. As a check, a series of micrographs were taken of the same area of crystal, after

---

Description of plate 2

Figure 6. Earliest stage in the transformation of OX1C to OX2C.

Figure 8. Rearrangement of OX1C to OX2C. (3 × 3) blocks are collected into irregular domains at A; there are incipient domains of *H*–Nb_2O_5, such as at D. F is a line of faulted structure.

Figure 10. Fully developed OX2C structure. (3 × 3) blocks are almost completely segregated into regular, elongated arrays, in a matrix of, largely, *H*–Nb_5O_5 structure. Rows of fault structure cross these domains.

successive exposures to irradiation, far exceeding that received in the normal course of microscopy. The results of this experiment are detailed in the Appendix, but the conclusion was that although beam-induced changes in the specimens occurred occasionally, they were rare events. No substantial and misleading artefacts are likely to have been produced in the course of the electron microscopy.

5. Rearrangement of the block structure: the disordered state

Electron microscopy shows that the alterations observed in the diffraction patterns (figure 2, figure 3*c*) correspond to the onset of an irreversible structural rearrangement, at constant composition. This has two effects: (*a*) the existing blocks are progressively rearranged, as a development of the type of localized stacking fault observed in OX1C; (*b*) new blocks are formed, with a different cross section. Blocks of (5×3) octahedra are needed to build up the ultimate *H*–Nb_2O_5 structure, but are not present in $Nb_{22}O_{54}$, $Nb_{25}O_{62}$ or their immediate oxidation products. They are formed by the disproportionation reaction represented by

$$2(4 \times 3) \text{ blocks} \rightarrow (5 \times 3) \text{ block} + (3 \times 3) \text{ block}. \qquad (1)$$

This disproportionation is responsible for the occasional faults found in OX1E. It is conservative in the number of blocks and of c.s. interfaces, and in the number of cation sites within blocks. Initiated at a number of uncorrelated sites, these processes of translocating blocks and creating new blocks necessarily generate a disordered structure. The oxidation products of the various lower oxides differ as to the temperature at which these two processes become significant. It is lowest for OX1C, and the individual steps can more conveniently be disentangled for that material. Hence that transformation was studied in considerable detail, and will be discussed first. At the higher temperatures needed for the transformation of OX1E, successive steps followed with great rapidity and were less easily isolated.

(*a*) *The transformation OX1C → OX2C. The early stages of transformation*

As already noted, the first detectable step is an extensive exchange of places between (3×3) blocks and (4×3) blocks. Figure 6 (plate 2) shows the typical structure at a very early stage. Over much of the region shown, the original '$Nb_{22}O_{54}$' structure (by '$Nb_{22}O_{54}$' is signified the block arrangement proper to $Nb_{22}O_{54}$, but with the actual stoichiometry $NbO_{2.500}$) remains unchanged, but pairs of blocks and also extended lines of blocks have exchanged places.

The fuller implications of these apparent interchanges of whole blocks can be brought out by a suitable mapping procedure. In figure 7, the region enclosed within the frame in figure 6, has been mapped on top of a map of the idealized '$Nb_{22}O_{54}$' structure. This at once shows where and how the local rearrangements have resulted from the displacement of atoms.

Thus, at A, where one pair of blocks has been interchanged, a single row of atoms (*a*) at the shorter edge of a (4×3) block, has been shifted to the position *b*. Two cations have been displaced by $\frac{1}{2}a_R \langle 110 \rangle_R$, from filled octahedral sites in the nearly invariant oxygen sublattice; two cations have been shifted by $\frac{1}{4}a_R \langle 111 \rangle_R$ to switch the position of the tetrahedral site around, and two oxygen atoms have also moved. (Here and subsequently, the subscript R relates to the underlying ReO_3-type, cubic sub-cell of the structure). The displacement of four cations and two oxygen atoms, in every layer of the structure, suffices to interchange the positions of two whole blocks. At A, the image contrast was normal and well resolved, indicating that this

process had run right through the thickness of the crystal flake imaged. At B and elsewhere, there is a band of dark contrast, 0.6 nm wide between what look like (3 × 3) blocks; this arises from an overlap, somewhere within the crystal flake, between original structure and transformed structure. It is evident that the atom row shift is propagated with ease up the unique axis, but is not an instantaneous, cooperative act.

This directly observed displacement of atoms in the c.s. interface is exactly that postulated by Andersson & Wadsley (1966, 1970) for the migration of c.s. planes. A cooperative jump of $\frac{1}{2}a_{\mathrm{R}}\langle 110\rangle_{\mathrm{R}}$ displaces the c.s. plane through a_{R} and, as applied to block structures, transfers a row of atoms from the edge of one block to that of its neighbour. It will subsequently be referred to as an A.W. shift. It is competent to effect the disproportionation process, and if A.W.

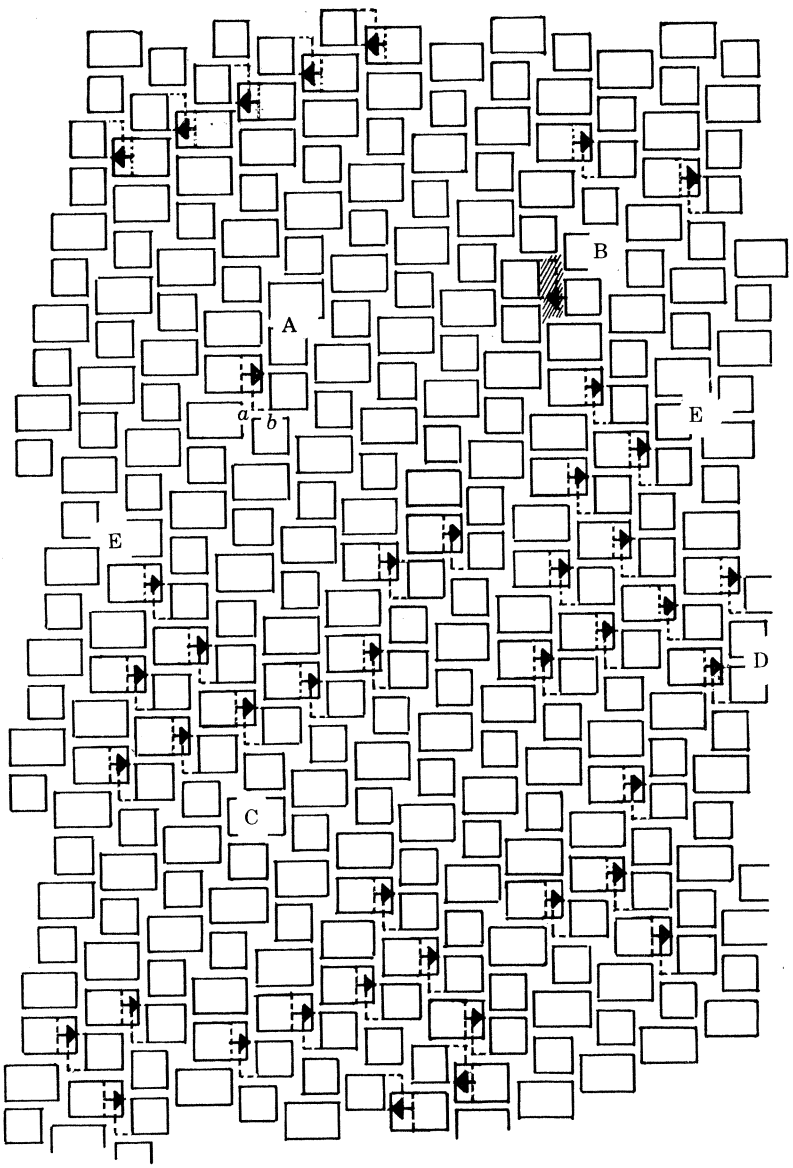

FIGURE 7. Displacement map of the area within the rectangle in figure 6. Original location of interfaces between blocks dotted; arrows mark the displacement of one row of atoms at such an interface.

shifts operate repeatedly, in the same sense, they serve virtually to transport a block of given cross section through the structure.

At C, a series of such A.W. shifts has run along a line of blocks, in the [001] ('$Nb_{22}O_{54}$') direction, thereby interchanging a row of (4×3) blocks and a row of (3×3) blocks. At D, a similar series of A.W. shifts has been propagated along [102] ('$Nb_{22}O_{54}$'); at E, A.W. shifts run up a file of blocks, along [100] ('$Nb_{22}O_{54}$). Cascades of displacement events have evidently been initiated, in an uncorrelated fashion, at various loci 6–10 nm apart, and have been propagated unequally along different crystallographic directions. The distribution, amplitude and direction of these shifts is displayed by the arrows in figure 7.

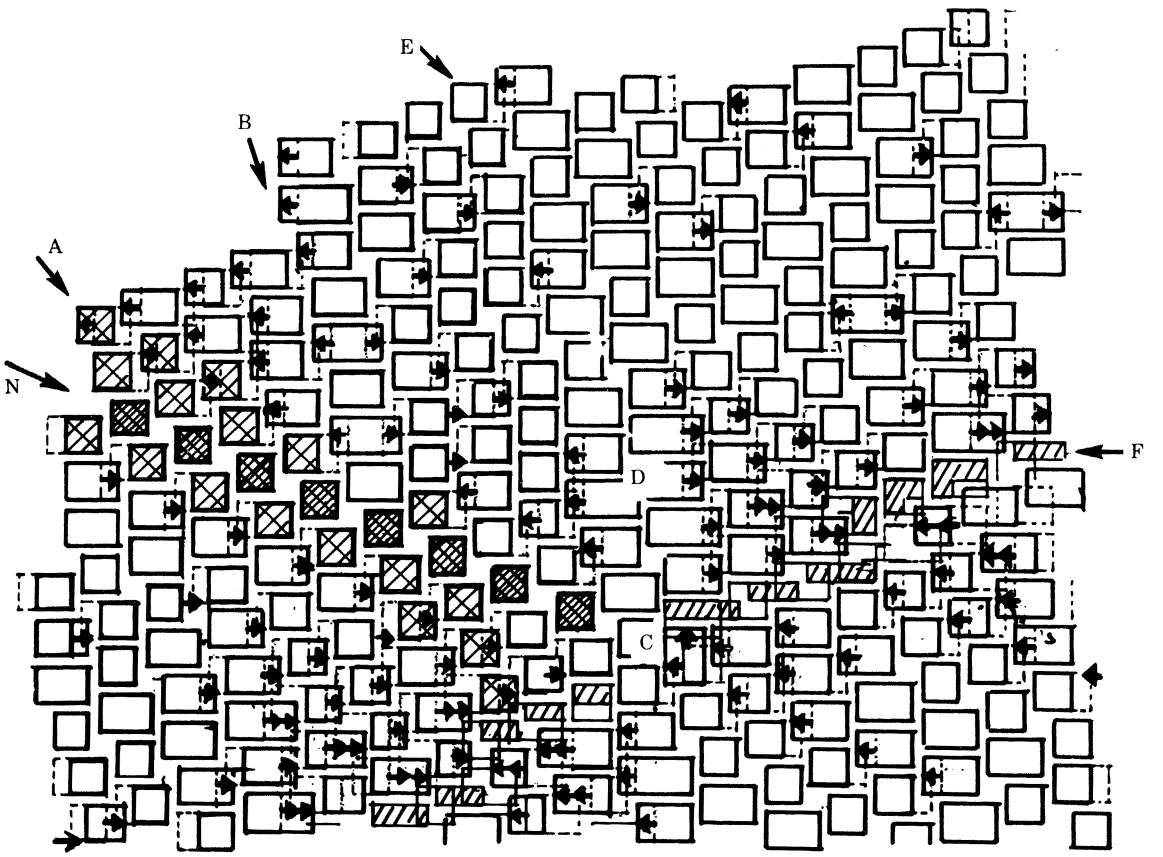

FIGURE 9. Displacement map of the area framed in figure 8.

A more advanced stage of transformation (in a sample of OX1C heated at 400 °C for 10 minutes) is shown in figure 8 (plate 2); a displacement map of the area within the rectangle is shown in figure 9. In the main, the structure is composed of the same structure elements ((3×3) and (4×3) blocks) as the original OX1C, but has been extensively rearranged. In addition, a small proportion of (5×3) blocks has been formed, stacked alternately with (4×3) blocks to form isolated units or very small microdomains of the *H*–Nb_2O_5 structure. It can be seen from figure 9 that the observed structure results from a high incidence of A.W. shifts, and that in a number of places two successive shift events must have operated, particularly in the immediate neighbourhood of disproportionations. There has been an extensive lateral displacement of the (3×3) blocks, which are now grouped into elongated strings of two kinds.

At E and elsewhere, a long, sinuous file of (3 × 3) blocks has been formed by the almost regular alternation of l → r (left to right) and r → l shifts, along the general [100] ('$Nb_{22}O_{54}$') direction. In these files, most of the blocks are linked to adjacent blocks by corner sharing, as in the structure of $TiNb_2O_7$, i.e. few tetrahedral sites have been created. A second configuration of (3 × 3) blocks is to be seen at A: a staggered array, in which each (3 × 3) block is surrounded by tetrahedral sites. Crossing this array is one row of blocks N that has not been subjected to any displacements; above N, all A.W. shifts are r→l, below it all are l→r. N is a sort of node, about which the c.s. planes that define the structure have pivoted, in the way discussed by Bursill & Hyde (1972). This reorientation of c.s. planes is the cumulative result of successive A.W. shifts, which fan out in density and amplitude on either side of the node.

Also noticeable at this stage is the incidence of the block disproportionation reaction, and its propagation along the [100] ('$Nb_{22}O_{54}$') direction, to produce incipient files with the *H*–Nb_2O_5 structure, as at B and D. In each case, the disproportionation reaction is associated with a set of r → l or l → r shifts, on either side of a nodal line; it could only be propagated laterally through a high incidence of cumulative shifts. The propagation of r → l shifts across every adjacent block, together with the creation of additional (3 × 3) blocks by the disproportionation reaction itself, is instrumental in building up the array of (3 × 3) blocks at A.

F is a meandering, discontinuous line of faulted structure. Its image corresponds to that expected for a row of narrow blocks, only two octahedra wide, although such blocks do not represent any stable crystal structure. The significance of such faults will be more fully considered later (§ 6), but their probable origin is evident from the displacement map. All the displacements appear to be propagated from independent initiating centres, with no long-range correlation between them. Immediately above F, all displacements are l → r: below F, all are r → l. Where these sets of independent displacements impinge, the structure cannot be reorganized into blocks three octahedra wide, and anomalous structure elements are formed. These may still represent an unstable configuration. At C, part of this faulted structure has been modified by the operation of an A.W. shift normal to the general direction. This has produced a (3 × 4) block, oriented with its longer edges at right angles to the general direction.

(*b*) *Maximization of disorder and the recovery of order*

Prolonged annealing (for example 7 days at 400 °C or 10 days at 350 °C) brought the material to a more or less reproducible state, corresponding to that designated OX2C by Hibst & Gruehn. In detail, the structure was highly variable from one crystal to another, but it conformed to a quite consistent pattern. This was typified (*a*) by the almost complete segregation of (3 × 3) blocks into small domains, and (*b*) by the minor role still played, up to this stage, by disproportionation to form (5 × 3) blocks (and hence of domains with the *H*–Nb_2O_5 structure).

Figures 10 (plate 2) and 11 (plate 3) typify this structural pattern, its lack of long-range order and its local variability. Figure 12 is a displacement map of the central area in figure 10, showing the incidence of A.W. shifts required to produce the structure as observed. In this structure, the (3 × 3) blocks are all grouped into elongated, staggered arrays, lying on the same orientation. Within each array, the (3 × 3) blocks are associated with tetrahedral sites and are arranged in tetragonal symmetry; their arrangement is isostructural with the known phases PNb_9O_{25} and VNb_9O_{25} (Roth *et al.* 1965). It follows that these arrays have the composition $Nb_{10}O_{25}$ and can be regarded as microdomains of another polymorph of niobium pentoxide,

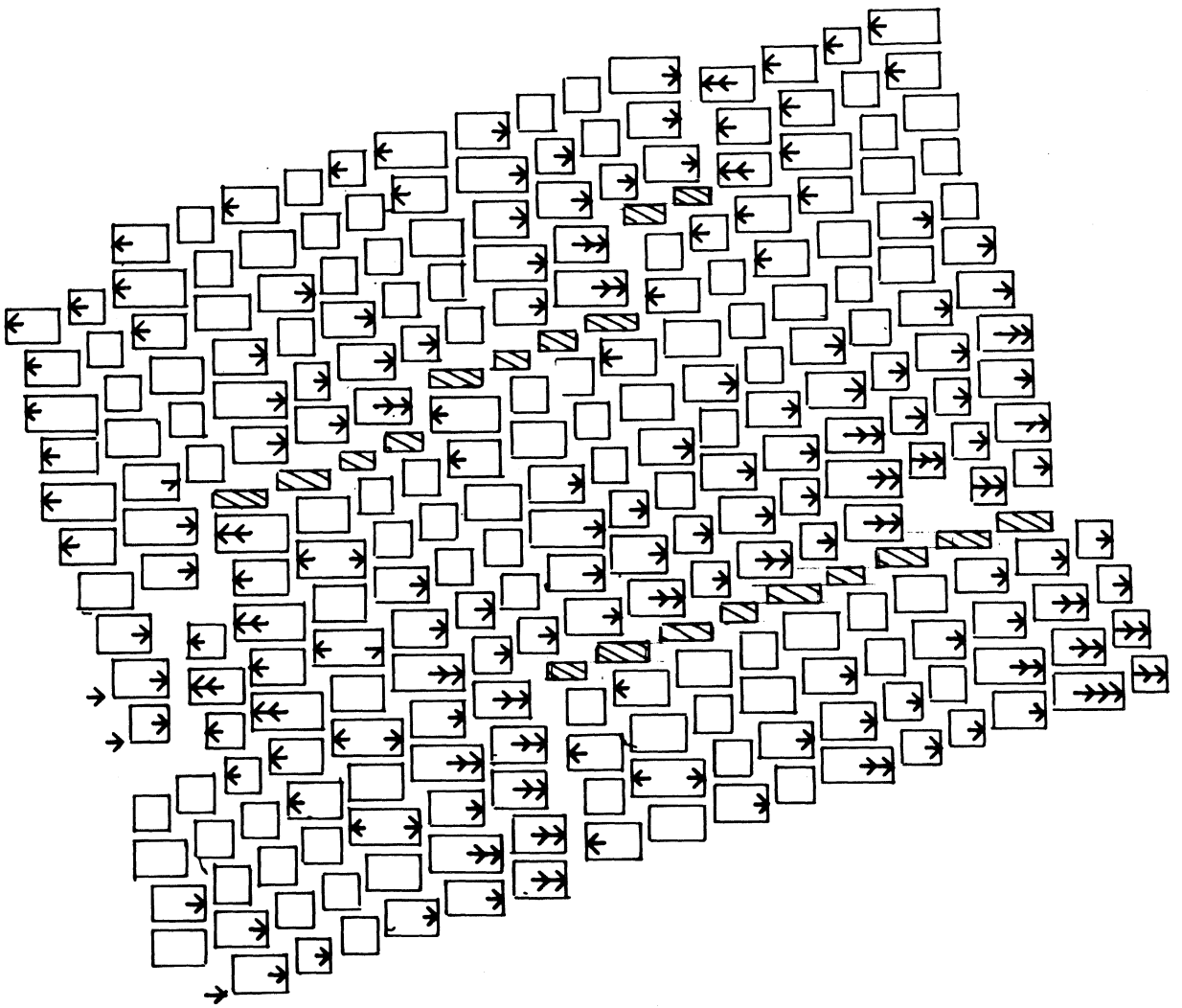

FIGURE 12. Displacement map of area covered by figure 10.

DESCRIPTION OF PLATES 3 AND 4

FIGURE 11. Fully developed OX2C structure, showing nearly regular recurrence of fault rows, with narrow blocks (arrowed). Occasional blocks are turned at right angles to the general configuration (X).

FIGURE 13. OX3C structure: long, regular arrays of (3 × 3) blocks ($Nb_{10}O_{25}$) and extensive domains of H–Nb_2O_5 structure. Fault rows, with narrow blocks, are undergoing replacement by walls of turned-around blocks.

FIGURE 15. OX4C structure: arrays of $Nb_{10}O_{25}$ structure and of H–Nb_2O_5 structure, intersected by walls of turned blocks with occasional anomalous faults.

FIGURE 16. OX4C: detail of typical structure in the intersecting fault walls. At Z is a block (6 × 3) octahedra in cross section; to the right of, and below, Z are a block two octahedra wide and a 'spliced' pair of blocks. This is the location of a dislocation.

FIGURE 17. Oxidation of $Nb_{22}O_{54}$ at 500 °C, with no annealing. Immediate effect is extensive interchange of block positions, but relatively little disproportionation.

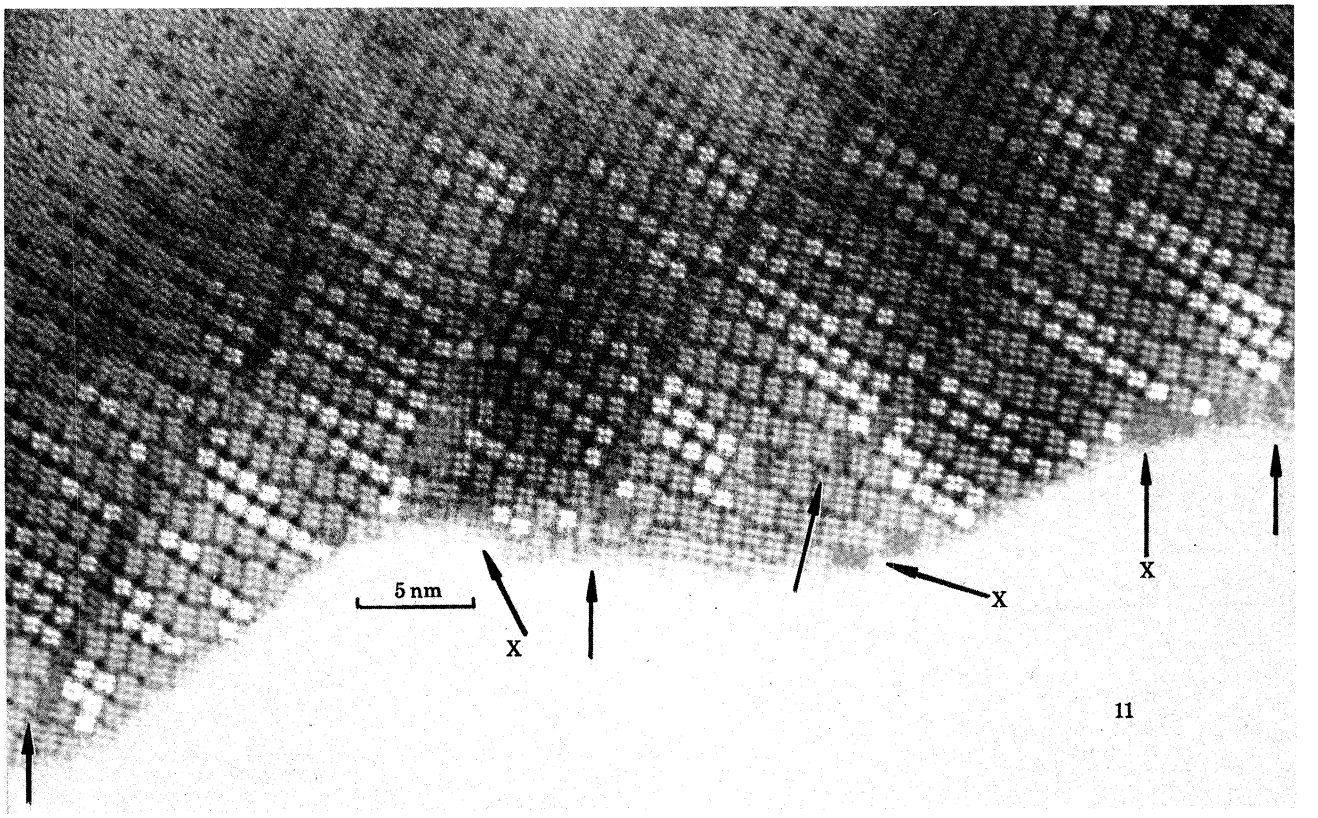

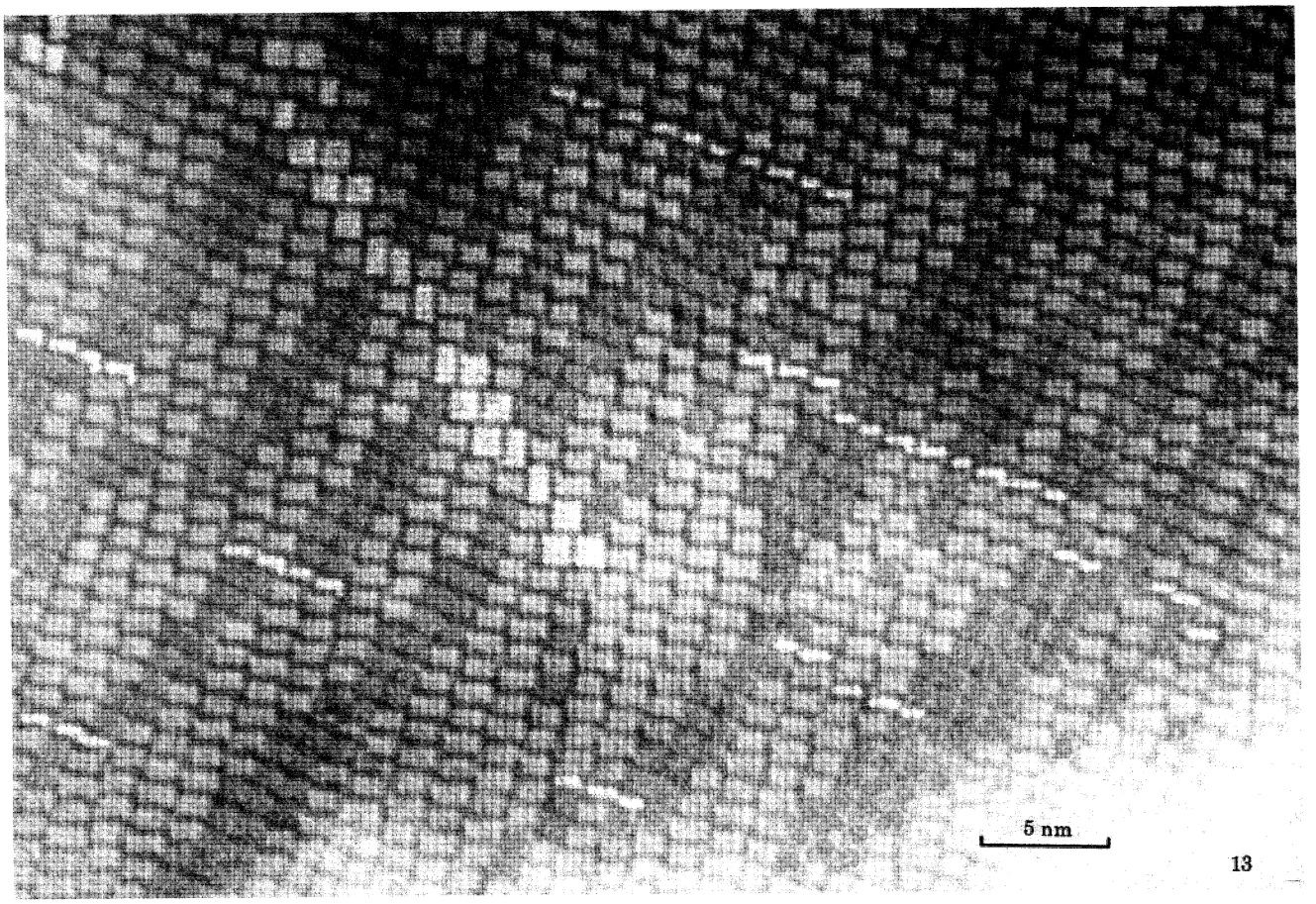

FIGURES 11 AND 13. For description see opposite.

(*Facing p.* 342)

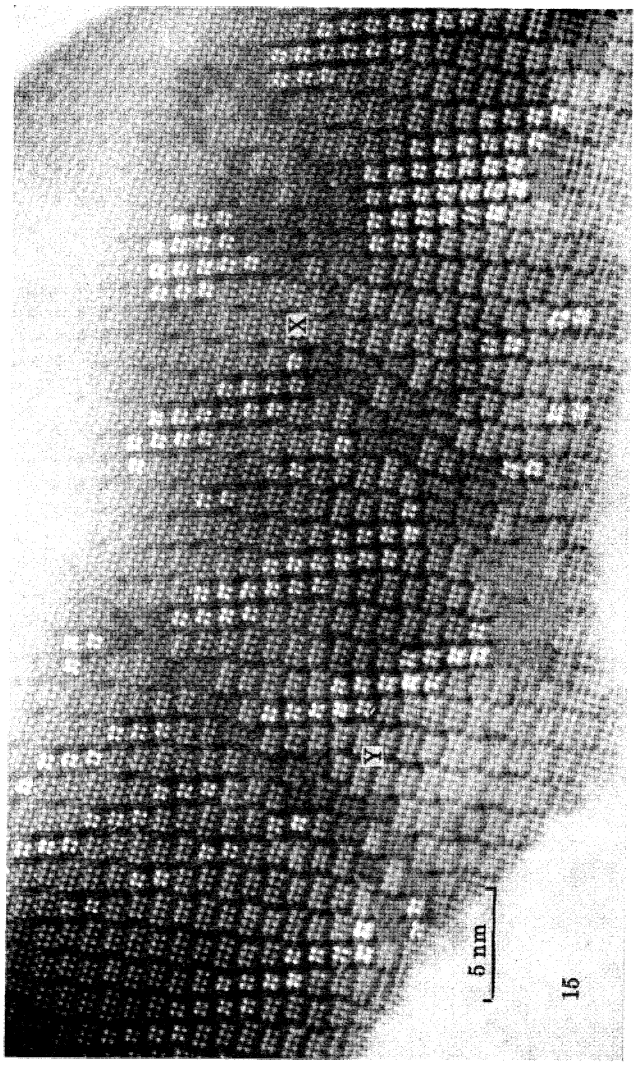

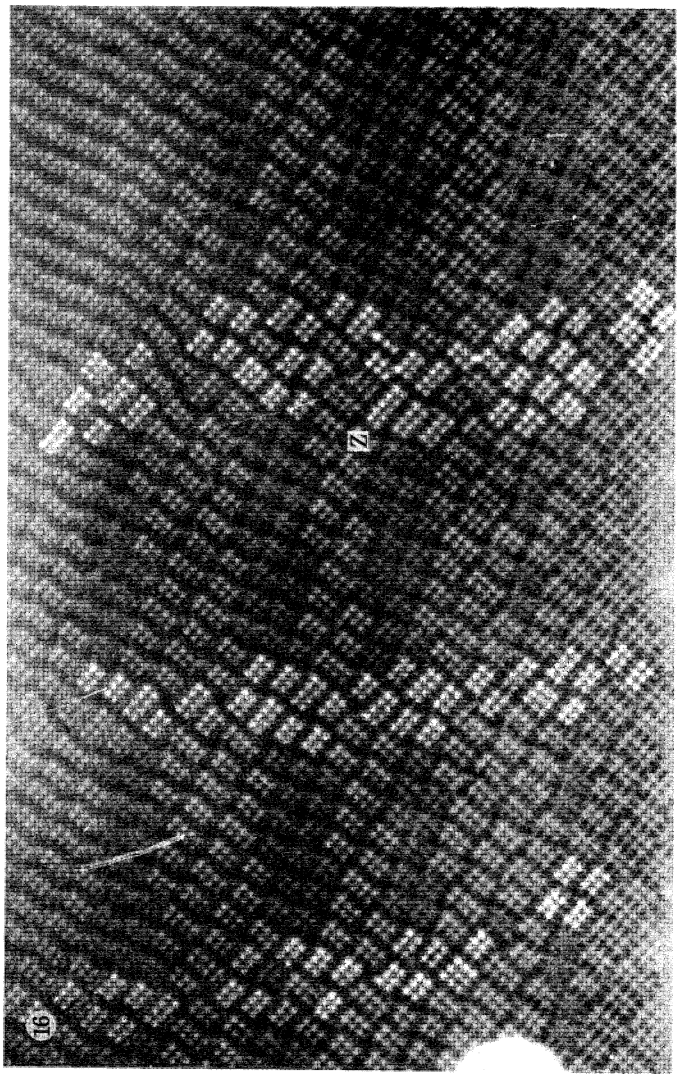

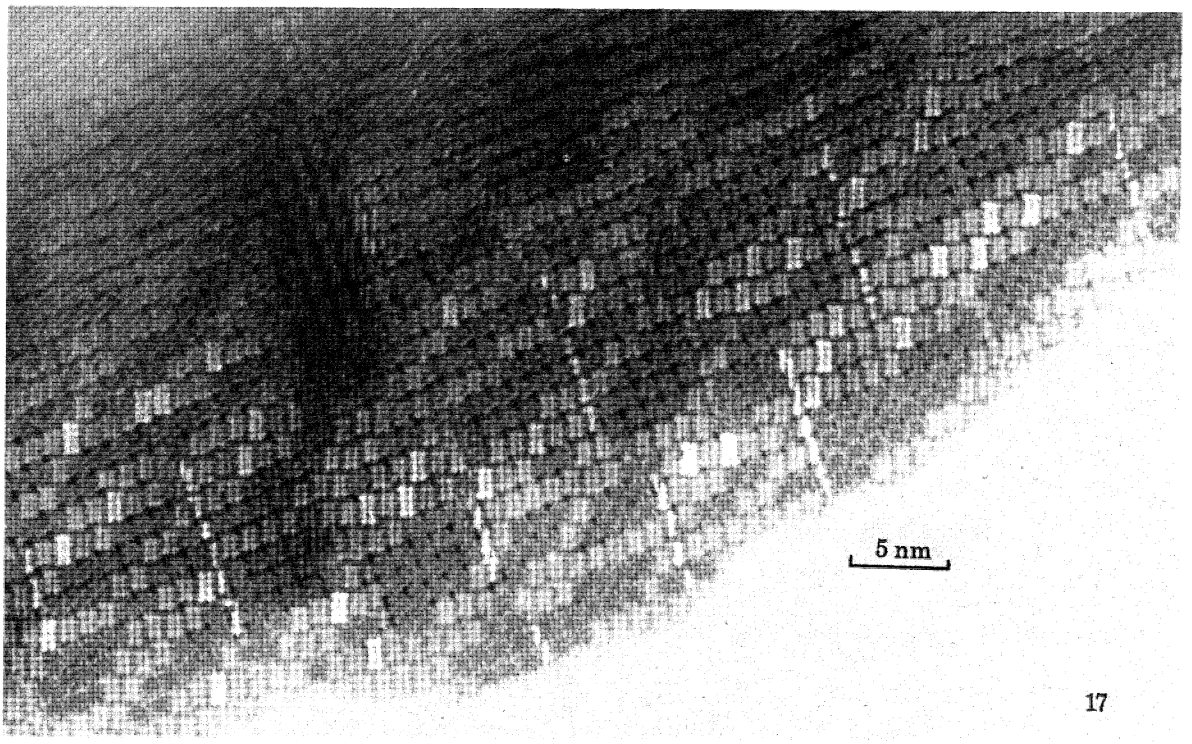

FIGURES 15–17. For description see p. 342.

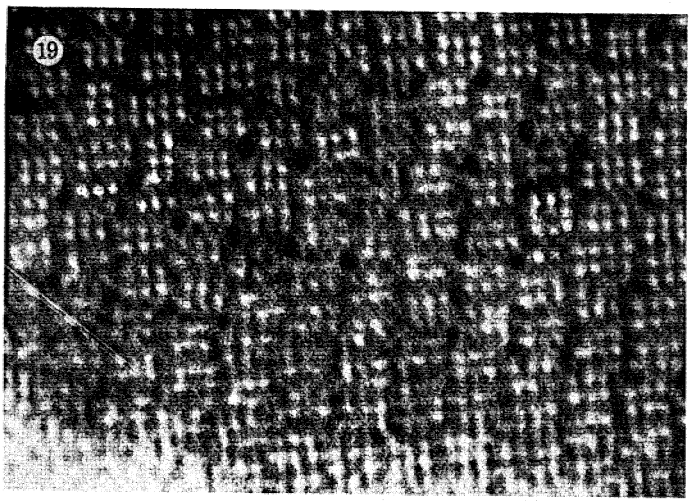

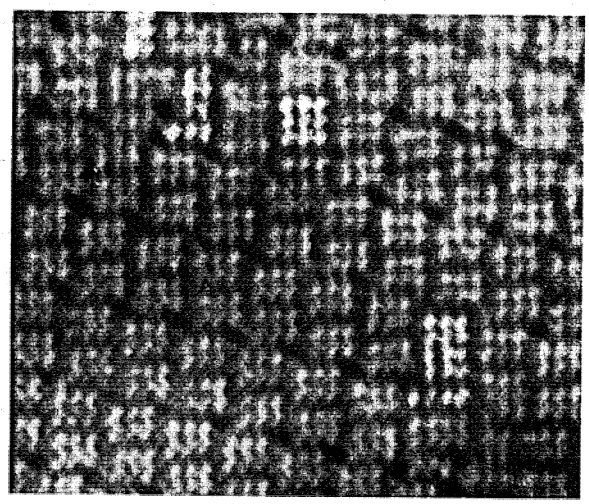

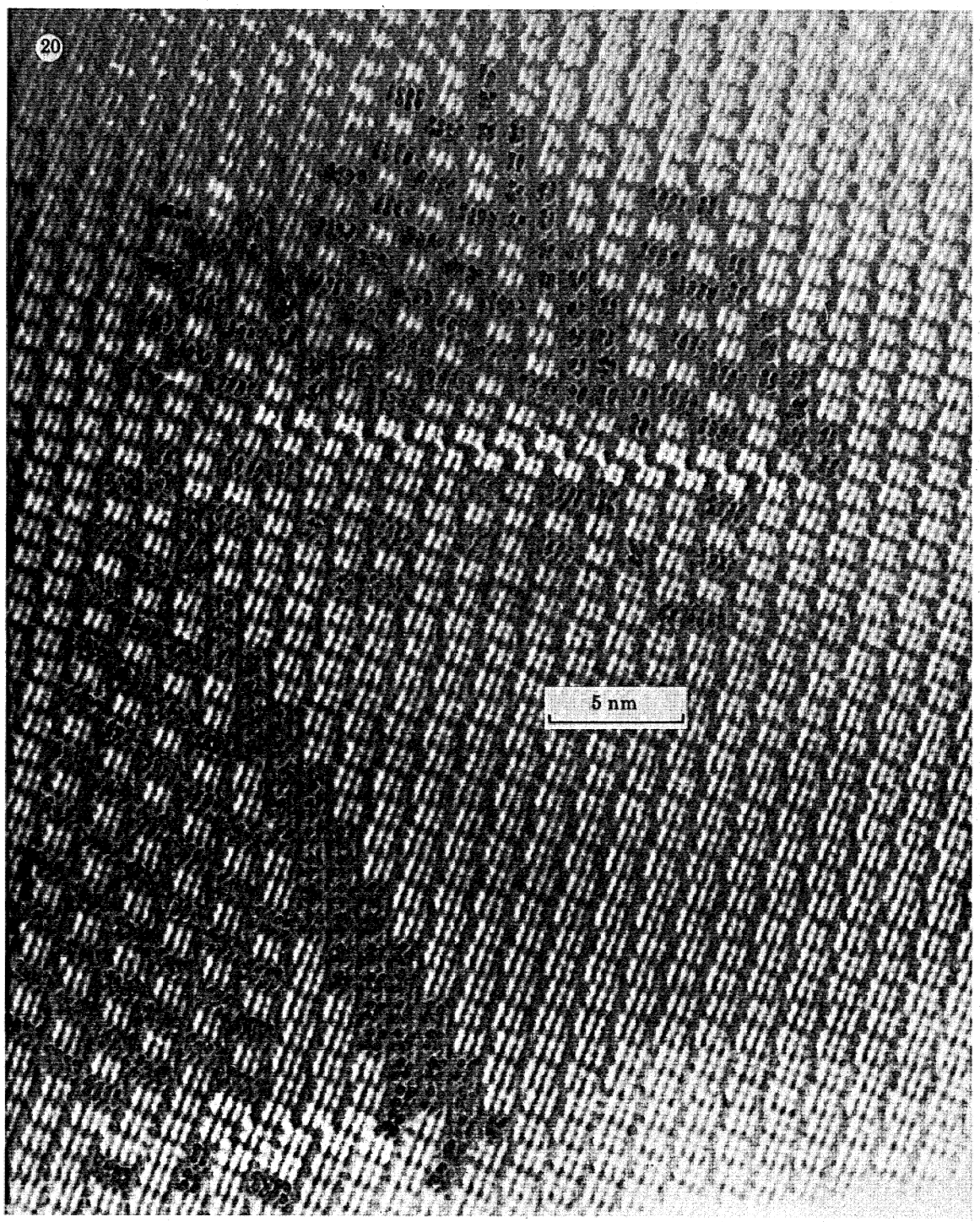

FIGURES 19 AND 20. For description see p. 343.

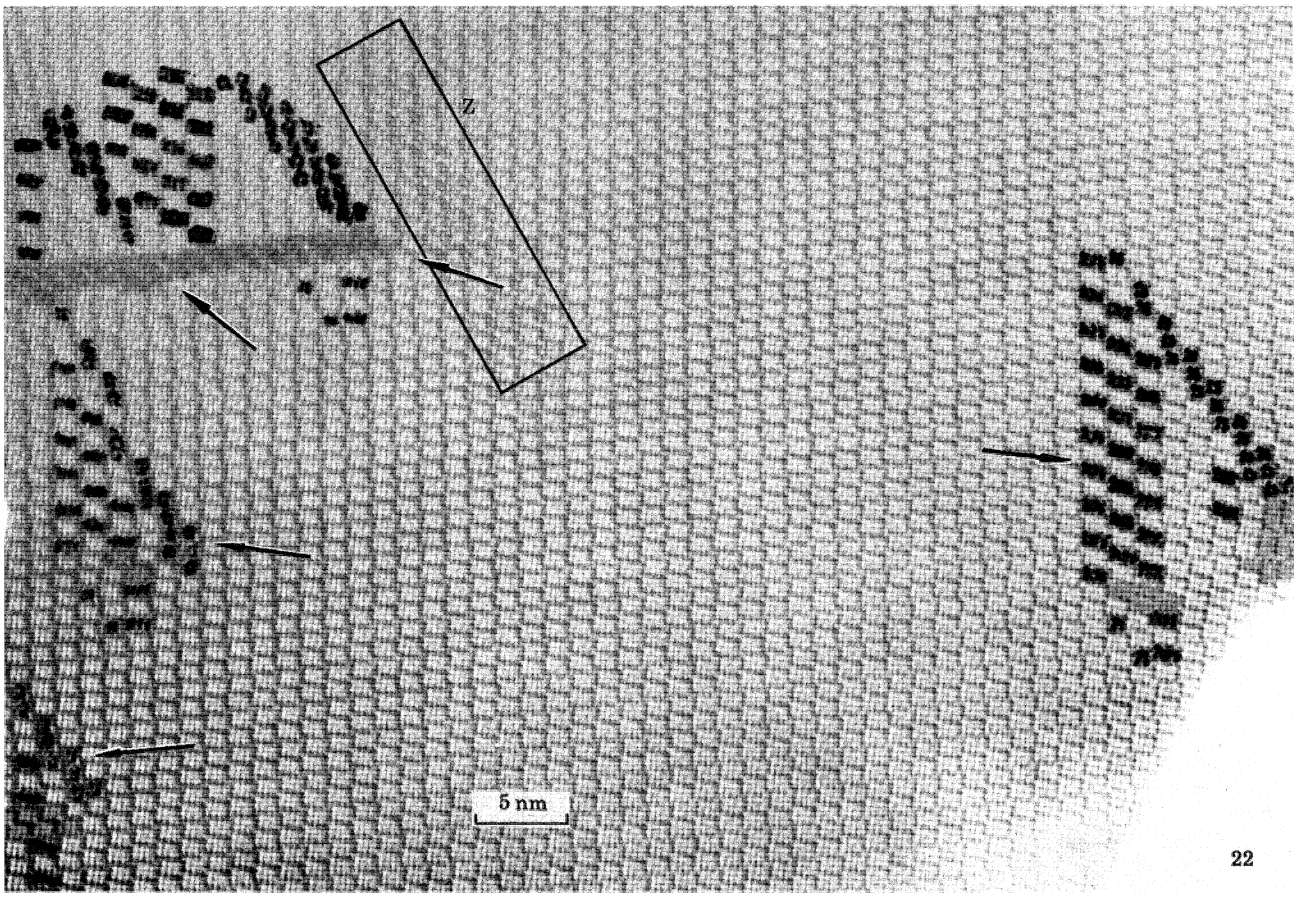

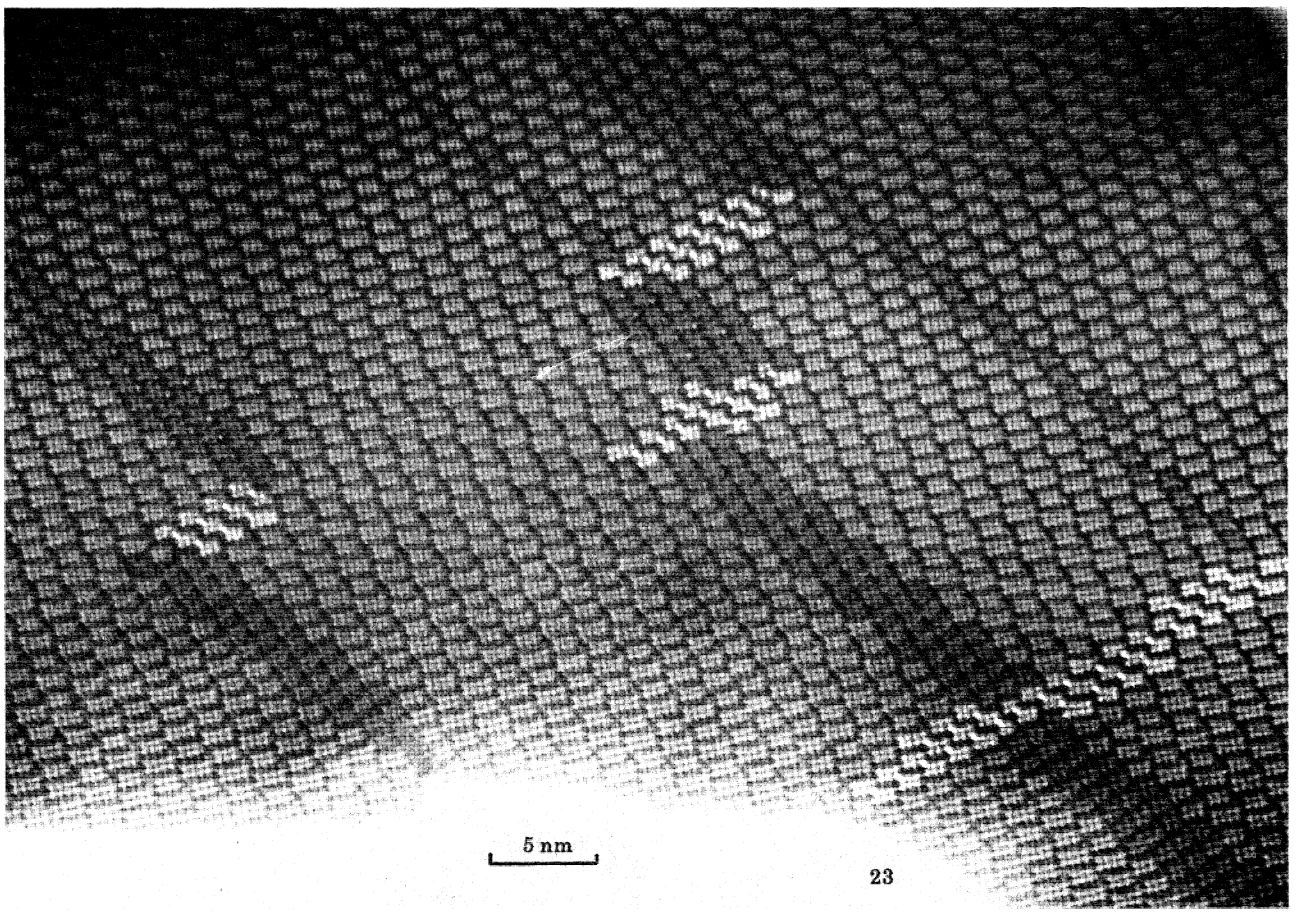

FIGURES 22 AND 23. For description see opposite.

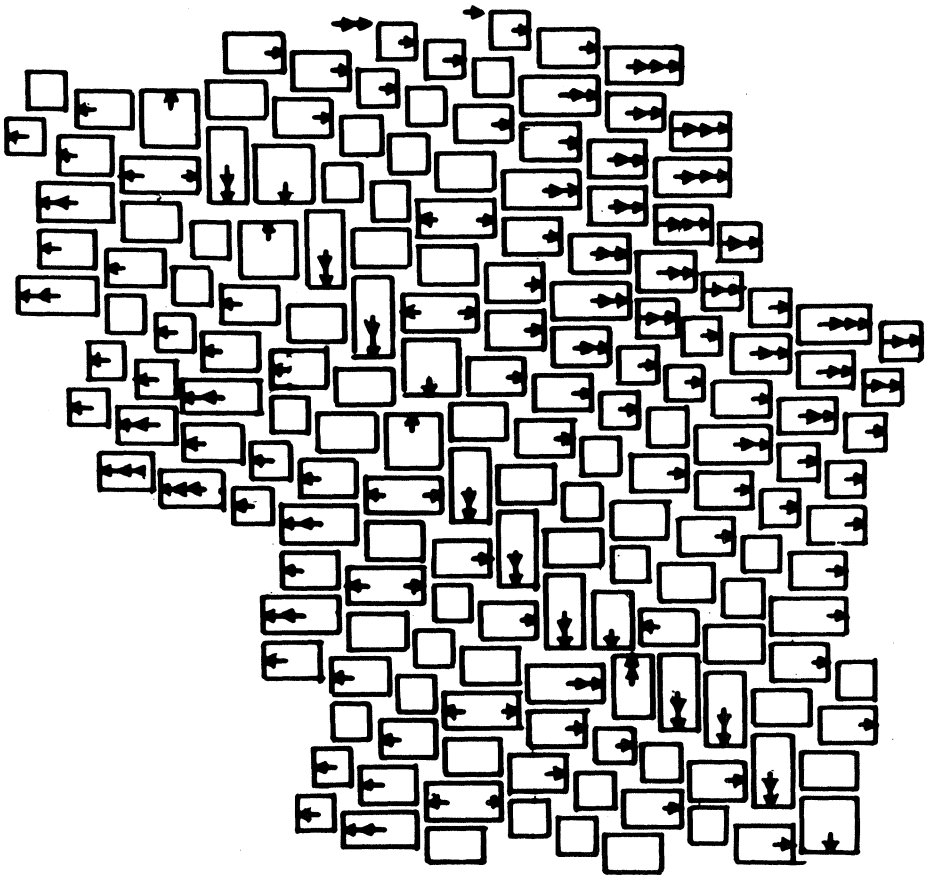

FIGURE 14. Displacements involved in forming the wall of turned-around blocks in figure 13.

which is not known as a stable species and can probably be formed only as a metastable, coherent intergrowth (cf. Browne & Anderson 1974). These arrays are bounded by (310) ($Nb_{10}O_{25}$) (i.e. $(60\bar{5})_R$). Between them are slabs, mostly two or three blocks in width, made up of (4×3) and (5×3) blocks; the latter create small microdomains with the H–Nb_2O_5 structure, but the extent of block disproportionation remains small and locally very variable at this stage. Disproportionation to form (5×3) blocks is invariably associated with a high local incidence of A.W. displacements, and usually with repeated displacement events. In figures 10 and 11 (5×3) blocks have been formed in several distinct ways: (*a*) from (4×3) blocks, by a single A.W. shift, on either side of a node that runs between files of blocks, thereby generating a strip of H–Nb_2O_5 structure, two blocks wide; (*b*) from (3×3) blocks, by two (perhaps

DESCRIPTION OF PLATES 5 AND 6

FIGURE 19. OX1E: occasional A.W. displacements across the longer edges of blocks.

FIGURE 20. Nucleation in the conversion of OX1E to OX2E: two adjacent triangular nuclei. Note abrupt transition from unchanged $Nb_{25}O_{62}$ structure to $Nb_{10}O_{25}$ and H–Nb_2O_5 structures at the edges of the nuclei.

FIGURE 22. Nucleation in the conversion of OX1E to OX2E: five nucleation events marked by arrows. In the area Z, the distribution of overlap contrast indicates that another array of $Nb_{10}O_{25}$ is in process of formation.

FIGURE 23. OX2E: merging of separate nucleation events creates large domains of H–Nb_2O_5 structure, long arrays of $Nb_{10}O_{25}$ and linking faults.

successive?) A.W. shifts, which may be either in the same sense or in opposite senses. In the latter case, a node runs up the centre of the file of blocks concerned. In either case, the lateral growth of the incipient *H*–Nb_2O_5 domain depends upon the occurrence of repeated, cumulative, displacements. As microdomains of the two kinds of Nb_2O_5 structure are formed, there is still a preponderance of (4×3) blocks in the matrix. Some of these are linked as elements of the $Nb_{25}O_{62}$ structure; others, associated with tetrahedral sites, correspond to the local composition $Nb_{13}O_{33}$. A balance sheet of block sizes and tetrahedral sites shows that the structure as a whole would not have the ideal stoichiometry $NbO_{2.500}$, but must still be cation deficient.

Intersecting this disordered microdomain structure is a series of linear faults, of the kind shown at F, figure 9. These recur at almost regular intervals, as is shown in figure 11, which is taken from a set of overlapping micrographs that mapped the structure in detail over 120–150 nm in both directions. It was found that, except where they step sideways, these faults run continuously through the crystal, and occur every 6–10 nm along the [100] ('$Nb_{22}O_{54}$') direction. They are an inherent feature of the transformation process, and all subsequent reorganization is to some extent restricted to rearrangement within the narrow slices of crystal contained between walls of fault. In a few places, as at X, figure 11, these fault walls are modified by conversion to 'turned-around' blocks (as previously noted, figure 9, C), but such features are rare.

Material brought to the stage termed OX3C (for example, annealed at 515 °C for 6 days) is typified by figure 13 (plate 3). It differs qualitatively from the preceding stage in that medium-range order has been established over larger domains. The arrays of $Nb_{10}O_{25}$ remain, and the zigzag strings have grown longer. The matrix in which they are set is largely made up of *H*–Nb_2O_5 structure, showing that the block disproportionation reaction has become more important at the higher temperature and with longer annealing times. The ordering process again appears to operate from numerous independent centres, since contiguous domains of *H*–Nb_2O_5 are usually out of phase with respect to their stacking sequences. As in OX2C, the structure is intersected by recurrent faults, rows of narrow blocks, but a process has started whereby these are ultimately completely eliminated, and replaced by walls of turned-around blocks. In these walls are frequent clusters and rows of (4×4) blocks, the structure elements of another known Nb_2O_5 polymorph, *N*–Nb_2O_5. Figure 14 illustrates how the structure is reorganized around such a wall. It may be noted that, although the absolute number of cumulative A.W. shifts needed to produce the observed configuration can no longer be identified with certainty, after such extensive rearrangement, the relative A.W. displacements are correct. It has not been possible to trace the full course of reconstruction of the fault walls. Whereas the original lines of narrow blocks run – subject to much segmentation and side stepping – along the rows of blocks, the general [001] ('$Nb_{22}O_{54}$') direction, the walls of turned-around blocks run diagonally, trending generally along $[101]_R$. The faults have thus been swung around as the narrow blocks were eliminated, and that necessarily entailed a complex set of A.W. shifts across the longer edges of blocks. At the same time, the domains of *H*–Nb_2O_5 structure have grown by propagation of the ordering process down the files of blocks.

This is still only a transient stage. The structural changes that set in at about 300 °C, mediated entirely by short-range processes – i.e. the step by step translocation of blocks and the disproportionation of blocks – first produce almost complete long-range disorder and then an increasing degree of a new, medium-range order. No electron microscope evidence points to

any essential constitutional difference between OX2C and OX3C; there is a continuous structural development that culminates in the quasi-regular domain structure of OX4C, discussed below. The two basic short-range processes presumably differ slightly in activation energy, since they dominate two distinct time–temperature-transformation régimes; in that sense, the distinction drawn by Hibst & Gruehn between OX2C (dominated by block translocation) and OX3C (dominated by disproportionation) is justified.

Long annealing (7 days) at 700 °C continues the ordering processes and produces a structure (OX4C) consisting essentially of alternating domains of *H*–Nb_2O_5 and $Nb_{10}O_{25}$; figure 15 (plate 4) is representative of this structure. Domains of *H*–Nb_2O_5 are invariably narrow, but the breadth of the $Nb_{10}O_{25}$ domains varies considerably from one crystal to another; at this stage there are numerous domains four–six (3×3) blocks wide. They form nearly continuous walls between slabs of *H*–Nb_2O_5 structure, but are intersected at intervals of 10–20 nm by walls of turned blocks, across which they are usually slightly offset. The fault walls completely replace the rows of narrow block faults found at earlier stages, but contain occasional narrow blocks (as at X) and 'spliced' blocks (as at Y). These are probably relics of uncompleted readjustments, as rows of narrow blocks become converted into walls of turned around blocks. Typical detail of the structure of the faults is seen in figure 16 (plate 4); blocks of unusual dimensions, such as the (3×6) block Z, an element from the hypothetical $Nb_{18}O_{45}$ structure for Nb_2O_5, are not infrequently found. Detailed mapping shows that these faulted structures involve unusual configurations for the c.s. interfaces between blocks and, occasionally, dislocations. The features observed would be consistent with the view that the structure had not reached its final stage and was still undergoing rearrangement. Further changes are, indeed, observed when the materials are heated to substantially higher temperatures (§ 7).

An experiment in which $Nb_{22}O_{54}$ was oxidized at 500 °C and held at that temperature for only 2 minutes, showed that translocation preceded disproportionation also at higher temperatures. Typical micrographs (figure 17, plate 4) showed that the main effects resulted from cascades of A.W. shifts along [001] ('$Nb_{22}O_{54}$'), which created broad bands of (3×3) blocks, while the extent of disproportionation, to produce (5×3) blocks, remained relatively small.

In principle, the progress of the transformation could be quantified by counting the population of blocks of each kind, in a representative region of crystal. If n_3, n_4, n_5 are the numbers of (3×3), (4×3) and (5×3) blocks present, then at any stage in the transformation, from equation (1),

$$n_3 = n_{3,0} + n_5, \quad n_4 = n_{4,0} - 2n_5,$$

where $n_{3,0} = n_{4,0}$ are the numbers of blocks originally present in the '$Nb_{22}O_{54}$' structure ($n_{5,0} = 0$). If the transformation went to completion, the balance sheet for the conversion of blocks could be written as

$$3(\text{'}Nb_{22}O_{54}\text{'}) \rightarrow (Nb_{28}O_{70}) + 4(Nb_{10}O_{25}), \tag{2}$$

$$3\{(3 \times 3) + (4 \times 3)\} \rightarrow \{(4 \times 3) + (5 \times 3)\} + 4(3 \times 3). \tag{3}$$

After complete transformation, the final population of blocks, n_3^*, n_4^*, n_5^*, would be

$$n_4^* = n_5^* = \tfrac{1}{3}n_{3,0} = \tfrac{1}{3}(n_4 + 2n_5).$$

The degree of advancement of the reaction at any stage could thus be expressed as

$$X = 3n_5/(n_4+2n_5), \tag{4}$$

and the predicted population of (3×3) blocks as

$$n_3 = n_4+3n_5. \tag{5}$$

The problem lies in taking a census over a representative region, since the structures are inhomogeneous on a scale comparable with the area covered by any one micrograph. The (5×3) blocks do not undergo the same extensive translocation as do the (3×3) blocks; their population should afford a good index of the degree of advancement of the transformation in any region. Counts over regions containing 600–1000 blocks showed that X varied from one region (or crystal) to another, but showed a consistent trend with the annealing history of the sample (table 3). It will be noted that the transformation does not go fully to completion in terms of equation (2), even after high temperature annealing. This is due, in part, to the topological requirement that an excess of (4×3) blocks is needed to preserve structural continuity in the final domain structure.

TABLE 3. EXTENT OF TRANSFORMATION IN OXIDIZED $Nb_{22}O_{54}$

heat treatment	n_3	n_4	n_5	$X = 3n_5/(n_4+2n_5)$ (%)	percentage of possible (3×3) blocks found
320 °C, 10 days	677	660	126	41.6	65
325 °C, 10 days	75	672	129	41.4	—
500 °C, 2 min	425	328	43	31	93
	333	276	46	37	80
515 °C, 6 days	188	215	63	55	46
	408	463	120	51	50
900 °C, 5 min	311	268	107	69	53
		487	198	67	
900 °C, 12 min	428	281	122	70	60
		873	376	69	
950 °C, 30 min		759	332	70	
		637	242	65	

Numbers of (3×3) blocks invariably fell short of those predicted from equation (5). This could be, in part at least, a sampling problem, since the (3×3) blocks undergo extensive translocation and form domains that may not have been representatively included in the image

---

DESCRIPTION OF PLATES 7 AND 8

FIGURE 24. OX2E: two types of fault-bounding domains of H–Nb_2O_5. Upper left, lines of spliced or overlapping blocks; lower right, meandering arrays of turned blocks.

FIGURE 25. Oxidized $Nb_{53}O_{132}$: fully annealed OXF structure. Compare with figure 23.

FIGURE 28. Faults: details of areas of turned blocks in OX2E. At X and Y, the turned blocks eliminate one row of cation sites; to the right of Z, two cation rows are eliminated.

FIGURE 30. Faults: spliced blocks in the earliest stages of conversion of OX1C to OX2C.

FIGURE 32. Broad bands of spliced blocks in OX2E, corresponding to a very large mutual displacement of the structure above and below the fault.

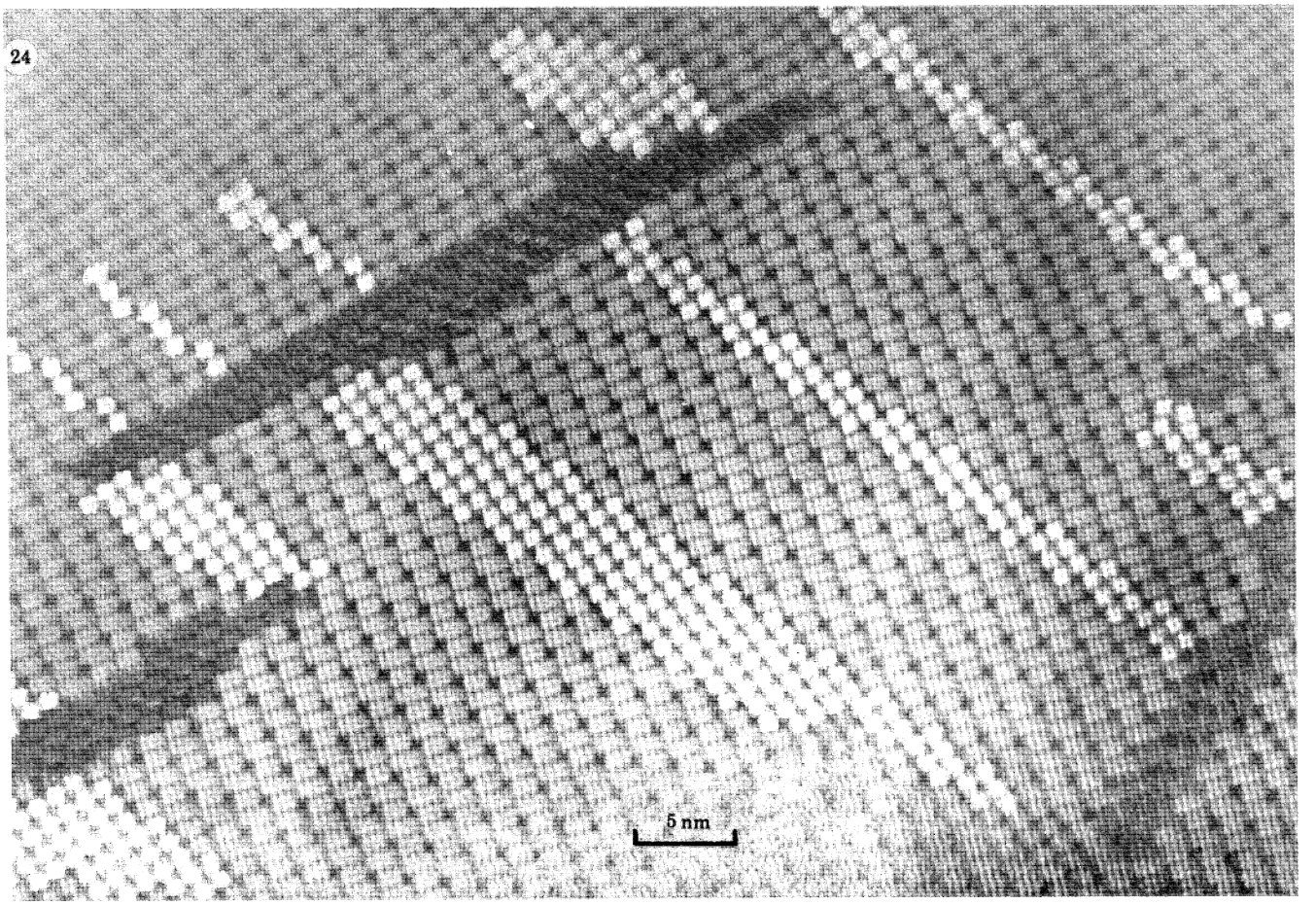

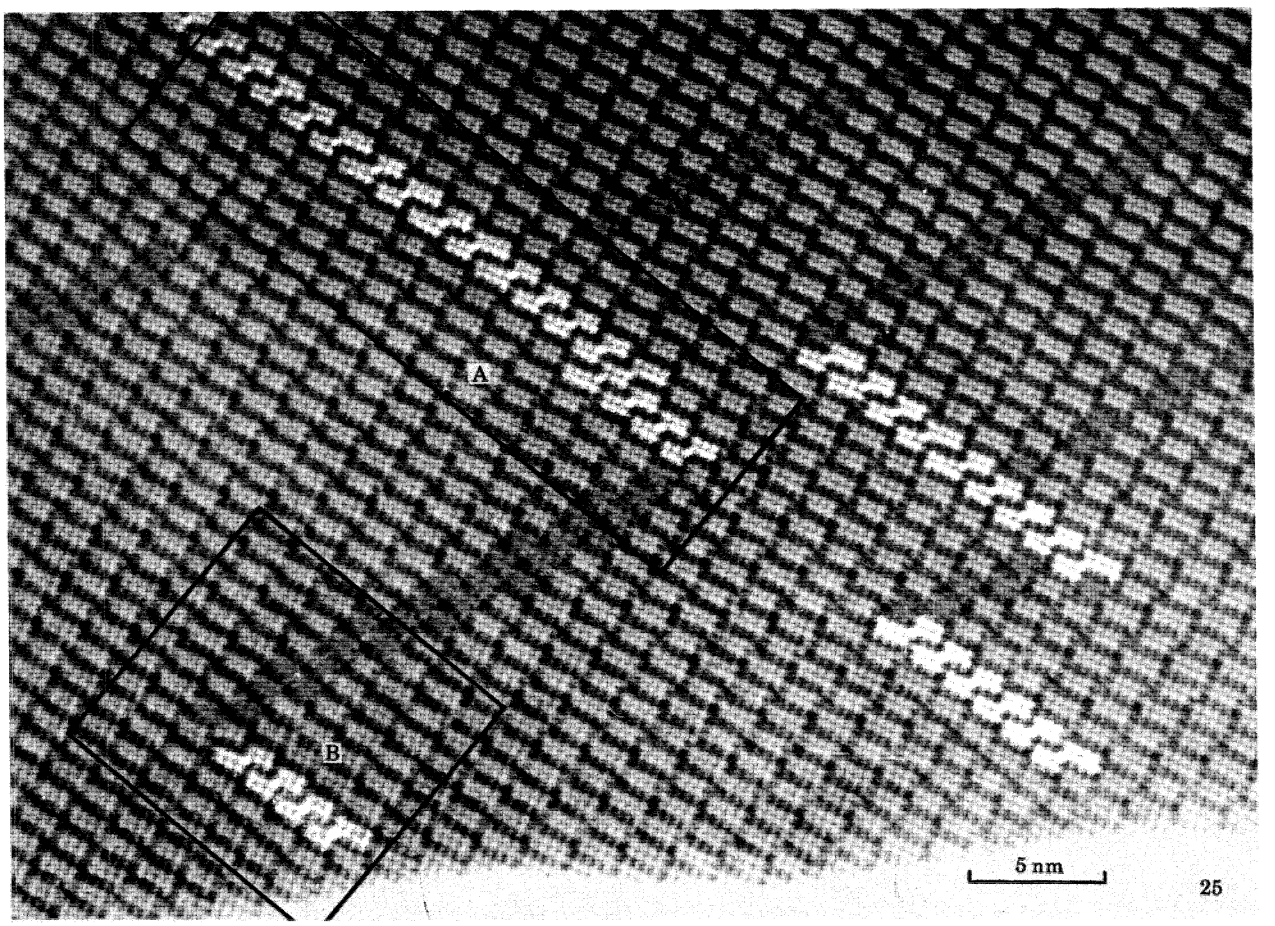

FIGURES 24 AND 25. For description see opposite.

(*Facing p.* 346)

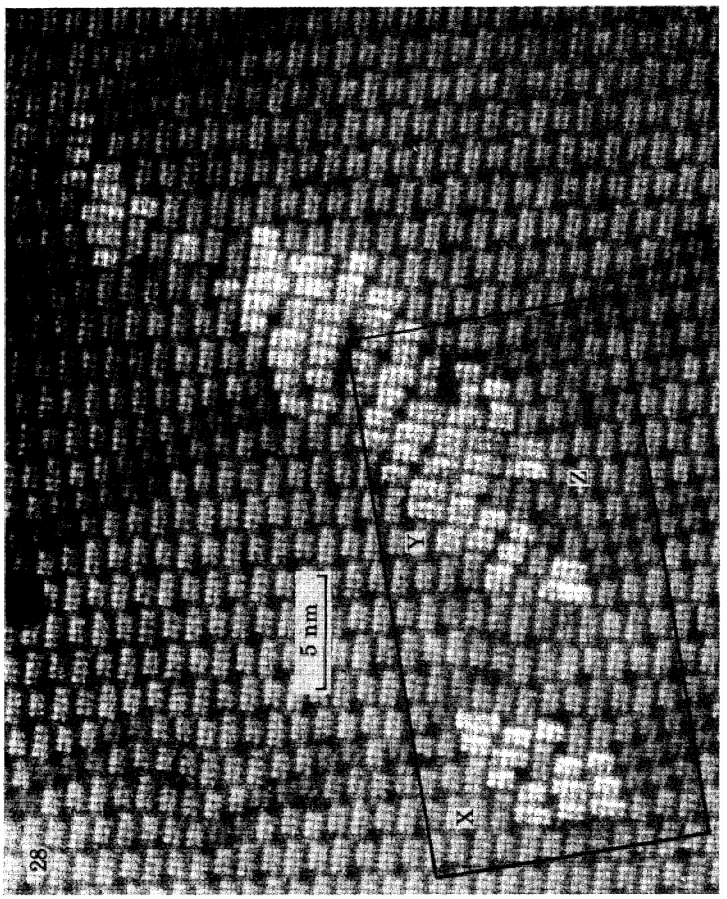

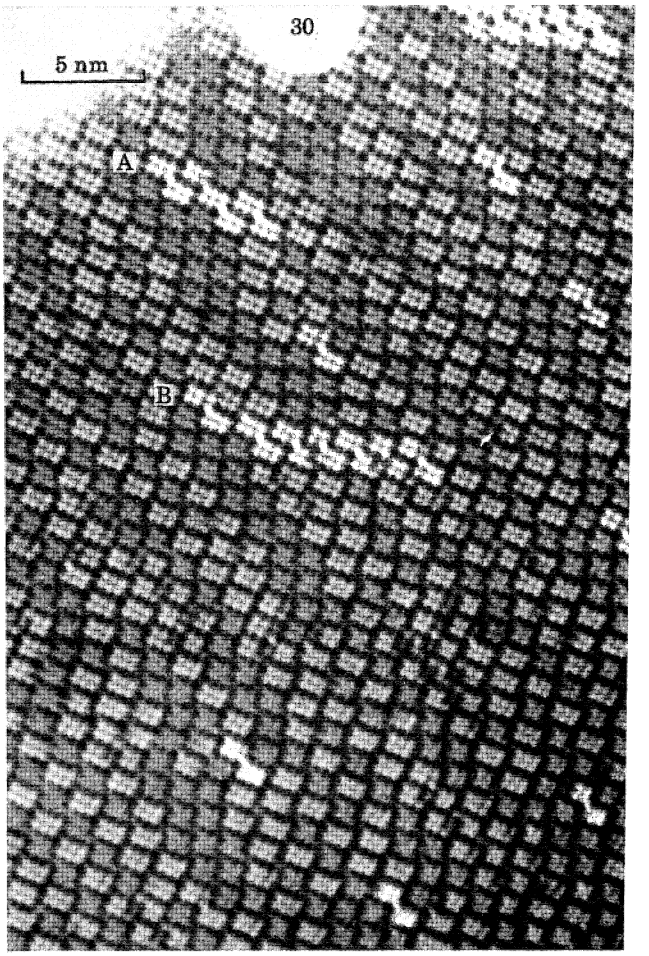

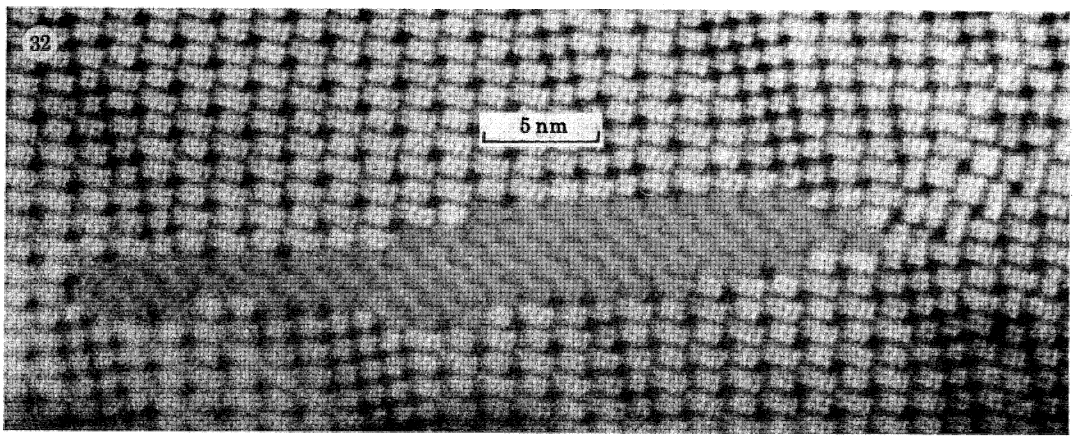

FIGURES 28, 30 AND 32. For description see p. 346.

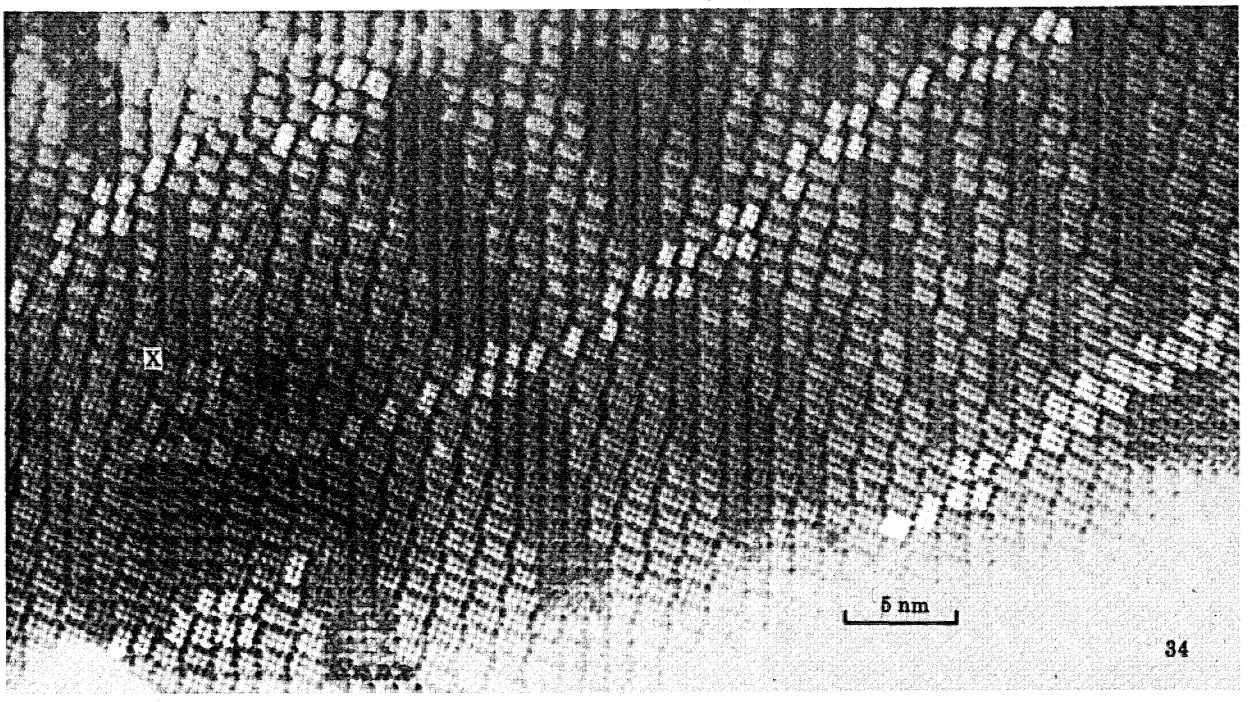

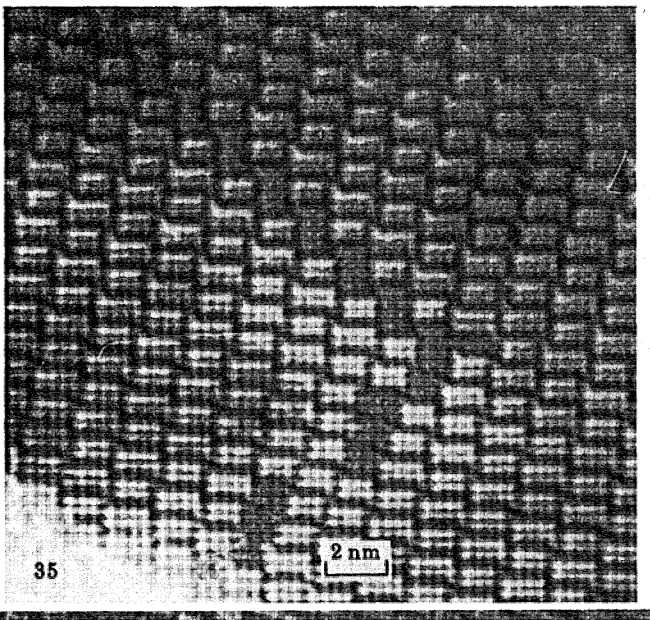

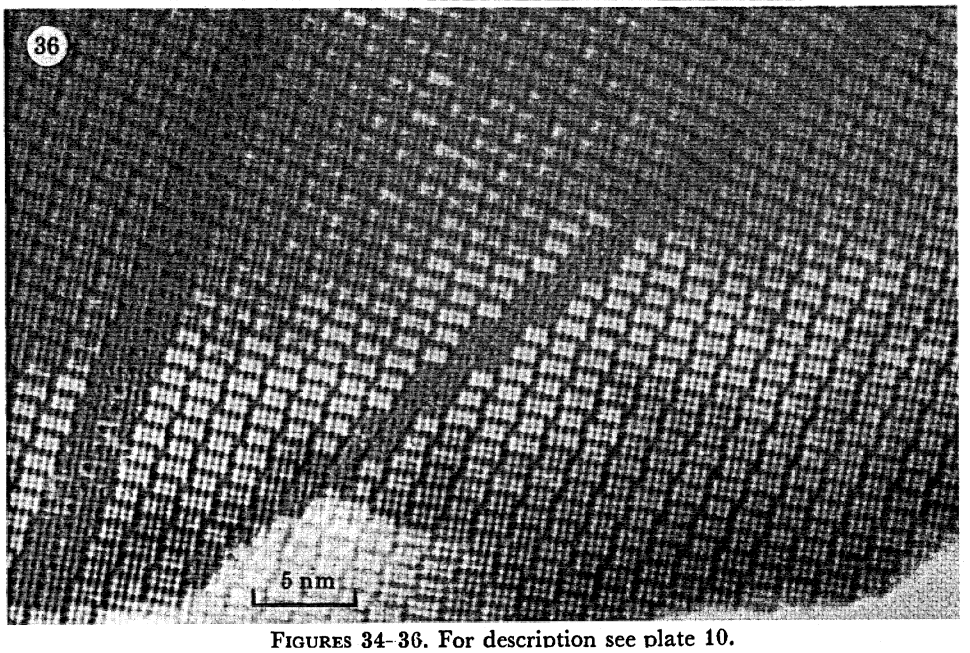

FIGURES 34–36. For description see plate 10.

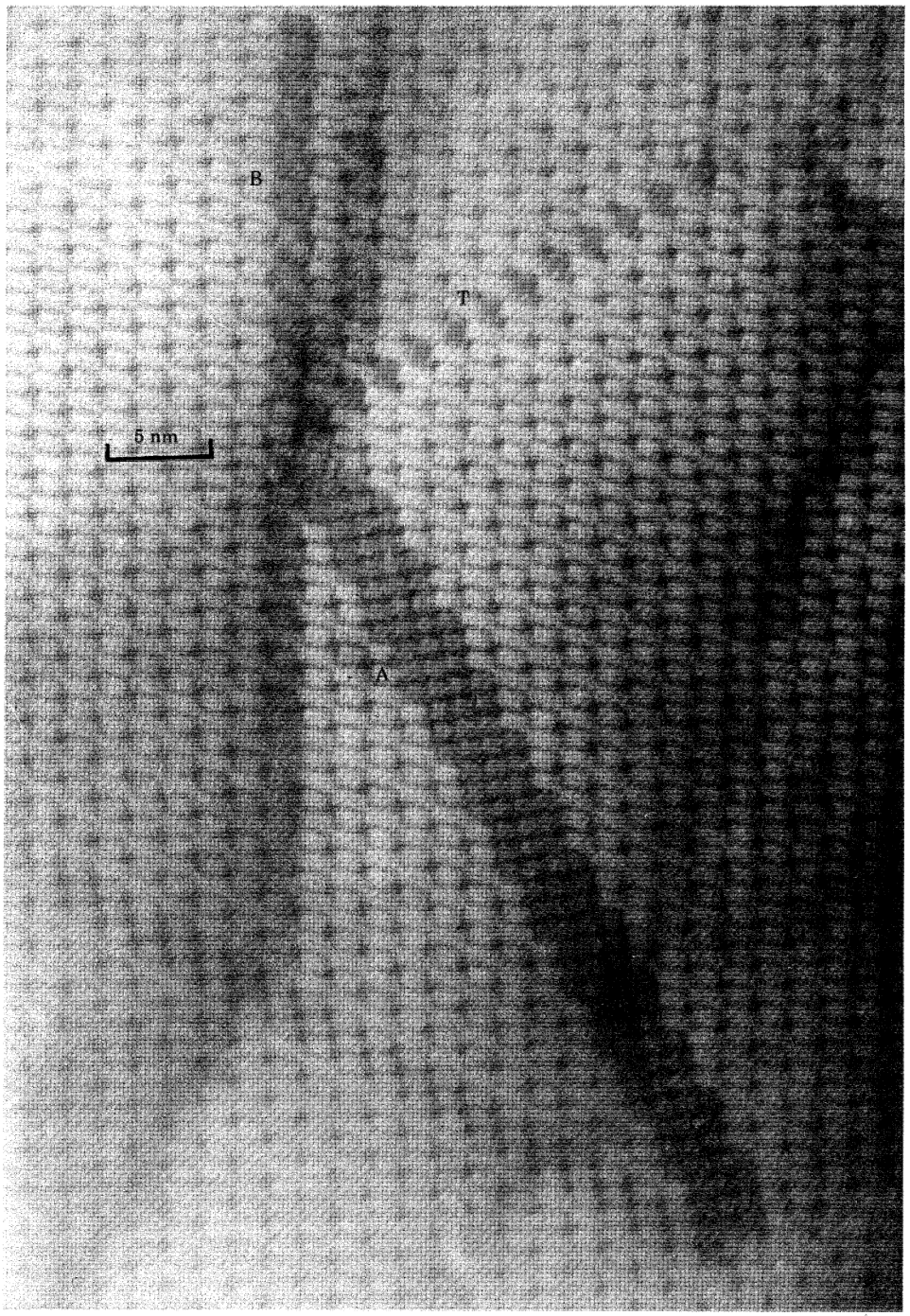

FIGURE 37. Final conversion of OX4C to H–Nb_2O_5: a residual domain of $Nb_{10}O_{25}$, A, ends at a line of twinned structure, T, and one file of a new structure for Nb_2O_5, B – a $(5 \times 3)_3$ block structure, $Nb_{46}O_{115}$.

DESCRIPTION OF PLATE 9

FIGURE 34. Structure of OX4C after annealing at a temperature (950 °C) above that at which direct conversion to H–Nb_2O_5 takes place.

FIGURE 35. Final conversion of OX4C to H–Nb_2O_5: remaining relic array of $Nb_{10}O_{25}$ and an antiphase boundary with the formal stoichiometry $Nb_{25}O_{62}$.

FIGURE 36. Final conversion of OX4C to H–Nb_2O_5: a relic array of $Nb_{10}O_{25}$ ending at a terminating twin band in the H–Nb_2O_5 structure. There is a dislocation at their junction.

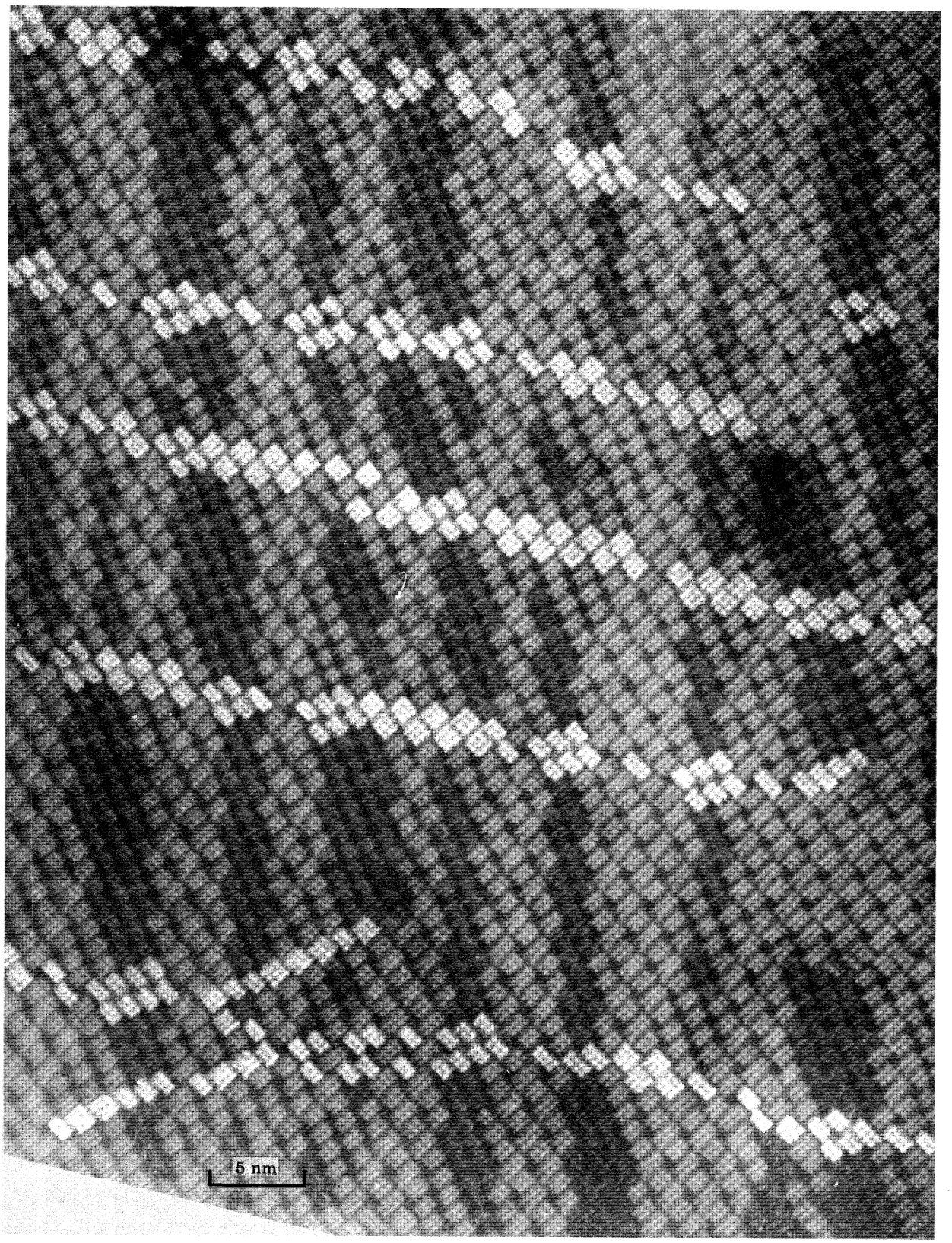

FIGURE 38. Heating above temperature of conversion to H–Nb_2O_5: OX4C after 90 s at 1000 °C. Fault walls largely transformed to N–Nb_2O_5 structure.

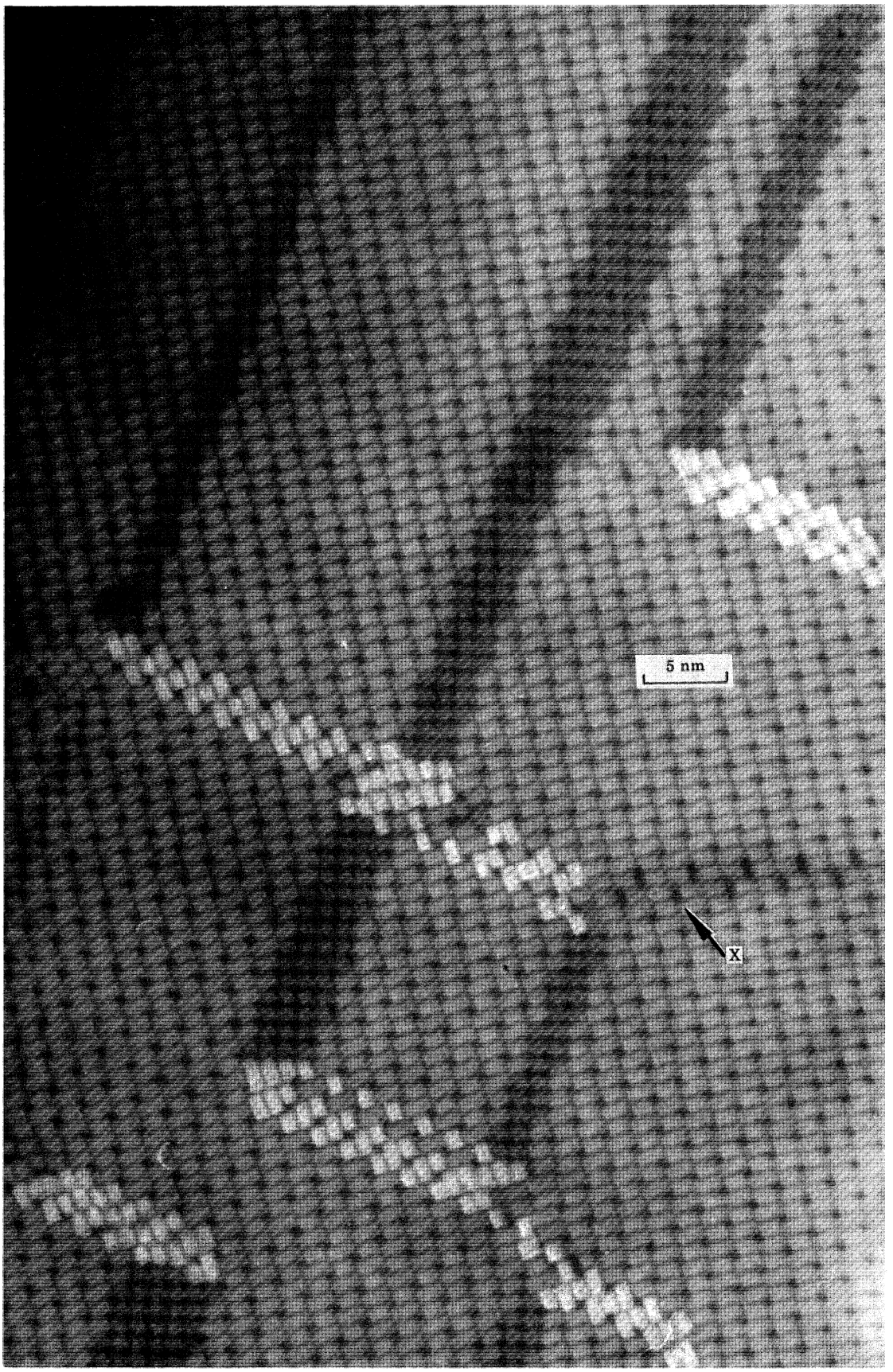

FIGURE 39. Heating above temperature of conversion to *H*–Nb_2O_5: OX2E after 205 s at 1000 °C.

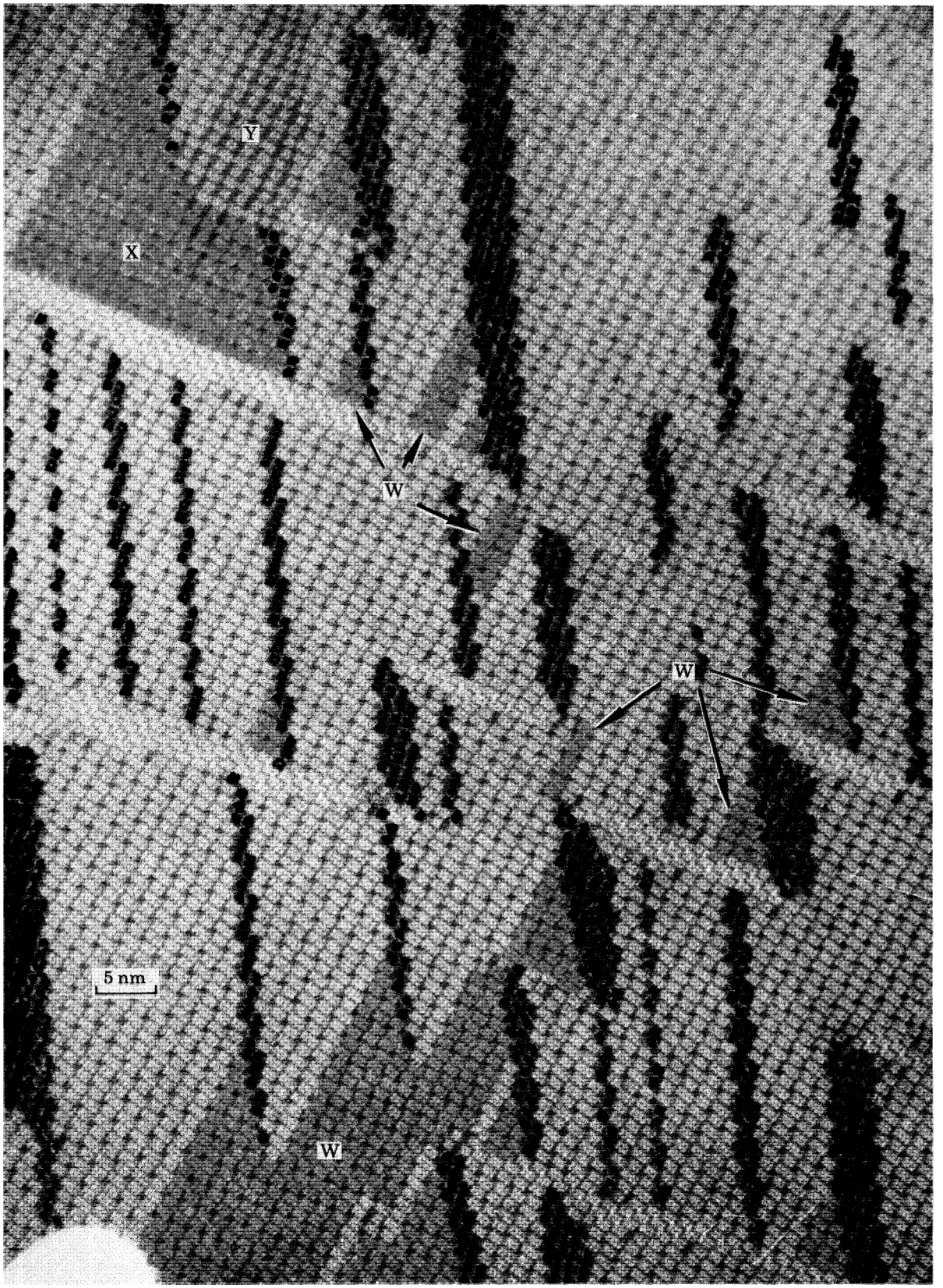

FIGURE 40. Heating above temperature of conversion to H–Nb_2O_5: OX2E after 180 s at 1120 °C. Areas marked W have retained or reverted to the $Nb_{25}O_{62}$ block structure. The similar area X abuts on a region Y where overlap contrast indicates frozen-in, uncompleted block rearrangements.

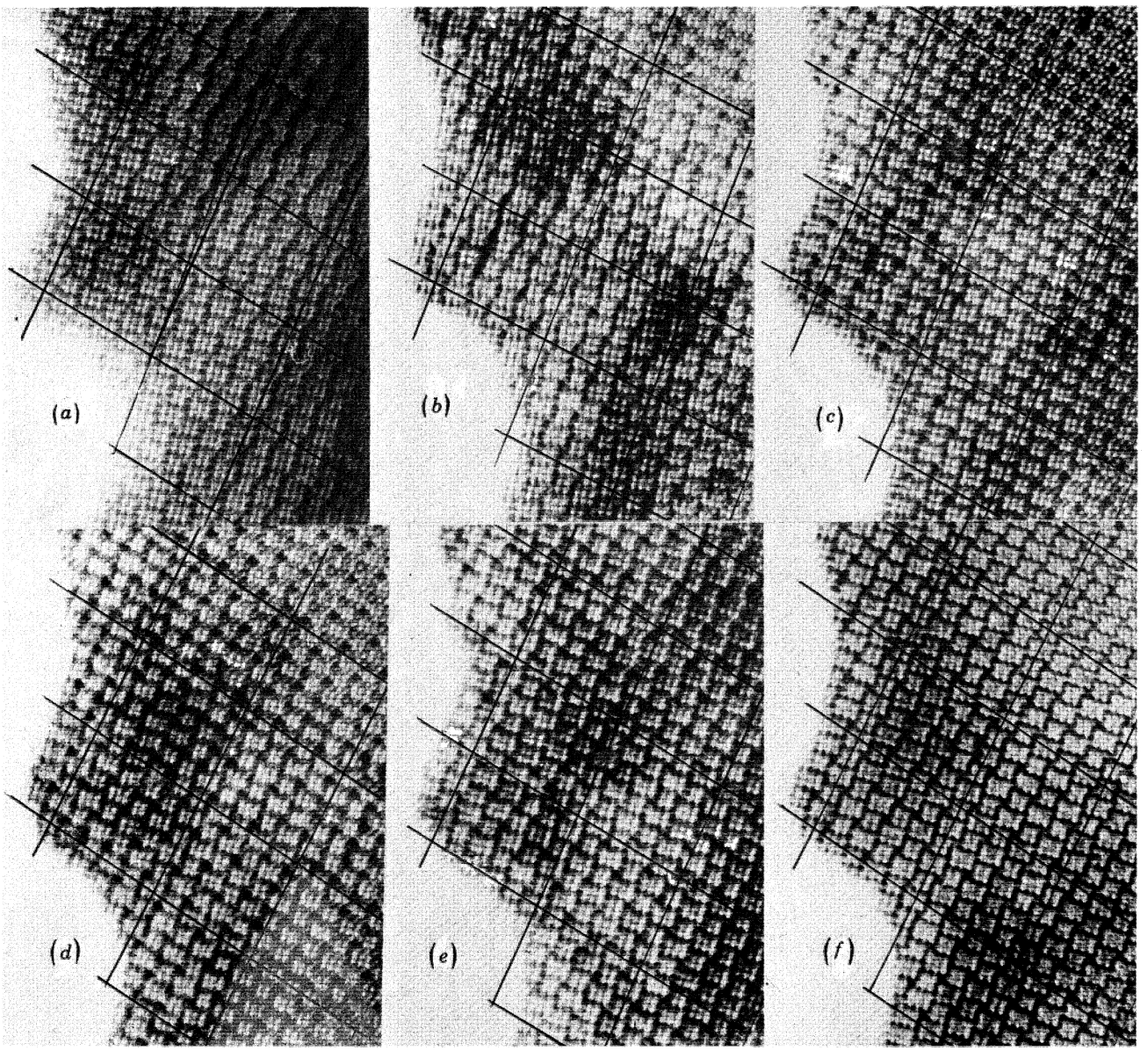

FIGURE 41. Beam stability: the same area of a crystal of OX1C after a series of intense irradiations in the electron microscope. Blocks found to undergo interchange of position at the next irradiation are enhanced in tone.

fields that were counted. The consistent shortfall suggests, however, that there is some undetected, parallel reaction that eliminates the metastable $Nb_{10}O_{25}$ structure, for example, by direct conversion to H–Nb_2O_5. Such a process does take place at higher temperatures, as is discussed in § 7.

(*c*) *Oxidized* $Nb_{25}O_{62}$: OX2E

Transformation of the cation-deficient OX1E structure ('$Nb_{25}O_{62}$' structure) into intergrown domains of H–Nb_2O_5 and $Nb_{10}O_{25}$ involves the same mechanism and the same, localized, primary reaction step as have been discussed above. It depends upon the disproportionation

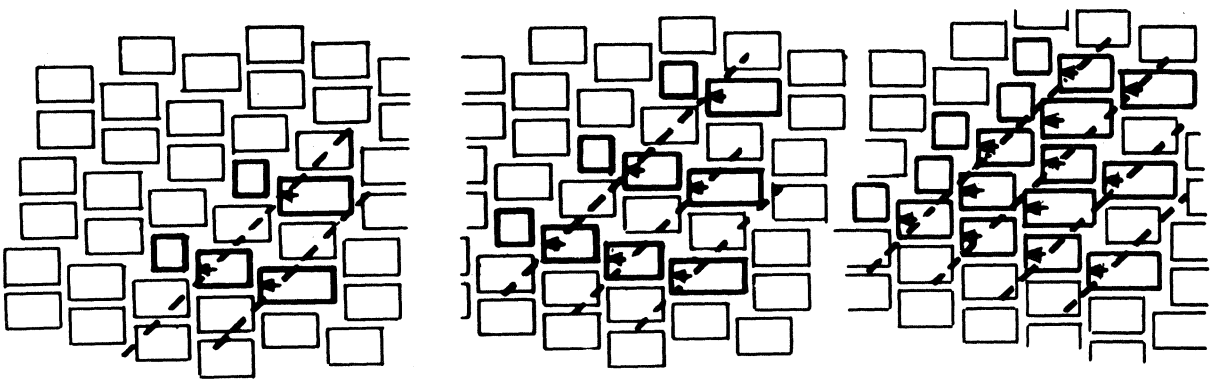

FIGURE 18. Propagation of A.W. displacements in the $Nb_{25}O_{62}$ structure.

reaction which, as noted earlier (§ 4.2), occasionally takes place during the oxidation reaction. The complementary pair of (5 × 3) and (3 × 3) blocks usually remains together, the product of a single A.W. shift, but occasionally the blocks are found separated, where a chain of A.W. shifts has run across several blocks. It is necessary for a unit A.W. shift to be propagated down a file of blocks to convert that file to the H–Nb_2O_5 structure; lateral growth, to form a domain of H–Nb_2O_5, requires an ordered sequence of repeated, cumulative A.W. shifts running along every row of blocks (figure 18). The complementary (3 × 3) blocks are thereby displaced sideways, building up an elongated array. It is probable that block disproportionation is the rate-determining factor, and at temperatures where this is fast, the succeeding block translocation steps can follow rapidly.

A.W. displacements across the longer edges of blocks may occur more readily in '$Nb_{25}O_{62}$', since they are occasionally observed in the OX1E material (figure 19, plate 5). They must involve a complex sequence of opposed displacements, and always create local faults, in the form of abnormal channels between blocks, 1.0 × 0.6 nm² in size, which probably eliminate tetrahedral cation sites.

While the earlier stages in the OX1E → OX2E conversion were not studied in detail, it is clear that transformation is again initiated at individual, random centres. The first step identified was the formation of small triangular nuclei of transformed structure. Figure 20 (plate 5) (from OX1E material heated at 750 °C for 3½ hours) shows two such nuclei, close together and just meeting, but apparently growing independently. Both of them, on the left, show an abrupt boundary between unchanged '$Nb_{25}O_{62}$' and a little domain of H–Nb_2O_5. It is evident that, in the lower nucleus, the complementary (3 × 3) blocks have been displaced to the right, to form a tapering array of $Nb_{10}O_{25}$ which, in turn, abuts on unchanged '$Nb_{25}O_{62}$'. The upper nucleus has grown larger, and the segregation of $Nb_{10}O_{25}$ structure, across its broad base, is not

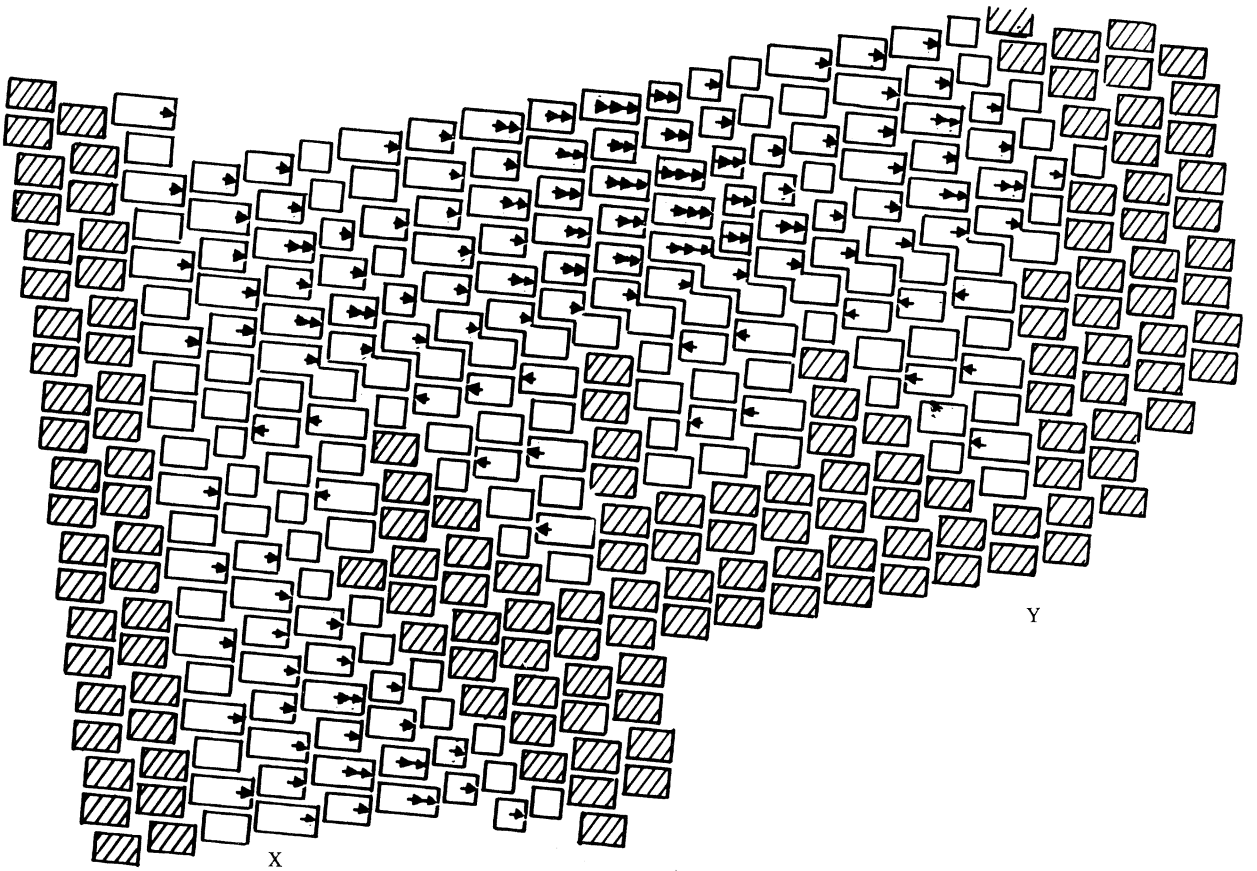

FIGURE 21. Displacement map showing processes involved in forming the nuclei of figure 20.

complete; it may indeed have been formed by the fusion of several original nuclei. At the base of the upper nucleus is a row of faulted structure, with blocks that appear to overlap or to be spliced together. Faults of this kind, which will be discussed more fully later (§ 6.2), occur very frequently in the OX2E material.

A displacement map of this region (figure 21) makes it clear how these features have been formed. In the lower nucleus, at X, l → r displacements have been propagated along every row of blocks, and upwards along each file, thus extending the transformed structure as a triangular domain. Repeated and cumulative A.W. shifts, along each row, are needed to broaden the microdomain of *H*–Nb_2O_5, but at no place in the region mapped have more than three successive shifts taken place. Where the same number of A.W. shifts have passed across every block, the effect has been to leave a small slice of the '$Nb_{25}O_{62}$' structure bodily displaced, as in the lower nucleus of figure 20. On the right of the region mapped, at Y, below the line of fault structure, a new set of r → l displacements is beginning to create new microdomains of *H*–Nb_2O_5 structure; the process is evidently being propagated downwards along each file. A triangular domain of *H*–Nb_2O_5 is necessarily associated with a tapering array of $Nb_{10}O_{25}$. If, however (as in figure 21), transformation is propagated in opposite senses in neighbouring nuclei, the net effect will be to build up parallel-sided domains of $Nb_{10}O_{25}$ such as are, in general, found in the fully developed OX2E structure.

These transformation nuclei appear to be initiated at irregular intervals of about 8–15 nm, as can be seen from figure 22 (plate 6), where a chain of nucleation events has taken place along

a particular direction through the structure. To the right of this, at Z, is a region of overlap contrast, which strongly suggests that a fresh set of cooperative A.W. shifts, representing another nucleation event, have been frozen in at an early stage in their development. As the triangular nuclei spread out, they impinge and join up, to form wide, irregularly shaped domains of *H*-Nb_2O_5 structure, separated by narrow elongated domains of $Nb_{10}O_{25}$ (figure 23, plate 6); these are usually 8–10 nm long and only a few (3×3) blocks in width. Adjacent domains of *H*-Nb_2O_5 are usually out of phase in their stacking, as is likely if they originated from independent nucleation events. Variation in the size of the domains reflects the area available for the unrestricted growth of each nucleus. The $Nb_{10}O_{25}$ domains are offset from one another, rather than forming nearly continuous walls, as in OX4C, but are usually linked through trailers of turned blocks, or through rows – often multiple – of apparently overlapping or spliced blocks (figure 24, plate 7). These faults correspond to the walls of turned blocks in OX4C. Their origin and location depends upon the random character of nucleation, but they have an important function that is discussed in § 6.

Transformation of '$Nb_{25}O_{62}$' could be represented as

$$3(\text{'}Nb_{25}O_{62}\text{'}) \rightarrow 2(Nb_{28}O_{70}) + 2(Nb_{10}O_{25}), \qquad (6)$$

$$3\{(4 \times 3) + (4 \times 3)\} \rightarrow 2\{(5 \times 3) + (4 \times 3)\} + 2(3 \times 3).$$

Hence (3×3) blocks and elements of the *H*-Nb_2O_5 structure should be present in equal numbers at every stage. While this holds as long as the growing nuclei abut on unchanged '$Nb_{25}O_{62}$' structure, the available evidence does not rule out the possibility that, as they merge, some $Nb_{10}O_{25}$ structure may be eliminated by a parallel direct conversion to *H*-Nb_2O_5. Many of the areas of crystal that were examined were deficient in (3×3) blocks but, for other crystals, detailed population accounts were in agreement with (6).

(*d*) *Oxidized* $Nb_{53}O_{132}$: OXF

No observations were made on the early stages of the transformation of '$Nb_{53}O_{132}$' ($Nb_{52.8}O_{132}$), but the end product of annealing at 700 °C (OXF of Hibst & Gruehn) was very similar in structure to the OX2E material. There is every reason to suppose that, *mutatis mutandis*, nucleation and propagation followed a similar path. There were fewer and narrower arrays of $Nb_{10}O_{25}$ in OXF (figure 25, plate 7). The block disproportionation reaction can be expressed as

$$3(\text{'}Nb_{53}O_{132}\text{'}) \rightarrow 5(Nb_{28}O_{70}) + 2(Nb_{10}O_{25}). \qquad (7)$$

As in the OX2E material, the arrays of $Nb_{10}O_{25}$ were joined by rows of apparently overlapping blocks, but lines of turned-around blocks were more rarely observed. Figure 26 maps the displacements that must have taken place to generate the structure, as observed, within the rectangular areas A, B of figure 25.

6. Faulted structures and extended defects

From the foregoing discussion of the structures of the various materials, it is evident that one simple, local mechanism effects the observed changes, and that transformation starts at numerous, roughly equidistant, but randomly situated centres. As transformation spreads out from these, the c.s. interfaces are so displaced that the structure in one part can get out of step with that around an adjacent centre. If coherence is to be preserved and strain minimized, some kind of faulted structure has to be formed where the effects impinge. At low temperatures,

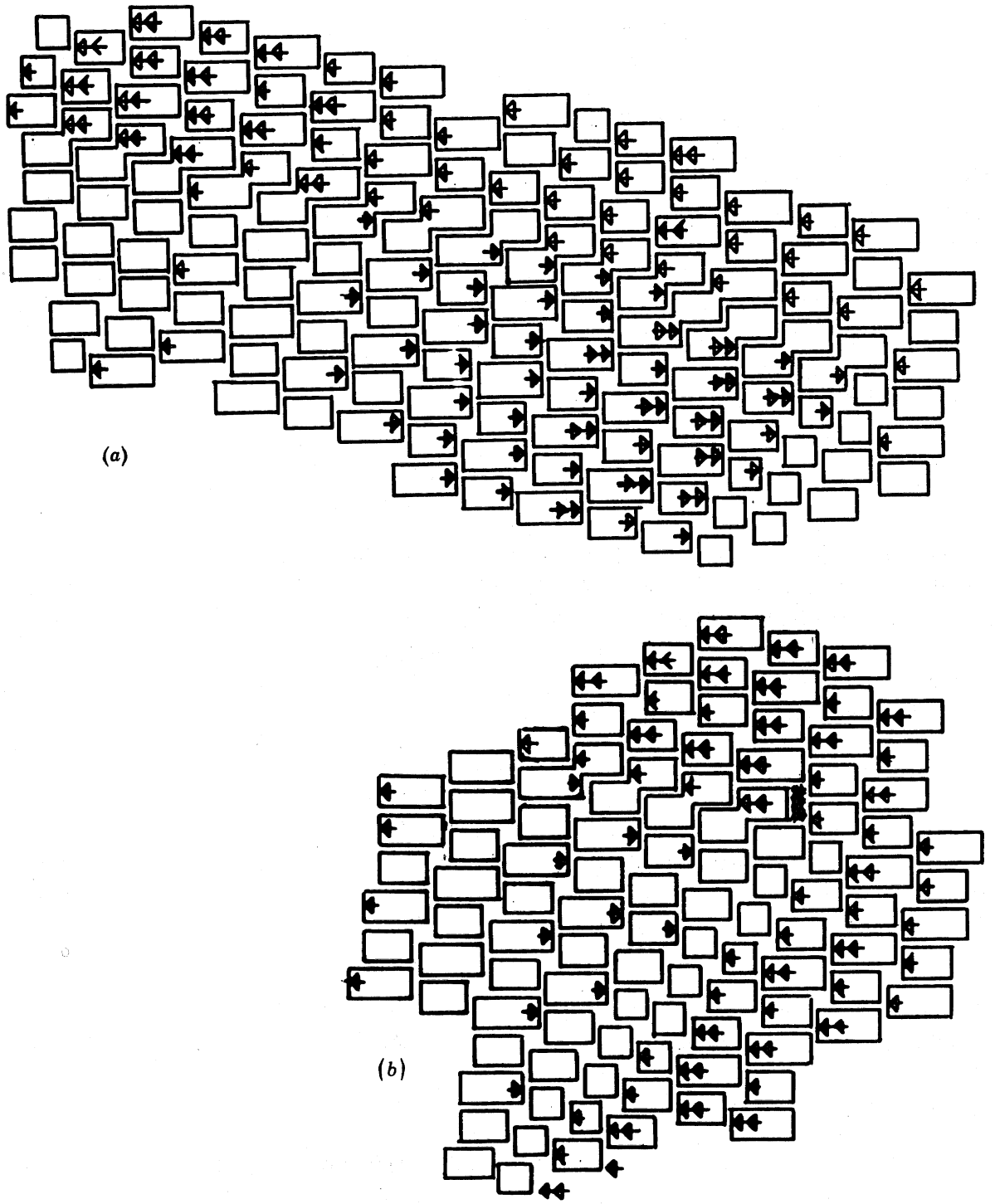

FIGURE 26. Displacement map of framed areas A, B in figure 25, showing processes involved in producing the observed structure from the original $Nb_{53}O_{132}$ structure.

any kind of far-reaching, cooperative reorganization, extending over many blocks, is improbable, but it can become important at higher temperatures. The extended defects formed are more than a structural compromise; they have an essential part in the redistribution of atoms over the crystallographic sites.

(*a*) *Rows of narrow blocks and turned-around blocks*

It has been shown that a high density of faults is inevitable as the oxidized '$Nb_{22}O_{54}$' structure (OX1C) undergoes rearrangement and passes through the disordered stage (OX2C). Where two expanding domains impinge along (100) ('$Nb_{22}O_{54}$'), they produce the rows of blocks only two octahedra wide. Where two adjacent files of blocks undergo displacements that are topologically incompatible, the rows of narrow blocks step sideways across several rows, leaving a boundary that is itself an extended defect, with c.s. interfaces of abnormal configuration between the blocks. These can be seen in the micrographs (e.g. figure 10; displacement map figure 12). Such defects frequently impose distortions and strain. The formation of a row of narrow blocks does not change the number of blocks, or of c.s. interfaces, in any file, so that it does not affect the alternation of cation levels between $y = 0$ and $y = \frac{1}{2}$.

At higher annealing temperatures, as the transformation OX2C → OX3C → OX4C proceeds, the rows of narrow blocks disappear and are replaced by walls of turned-around blocks, including some of abnormal dimensions (e.g. (6×3) and (7×3) blocks), and by the (4×4) elements of the *N*–Nb_2O_5 structure. This is evidently a more stable configuration, which persists up to the final stage of recrystallization. Formation of these walls of turned blocks must involve a complex and cooperative set of A.W. shifts along both *x*- and *z*-directions, since it changes the orientation of the faults and, in so doing, the length of uninterrupted files of blocks. Whereas the broken lines of narrow blocks have their segments lying on (100)*('$Nb_{22}O_{54}$'), the continuous walls that replace them follow an orientation that maximizes their compatibility with adjacent domains of *H*–Nb_2O_5 structure. They vary in width and frequently follow a meandering course, but their general trend is invariably along the permitted twinning plane of *H*–Nb_2O_5.

If turned-around blocks, (3×4) or (3×5) octahedra in cross section, are formed by eliminating narrow blocks, the process could be represented schematically by the following equations (8*a*) or (8*b*); these are in agreement with the A.W. displacements directly mapped:

$$(3 \times 3) \text{ block} + (3 \times 2) \text{ block} \rightarrow (3 \times 5) \text{ block}, \tag{8a}$$

$$2(3 \times 3) \text{ blocks} + (3 \times 2) \text{ block} \rightarrow 2(3 \times 4) \text{ blocks}. \tag{8b}$$

These processes are not conservative in the number of c.s. interfaces, and therefore break the regular alternation of cation levels along the files that contain the turned blocks, in the same way as a dislocation (Hutchison *et al.* 1977). In real space, the octahedral coordination groups have to be edge-linked at the interface between blocks, and, in a formal sense, this could be achieved by tilting the layers of atoms in the turned blocks; the implication is that the structure is locally warped. A finite wall of turned blocks, ending within the crystal, necessarily terminates at a dislocation, but by extending the fault wall right across the crystal, the dislocation climbs out, leaving a relaxed structure that has undergone a virtual slip of $\frac{1}{2}a_R \langle 010 \rangle_R$ across the fault wall. Release of strain energy is thus a driving force in the elimination of narrow blocks.

These extended faults also impose dimensional misfits. In principle, block structures are modular, based on the unit $\frac{1}{2}a_R \langle 100 \rangle_R$, or *ca.* 0.2 nm. If the structure around any segment of

a line of narrow blocks, as observed, is mapped on that basis, it can be seen that the real structure involves distortions, the interatomic distances being stretched or squeezed. Figure 27 maps such a segment, between two side steps. The upper row A, of eight blocks, extends over a nominal 8.6 nm; the lower row, B, with seven blocks, extends over a nominal 8.8 nm. It also incorporates one more row of oxygen atoms than row A. Between A and B is the row of narrow blocks and in the crystal the structure closes coherently around this segment. The micrograph from which the structure was mapped shows that there are detectable distortions close to the fault, but these attenuate rapidly in the surrounding structure. A row of blocks two octahedra wide does not ideally fill the space between the rows A and B, and in several places the micrograph showed ill resolved, probably disordered structure.

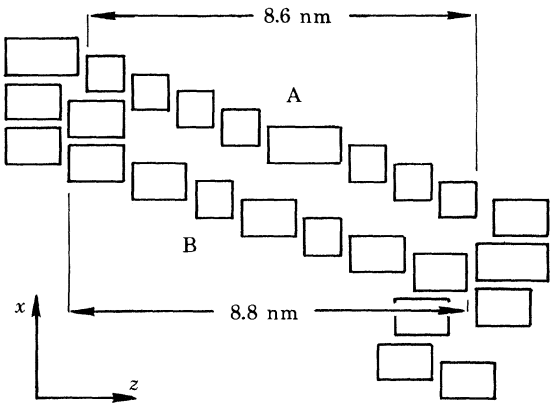

FIGURE 27. Faults: dimensional misfit around a row of narrow blocks.

A systematic dimensional change is involved in the elimination of the narrow blocks. Processes (8*a*) and (8*b*) represent the replacement of edge sharing by vertex sharing between octahedra at the original c.s. interface, and this expands the structure by 0.2 nm. Modular mapping around sites where turned blocks have been formed shows there is, nevertheless, a net contraction of 0.2 nm; the structure was originally stretched around the narrow blocks, and their replacement releases part of the strain.

The situation is rather different in the transformation of $Nb_{25}O_{62}$, OX1E → OX2E. There is a less radical reorganization of block cross sections, fewer new tetrahedral sites are created and there is, consequently, less change in the profile of the rows of blocks. As a result, out-of-step relations between adjacent domains do not develop to the same extent as in the transformation OX1C → OX2C → OX3C → OX4C. The process also takes place at higher temperatures, and no rows of narrow blocks are formed. It is not always possible, however, to effect a fault-free junction between adjacent, growing domains. This appears to be the origin of the sometimes extensive areas of turned-around blocks that link the arrays of $Nb_{10}O_{25}$ structure; these demarcate the boundaries of individual domains of transformed structure.

This recurring feature of the OX2E structure is exemplified in figure 28 (plate 8), illustrating an area that lends itself to further analysis. At X, a short, isolated area of turned blocks runs between two arrays of $Nb_{10}O_{25}$; at Y, another longer and broader band of turned blocks runs across the termination of several $Nb_{10}O_{25}$ arrays. Figure 29, a map of the area enclosed by the rectangle, shows that the turned blocks at X have been formed where a domain propagated by l → r displacements impinges on a domain formed by r → l shifts. The topological incompati-

bility has been resolved by a complex set of displacements of atom rows to generate the turned blocks; such a high density of interlocked shifts suggests that the local reorganization may take place by a cooperative and catastrophic process, rather than through a progressive sequence of unit shifts. However, apart from a fault at F, a channel 0.8×0.6 nm^2 replacing a tetrahedral site, region X shows no dimensional misfits or mismatch of cation levels. Along file A, two (3×5) blocks and one (3×4) block replace five (4×3) blocks; along the files B, one (3×5)

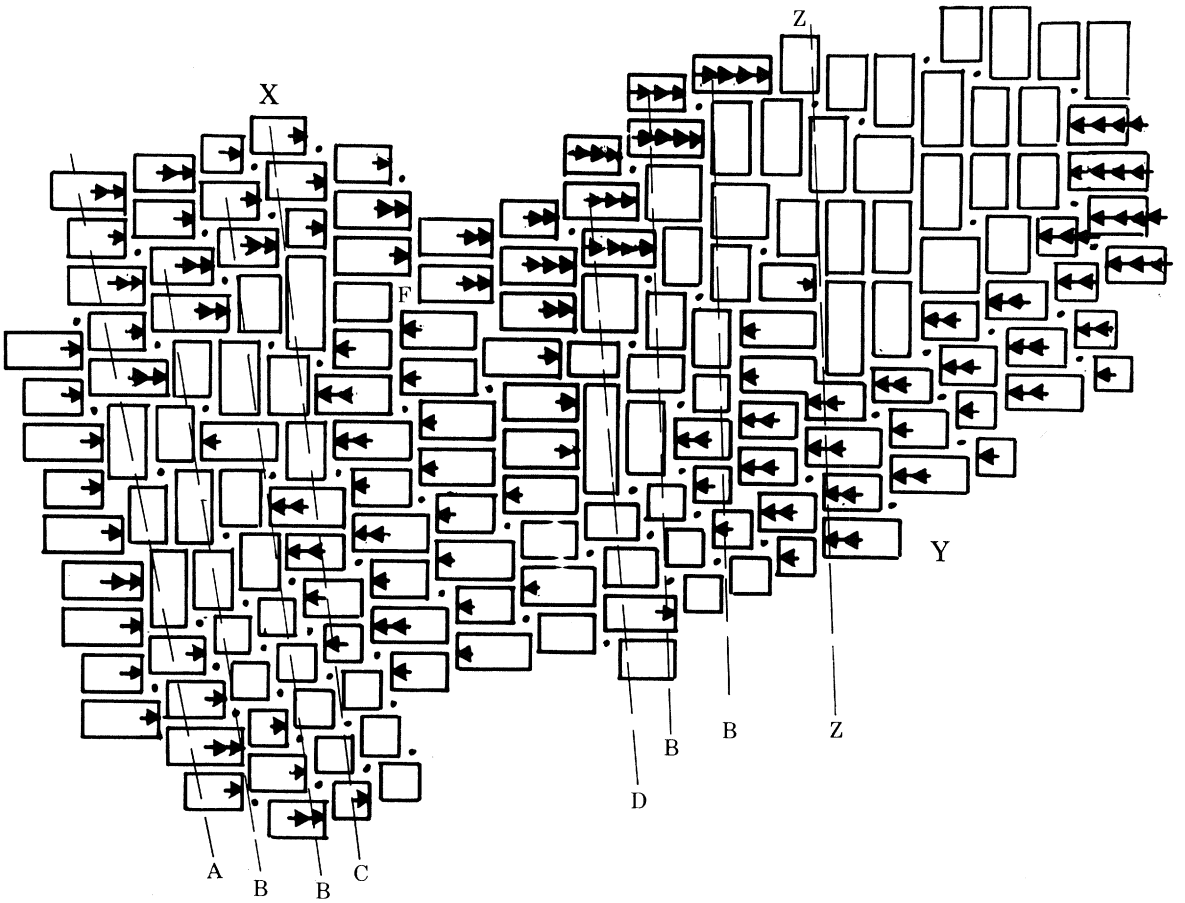

FIGURE 29. Displacement map of the framed area in figure 28.

block and three (3×4) blocks replace six (4×3) blocks; in file C, one (3×6) block and two (3×4) blocks replace five (4×3) blocks; in file D, one (3×7) block and one (4×4) block replace four (4×3) blocks. In each case, an even number of c.s. interfaces is eliminated and the sequence of cation levels is preserved. These replacements leave the number of rows of oxygen atoms, and hence the dimensions, unchanged, but one row of cations has been omitted from every file. Complex as the pattern of displacements was, no niobium atom needed to execute more than a unit jump into a next neighbour site. In the longer trail of turned blocks at Y, analysis shows that one row of cations was eliminated from all files to the left of Z, and two rows of cations from the area to the right of Z. The *H*–Nb_2O_5 matrix structure is not unbroken and fault free between the two areas of turned blocks; there are abnormalities in the stacking sequence and, in several places, tetrahedral sites are replaced by tunnels 0.8×0.6 nm^2 in section.

Areas of turned blocks that involve the elimination of cation sites are occasionally linked together by twin bands in the *H*–Nb_2O_5 structure. These twin bands serve to compensate for the configurational misfit between adjacent domains, without the elimination of more cation sites.

(*b*) *Overlapping or spliced blocks*

Faults of this kind are found at all stages of the transformation. They are occasionally to be seen in the very earliest stages of the transformation of the OX1C material, but are infrequent in the fully transformed OX4C. They are prominent features in the transformed, oxidized $Nb_{25}O_{62}$ (OX2E) and $Nb_{53}O_{132}$ (OXF) materials; in OXF they tend to recur at quasi-regular intervals of 20–25 nm.

Their nature and origin is most clearly seen by analysing their formation during the earliest stages of the OX1C → OX2C transformation. Figure 30 (plate 8) shows isolated units and

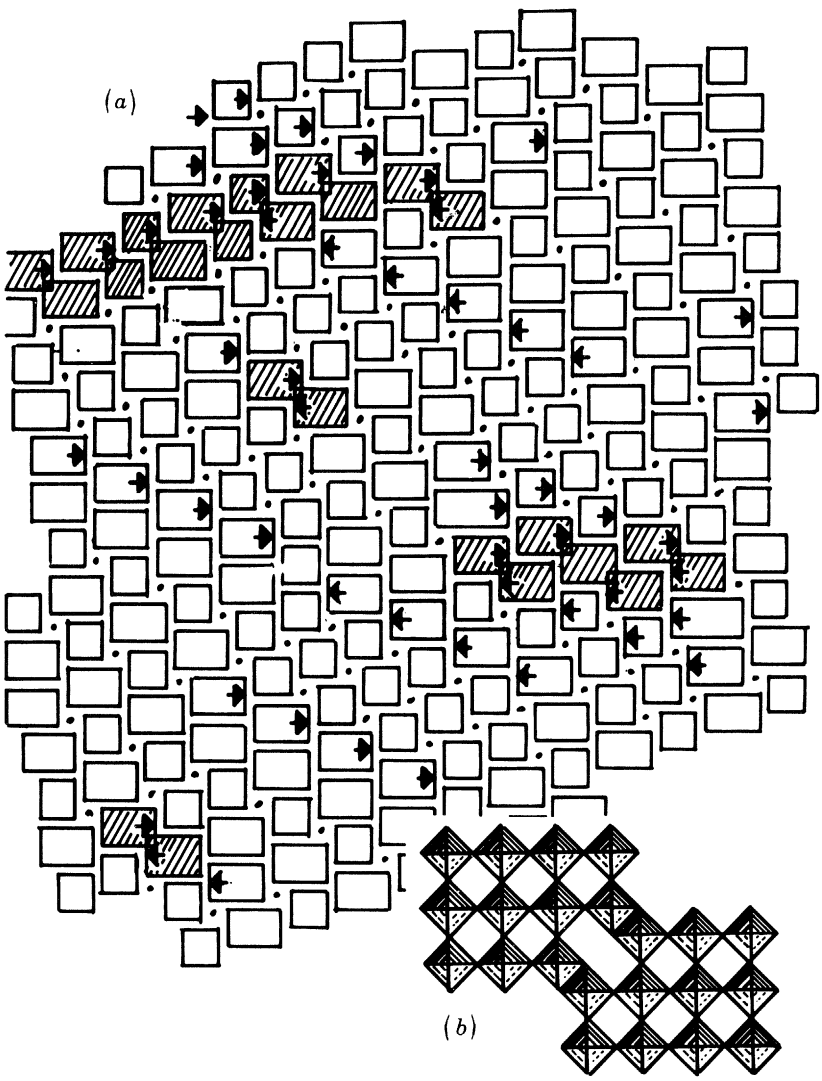

FIGURE 31. (*a*) Displacement map of the upper part of figure 30. (*b*) Structure of the 'spliced' or 'overlapping' blocks.

small groups of them, and the A.W. shifts needed to create the observed configuration are mapped in figure 31*a*. At A and B, a cascade of l → r shifts in one (100) ('$Nb_{22}O_{54}$') row impinges on a cascade of r → l shifts in the next row below it. The result, in these cases, has not been to leave a fault strip, with blocks of abnormal width, but to form a structure element that fits without distortion into the surrounding network, with a structure image that is characterized by a prominent, apparently diagonal, streak of light contrast where the blocks 'overlap'. This light contrast feature indicates that there is a channel or tunnel through the structure, and there can be no doubt that the structure is as represented in figure 31*b*. 'Spliced' blocks of this kind have been observed previously (Hutchison & Lincoln 1973). The unit formed by splicing two (4 × 3) blocks (i.e. $2 \times Nb_{12}O_{29}$) in this way would have the composition $Nb_{22}O_{52}$. Thus every spliced block represents the localization of two of the vacant cation sites in the crystal. Since the structure images show no sign of overlap contrast, the structure as seen in projection must run right through the crystal flake imaged. In effect, vacant cation sites have been collected and ordered into a wall of new structure.

Rows of spliced blocks fill the same role in the other materials. Thus it can be seen in figures 25 and 26 how long rows of spliced blocks have been produced in OXF, by displacements of opposite sense, in adjacent rows of blocks. These long arrays of spliced blocks represent the localization of a considerable number of vacant cation sites. Turned blocks have been found relatively infrequently in the OXF structure, so that few rows of cation sites are eliminated by that means.

One probable origin of long arrays of spliced blocks in OXF and OX2E is thus explicable. As can be seen in the lower portion of figure 26*a*, transformation spreads out on either side of some nodal file of blocks, by oppositely directed A.W. shifts. In OX2E, the original sharp boundary of a triangular nucleating event constitutes such a node. If the fortuitous nature of nucleation gives rise to nodes that are mutually separated in adjacent domains, arrays of spliced blocks can be formed where they meet. The array seen in figure 20 is of this kind.

Long arrays of spliced blocks do not necessarily originate in the cascades of A.W. shifts that produce the nuclei of the transformed structure. Triplets of spliced blocks can undoubtedly be formed in that way (see figures 30, 31), but numerous micrographs of OX2E, in particular, show wide banks of blocks spliced together, corresponding to a very large apparent displacement of one section of the structure with respect to the adjoining domain (figure 32, plate 8). We suspect that these have a different origin that reflects the inherent mobility of the structure at high temperatures. In all the end-product-domain structures OX4C, OX2E and OXF, any translocation of blocks would require the transmission of an A.W. shift along a row of blocks. If such a cascade of displacements occurred cooperatively, across a slab of structure, a (3 × 3) block could be transferred from one $Nb_{10}O_{25}$ array to another, in what is essentially a single act. The residual, visible consequences of this would be to introduce a sigmoid kink into the files of blocks and an abrupt change in the width of the $Nb_{10}O_{25}$ arrays on either side of the matrix slab affected.

Structures that have frequently been found in OX2E, after short periods of heating at high temperatures, are in accord with this scheme. They consist of long multiple arrays of spliced blocks, which separate domains in which the observed structure can be rationally related to the original '$Nb_{25}O_{62}$' structure, through the operation of a few A.W. shifts. These domains are mutually displaced by a large amount across the arrays of spliced blocks, and associated with those arrays are detached, single strings of $Nb_{10}O_{25}$ and abrupt changes in the breadth of larger $Nb_{10}O_{25}$ domains. Figure 33 maps part of a fault of this kind, showing the displacements

that produced the observed configuration from the original '$Nb_{25}O_{62}$' structure, and the drastic shearing localized across the rows of spliced blocks. On the left, where blocks are spliced in triplets, the upper part is displaced 1.2 nm (three A.W. shifts) to the right, with respect to the lower. On the right side, this shear is augmented by a cascade of r → l shifts in the lower part, to produce blocks spliced in groups of four, giving a total relative displacement of 1.6 nm. Associated with this cascade is the formation of a file of *H*–Nb_2O_5 structure at X and the transfer of (3 × 3) blocks from r → l, to a domain of $Nb_{10}O_{25}$ at Y. Across the bank of spliced blocks, the c.s. planes and files of blocks are sharply kinked. This configuration, frequently to be found in the micrographs, is suggestive evidence that shearing displacements between different domains of matrix structure take place after the original domain structure has been established, to modify and relocate the arrays of $Nb_{10}O_{25}$.

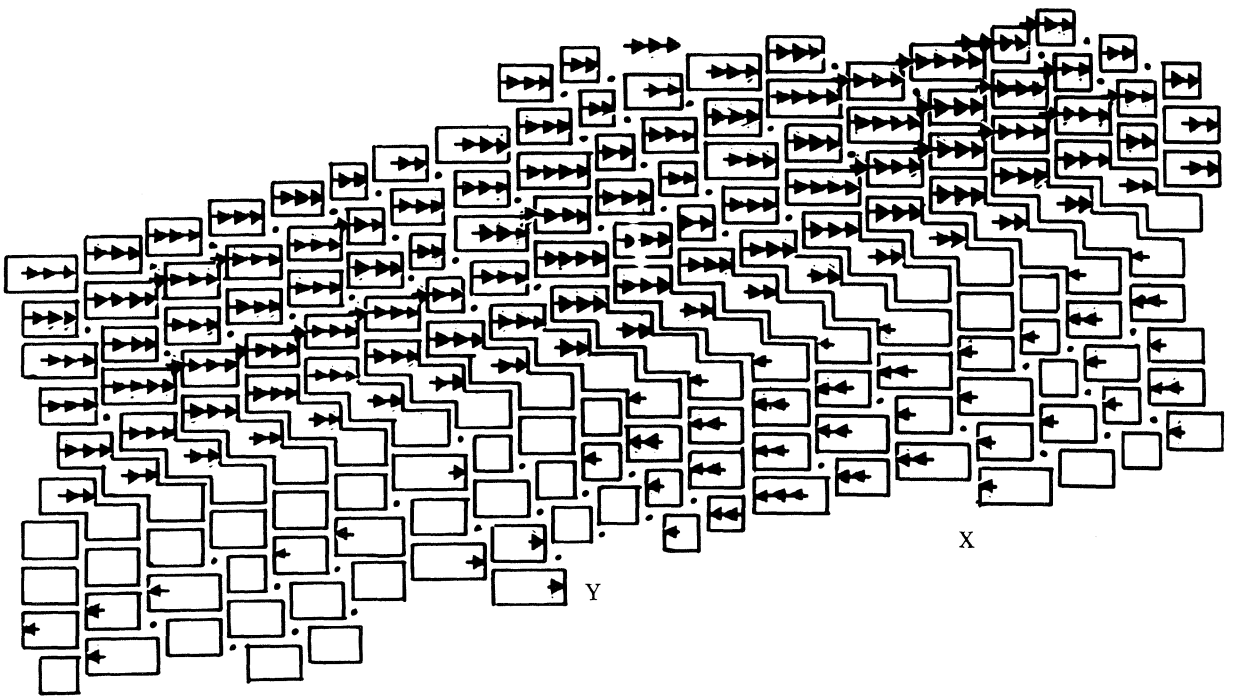

FIGURE 33. Displacement map from a micrograph of OX2E, showing relative displacements in the production of a long array of spliced blocks from the original $Nb_{25}O_{62}$ structure.

(*c*) *Extended defects and the elimination of cation vacancies*

As already stated, an array of spliced blocks is equivalent to a wall of cation-deficient structure; a wall of turned blocks is a structure from which cation rows have been eliminated, as are the rows of narrow blocks from which the wall was formed. Equations (2), (6) and (7) correctly represent the redistribution of cation sites within the blocks, during the transformations OX1C → OX4C, '$Nb_{25}O_{62}$' → OX2E, '$Nb_{53}O_{132}$' → OXF; they do not show the whole mass balance for converting cation-deficient structures (which correspond to stoichiometries lower than $NbO_{2.500}$) into an intergrowth of two structures, each with the stoichiometry Nb_2O_5. That process involves the creation of additional tetrahedral sites. The condition determining the total mass balance is that the number of oxygen atoms in any crystal remains constant; oxygen and niobium atoms required for creating tetrahedral sites can come only from the destruction of some of the blocks originally present.

Thus the true mass balance for the complete transformation of '$Nb_{25}O_{62}$' should be written as

$$95(Nb_{24.8}O_{62}) \rightarrow 62\ (Nb_{28}O_{70}) + 62(Nb_{10}O_{25}). \quad (9)$$

In this process, out of every 190 (4 × 3) blocks originally present, four have been 'cannibalized' and 29 new tetrahedral sites have been formed. All the cation sites are occupied in the products. Similarly, for oxidized $Nb_{22}O_{54}$, the overall process is

$$85(Nb_{21.6}O_{54}) \rightarrow 27(Nb_{28}O_{70}) + 108(Nb_{10}O_{25}), \quad (10)$$

with the net disappearance of eight (4 × 3) blocks out of every 85 originally present, and the creation of 50 tetrahedral sites. For oxidized $Nb_{53}O_{132}$, the process is

$$95(Nb_{52.8}O_{132}) \rightarrow 157(Nb_{28}O_{70}) + 62(Nb_{10}O_{25}). \quad (11)$$

Four out of every 285 (4 × 3) blocks originally present have been consumed and 29 tetrahedral sites created. If transformation goes to completion, the cation-deficient structures are completely replaced by perfect structure.

It is evident that although the locations at which faults are found depend fortuitously on how the transformation is initiated and propagated, the faults themselves have an essential function. They are the loci from which crystallographic sites are eliminated, in accordance with equations (9), (10) and (11). As such, they are sinks for cation vacancies, which must drift outwards as the two sorts of ordered domains of Nb_2O_5 grow in extent. The faults serve either to delete cation sites (turned blocks) or to order them into walls (spliced blocks). Faults are also sources for the inward drift of oxygen atoms needed to form tetrahedral sites. That drift does not require any long-range transport; detailed examination of what is implicit in the cumulative A.W. shifts shows that no oxygen atom need execute a longer diffusion jump than to a second or third neighbour site, in any one act. The observed spacing between lines of faulted structure is such that the mean total drift path, over a series of repeated A.W. shifts, is short.

7. Conversion to *H*–Nb_2O_5 and recrystallization

There is no definite temperature at which the metastable polymorphs of Nb_2O_5 are converted into *H*–Nb_2O_5, but in general the relevant processes become important above about 950 °C; at lower temperatures, conversion is very slow. This OX4C material, formed by annealing at 700 °C, as typified by figure 15, undergoes no further, significant change of microstructure when it is reheated to 900 °C (figure 34, plate 9). Occasional files of spliced blocks, as at X, indicate that some rearrangement processes have been frozen in, in an uncompleted stage; this particular fault appears to be associated with the reorganization of a wall of turned blocks, and affords some insight into the reaction steps involved in that process.

Above about 950 °C, all the domain structures – OX4C, OX2E and OXF – transform fairly fast, the domains of $Nb_{10}O_{25}$ disappearing and the antiphase domains of *H*–Nb_2O_5 structure undergoing recrystallization. The domain structures of OX4C, OX2E and OXF are all based upon the same principle; they differ only in their relative proportions of $Nb_{10}O_{25}$ domains and *H*–Nb_2O_5 domains. It is likely that the same transformation mechanism will operate for all three; OX4C, with its high proportion of $Nb_{10}O_{25}$ domains, probably transforms more rapidly than OX2E or OXF.

The mechanism of this transformation has proved elusive. In any of these materials heated

above 950 °C, all crystals (or regions of crystal) were found either to be completely transformed into H–Nb_2O_5 or to retain the domain structure, apparently unchanged. No informative transition structures could be found. This evidence suggests that the process is catastrophic, and possibly heterogeneous, as contrasted with the progressive structural evolution of the preceding stages. In particular, there is no experimental evidence for the mechanism by which the metastable $Nb_{10}O_{25}$ domains are transformed. Hypothetically, the tetragonal $Nb_{10}O_{25}$ structure of (3×3) blocks could be smoothly converted into the H–Nb_2O_5 structure by recurrent glide on (310) ($Nb_{10}O_{25}$), the composition plane with the H–Nb_2O_5 structure. Such a glide cannot, however, be propagated through the H–Nb_2O_5 matrix surrounding an enclosed domain, so that it does not provide a mechanism for homogeneous transformation. It could take place in $Nb_{10}O_{25}$ domains exposed at a free surface, as could other reconstruction processes.

In materials heated for relatively short times (for example, less than 1 hour) at 950–1000 °C, the regions of H–Nb_2O_5 structure were not free from faults. Twin bands occurred frequently, but did not recur at the quasi-regular intervals of the walls of turned blocks in OX4C or the corresponding features in OX2E and OXF, so are not necessarily related to the antecedent fault structure. There were also occasional relic strings of (3×3) blocks and antiphase boundaries (figure 35, plate 9). In a few cases, twin bands were seen to terminate within the crystal, at a relic string of (3×3) blocks (figures 36 (plate 9) and 37 (plate 10)); such terminating faults necessarily introduce a dimensional mismatch, with dislocations and antiphase boundaries. Thus, a Burgers' circuit mapped around the end of the twin band in figure 36 shows that a dislocation of partial edge character, with a closure gap of 0.2 nm, is located at the two-octahedron-wide block. In figure 37, a narrow domain of $Nb_{10}O_{25}$ is completely enclosed within H–Nb_2O_5 structure. The structure around its lower extremity is not decipherable, but its upper end is a junction with two other faults, B and T. Fault T is a twin band in the H–Nb_2O_5 structure; B is a file of (5×3) blocks, which are so stacked as to constitute a strip of the (not hitherto observed) $(5 \times 3)_3$ structure. The unit cell of this structure would have the composition $Nb_{46}O_{115}$; it is another possible polymorphic structure for Nb_2O_5. The junction of the three faults A, B and T compensates for mismatch of dimensions and cation levels; no dislocation is involved. Twin bands also occasionally stepped sideways across several files of blocks; between the ends of those segments, there was a row of narrow blocks. The evidence is consistent with the onset of a large-scale, cooperative sequence of transverse A.W. shifts, as part of the mechanism of recrystallization.

The regions of crystal that retain the domain structure do show some changes. Figure 38 (plate 11) shows such a region in OX4C, after heating at 1000 °C for 90 s. The meandering fault walls have been largely replaced by arrays of (4×4) blocks, narrow domains of the N–Nb_2O_5 structure; the average orientation of the faults has been altered thereby. The average proportion of (3×3) blocks in such OX4C material tends to be smaller than in OX4C annealed at 700 °C, suggesting that some direct transformation has occurred, but the matrix slabs of H–Nb_2O_5 structure between them have much the same average width. This reflects a higher proportion of narrow $Nb_{10}O_{25}$ arrays. For OX2E, it is less easy to discern how far the structure attained at 700 °C is modified at higher temperatures, without undergoing complete transformation. The important question is whether that structure is a static configuration, awaiting transformation, or whether the structure observed after any heat treatment represents a mobile, high temperature state.

In a series of experiments to test this, OX2E was subjected to progressively more severe heat

treatments, and micrographs taken to cover the largest possible image fields in order that the observed structures should be as representative as possible. Figures 33, 39 (plate 12) and 40 (plate 13) are from material reheated to 980 °C for 2 s, 1000 °C for 205 s and 1120 °C for 180 s respectively. As compared with OX2E annealed at 700 °C: (*a*) there is an undoubted increase in the incidence of bands of spliced blocks, indicative of cooperative, multiple A.W. shifts; and (*b*) there is probably an increase in the concentration of rows of single, detached strings of (3 × 3) blocks, although this is variable from one area to another. The evidence favours the view that the structure is mobile at high temperatures; what is observed in any specimen is a configuration that existed at the moment of quenching. In figure 39, at X, the overlap contrast in two adjacent rows clearly reveals the uncompleted passage of a set of A.W. shifts in two opposed directions, which thereby sheared the structure in the course of forming a line of turned blocks at the end of an array of $Nb_{10}O_{25}$.

If these domain structures are mobile at high temperatures, several implications follow. A mechanism is provided for translocating (3 × 3) blocks to existing domains of $Nb_{10}O_{25}$, thus enabling them to grow into viable nuclei. Mobility also serves to 'dissolve' (3 × 3) blocks from the edges of $Nb_{10}O_{25}$ domains, for relocation elsewhere. Comparing the average breadth of $Nb_{10}O_{25}$ domains in OX4C annealed at 700 °C (figure 15) and at 1000 °C (figure 38), or the large proportion of detached, single strings of (3 × 3) blocks in OX2E (figures 33, 39, 40), it is evident that the $Nb_{10}O_{25}$ domains show no evidence of continued growth in their size; if anything, there is some tendency to disperse the (3 × 3) blocks. The strings of (3 × 3) blocks retain their linearity and their orientation; isolated blocks or irregular formations have rarely been seen.

It may also be relevant that unexpectedly large patches of '$Nb_{25}O_{62}$' structure were frequently found in OX2E quenched from high temperatures, for example, after heating to 1120 °C for 540 s. While it is not impossible that these are residual structures that had survived through the heat treatment, they could also be evidence that the process of equation (5) had been reversed, as a necessary first step in the 'dissolution' and translocation of (3 × 3) blocks. Several such domains of '$Nb_{25}O_{62}$' structure can be seen in figure 40; most of them are closely associated with multiple rows of spliced blocks. The area X merges into a triangular region where overlap contrast suggests that a set of cooperative A.W. shifts, extending across about 15 rows of blocks, was active at the moment of quenching.

8. Discussion

The evidence reviewed in the preceding sections confirms that a single operative step underlies the whole transformation process, and that this step is the process postulated by Andersson & Wadsley. More significant is that it has been possible to trace, in considerable detail, how that process, beginning with independent and purely localized fluctuations, is propagated throughout each crystal.

It appears to be characteristic of c.s. structures that sites along the unique crystallographic axis, with alternating cations and anions, are strongly correlated. If a displacement reaction is effected in one layer, it is propagated along a whole rod of sites, and one-dimensional order is conserved. Our numerous observations of overlap contrast, which indicates that reaction has not gone to completion throughout the thickness of the specimen, show that although the co-operative process may be rapid, it is not instantaneous; it is more likely to result from individual,

local A.W. shifts in each layer than from the passage of a strong, transverse vibrational displacement along a rod of sites. Propagation of A.W. shifts from block to block along a row is the mechanism for translocating blocks, which segregates and builds up arrays of (3×3) blocks. The growth of domains with the *H*–Nb_2O_5 structure is dependent upon propagation in the third direction, along files of blocks. Once embryo domains of the two stoichiometric Nb_2O_5 structures have been formed, it is evident that energetic considerations favour those subsequent displacement events that augment these local ordering arrangements. What is observed at any stage is the rearrangement of structure brought about cumulatively, by repeated and separate A.W. displacement events. On the displacement maps, these appear as cascades of A.W. shifts along rows or up files. The l → r and r → l shifts spread out on either side of nodes, which mark the origin of each region of local transformation; the size of each region, and of the domain of *H*–Nb_2O_5 structure into which it develops, is fortuitously determined by the random incidence of initiation. Up to the stage at which some reorganization of the domain structure sets in, through modifications in the walls of faults between adjacent regions, the structures observed are those that could be produced by a very small number of consecutive, cumulative, A.W. shifts.

De Fontaine (1975) has discussed homogeneous reactions, with particular reference to the simpler metallic structures, in terms of replacive or displacive waves of perturbation, polarized along specific crystallographic directions. This idea provides a suggestive *post hoc* interpretation of order–disorder transformations, the formation of ω-phases and similar non-reconstructive processes, but leaves it uncertain whether the perturbation waves should be envisaged as synchronously affecting a whole region of crystal, or whether they spread out from some purely localized fluctuation. In the latter case, it might be expected that they would be propagated at a rate that was related to the vibrational spectrum of the crystal. Our results relate to a different and more complex type of structure, and make it certain that displacive perturbations do not affect a whole region of crystal synchronously, but start as strictly localized phenomena and are propagated outwards along specific, structurally favourable crystallographic directions. The observed structures look as if they had been formed by a set of discrete events, rather than by the passage of a wave of displacement, but the displacements, as mapped, may not be incompatible with the occurrence of instantaneous pulses of perturbation, of varied intensity in different locations, and attenuating rapidly so that each is effective over a limited range. At the higher temperatures, where the rates of propagation along rows and up files appear to be comparable, the transformation moves through the crystal as a one-dimensional process within each self-contained region. It must remain open whether that process should be regarded as the passage of a planar wave front, or as a highly correlated set of discrete events.

It is not clear how the formation of the ultimate domain structure should be categorized. Up to the stages of forming OX4C, OX2E and OXF, it follows the behaviour of a typical time–temperature-transformation process that attains an incomplete, but almost stationary, state at every temperature. Thus (table 3) OX4C hardly proceeds beyond 70 % transformation up to 900 °C. At higher temperatures, any region of crystal either recrystallizes completely or it retains the domain structure, at much the same degree of transformation. Formation of the domains of *H*–Nb_2O_5 and $Nb_{10}O_{25}$ cannot properly be described as ordinary homogeneous nucleation; the domains do not progressively grow in size as heat treatment is continued. Even in the régime where substantial regions of crystal are converted to recrystallized *H*–Nb_2O_5, the domains of $Nb_{10}O_{25}$ remain narrow, with much the same width distribution and spacing

between them. As noted above, the proportion of single strings of (3 × 3) blocks is higher, if anything, in materials quenched from high temperatures, as if the structures were being dispersed.

The domain structures bear some resemblance to models of spinodal decomposition. In general, both spinodal decomposition and homogeneous nucleation are considered in relation to solid solutions, from which domains with different compositions, but the same structure, are segregated. The present case is different; the original, disordered state (e.g. OX2C) is stoichiometric in composition, and the domains that segregate from it have identically the same composition, but different, though topologically compatible, structures. It is permissible to treat the establishment of two kinds of medium-range order in such a system on the same basis as the establishment of compositional order in a solid solution system. In a formal sense, the disordered state everywhere has the DO_9 structure, collapsed by randomly distributed segments of c.s. planes (linear groups of edge-sharing octahedra). These segments of c.s. planes are conserved during the transformation and they could be formally regarded as pseudo-components of the system; the transformation process redistributes and orders them, to build up domains with two variants of medium-range order. In principle, it would be possible to construct an equilibrium diagram, showing how the free energy of the system varied with some parameter that expressed the concentration and configuration of the c.s. segments. A free energy-configurational parameter diagram of this kind would be analogous to the free energy-composition diagram of a solid solution system, and it would lead to similar considerations about the viability of fluctuations within an originally random system.

There are, however, significant differences between the domain structures and the spinodal structures, as treated theoretically by Cahn (1961, 1962*a*, *b*) and others. The micrographs show that there is no simple, even if only approximate, regularity in the spacing of the domains. We defer consideration of whether those spacings show any regular relationships, or whether they correspond to a chance distribution, corresponding to the fortuitous location of strings of (3 × 3) blocks at the moment when mobility was quenched. There is no immediately identifiable dominant wavelength for the perturbations and, since the breadth of the *H*–Nb_2O_5 matrix domains does not increase with continued heat treatment, there is no obvious increase in wavelength as transformation proceeds, such as is required by Cahn's theoretical treatment. Moreover, apart from the retention of those extra (4 × 3) blocks that are needed to preserve coherence between the two structures, the transition from *H*–Nb_2O_5 to $Nb_{10}O_{25}$ domains is sharp. The matter is not altogether clear cut, however. Theories of homogeneous nucleation and spinodal decomposition have been largely expressed in the language of continuum structures. It is not clear what meaning attaches to 'concentration' or 'concentration gradient' (for composition changes within the solid solutions), when the crystal structure is viewed on the atomic scale; nor is a 'diffuse boundary' a concept of clear meaning on that scale, or one that is applicable to the segregation of different structures. The observations that have been described here are subject to these ambiguities, relating, as they do, to strictly local structure and local composition within crystals. Care must be exercised in applying to this situation the terminology and the reasoning that are valid for statistical models of macroscopic systems. The transitions discussed here may not fit easily into the usual categorization of phase reactions, but they are of a type that probably has its counterparts in the reactions of other polyhedron network structures.

It is evident that the first stage oxidation products are unstable, but it is not clear what factors determine the relative stability of the numerous possible polymorphs of Nb_2O_5. In the

rearrangements discussed, local ordering creates fragments of several configurations that have the ideal stoichiometry Nb_2O_5: elements of the *N*–Nb_2O_5 structure $Nb_{16}O_{40}$, $(6 \times 3)_\infty$ elements of $Nb_{18}O_{45}$, $(5 \times 3)_3$ elements of $Nb_{46}O_{115}$ as well as the main products, $Nb_{10}O_{25}$ and $Nb_{28}O_{70}$. There is no thermochemical evidence about the relative stability of any of the Nb_2O_5 polymorphs, nor are lattice energy calculations sufficiently precise; the differences in free energy between *H*–Nb_2O_5 and all its well defined, metastable polymorphs are certainly very small compared with the large cohesive energy of the structures. In most contexts, and to simplify discussion, the block structures can be idealized as regular, modular structures, but they do show small differences in the dimensions and distortions of their component coordination octahedra. As table 4 shows, the mean volume per niobium atom is actually greater in *H*–Nb_2O_5 than in the lower oxides (assuming that these have the same cell dimensions as their analogues in the TiO_2–Nb_2O_5 system). Since the interlayer spacing is practically constant, the area per atom in each layer must increase as OX1C and OX1E are transformed into domains of *H*–Nb_2O_5. If $Nb_{10}O_{25}$ is identical in dimensions with PNb_9O_{25}, it is formed with a decrease in the area per niobium atom; in the domain structure, the two constituents partially compensate for the dimensional changes. Elastic strains are undoubtedly introduced locally, as transformation proceeds, but the final microstructure lowers the total strain energy.

TABLE 4. DIMENSIONAL DIFFERENCES BETWEEN BLOCK STRUCTURES

compound	interlayer separation / nm	volume per Nb atom / 10^{-3} nm^3
$Ti_2Nb_{10}O_{29}$†	0.3814	46.54
$Nb_{22}O_{54}$	0.3822	47.76
$TiNb_{24}O_{62}$‡	0.3821	47.89
PNb_9O_{25}§	0.3828	46.58
H–Nb_2O_5	0.3822	48.50

† $Nb_{12}O_{29}$ assumed identical in dimensions.
‡ $Nb_{25}O_{62}$ assumed identical in dimensions.
§ $Nb_{10}O_{25}$ assumed identical in dimensions.

A simple calculation for the reorganization of OX1E structure, based on equation (9), indicates a small net shrinkage of about 0.6 %. For the reorganization of '$Nb_{22}O_{54}$', OX1C, equation (10) would imply a decrease in area by about 2 %. Some of the differences in behaviour between the OXC and OXE systems – for example the incidence of narrow block faults that create dimensional misfits and dislocations, and the greater importance of direct conversion of $Nb_{10}O_{25}$ to *H*–Nb_2O_5 in the OXC system – could arise from the larger elastic strain in OX2C, OX3C and OX4C, as compared with OX2E. The elastic strain energy could well be regarded as that property of the crystal as a whole that progressively imposes long-range order on the initially disordered structures.

Initiation and nucleation have been referred to as random events, but regions such as that shown in figure 22, with a chain of nuclei lying along the [100] direction of '$Nb_{25}O_{62}$', suggest that they may tend to recur along certain trajectories through the crystal. The strain field around a nucleus may well be anisotropic, and could predispose the next initiation event to take place preferentially along a specific crystallographic direction. On this, as on other matters discussed, more experimental evidence is needed.

The authors would thank Mr J. Ll. Jenkins for invaluable technical assistance, and the Science Research Council for its support of this work.

Appendix. Radiation damage and artefacts

Inelastic scattering raises the temperature of the crystal area under examination, to an indeterminate degree, during the manipulations of electron microscopy. Since the transformation of oxidized $Nb_{22}O_{54}$, in particular, sets in at a relatively low temperature, it seemed possible that some of the observed A.W. displacements could have been induced during the microscopy, rather than by the heat treatments. To test the extent of this, a representative region of an OX1C crystal was imaged (figure 41*a*, plate 14). The crystal was then irradiated, under the usual imaging conditions for 30 s (about four–five times the usual exposure), and a micrograph taken of the same area (figure 41*b*). The condenser aperture was removed, and the crystal was irradiated again. A series of such drastic irradiations was made, and structure images of the same area were recorded after each. Figure 41 *c–f* shows images from this series, taken after 30, 75, 135 and *ca.* 1150 s of beam heating, respectively. A grid has been drawn on the micrographs, with its origin on the same identifiable (3×3) block, to facilitate detailed comparison. On each micrograph, those blocks that will be changed in dimensions – i.e. that will undergo an A.W. shift – during the next irradiation are tonally emphasized.

It can be seen that some A.W. displacements are, indeed, induced by strong or prolonged beam heating, but that those occurrences are relatively rare. Only single shift events occur; in no case are they propagated along rows or files of blocks. In many of them, overlap contrast shows that the displacements have not been propagated from layer to layer, right through the thickness of the crystal. The artefacts are not uniformly distributed, but tend to occur in certain areas of crystal, and especially where some disorder is already present; their general effect, indeed, is to improve local order, by correcting interchanges between (3×3) and (4×3) blocks that had occurred during the preparation of the sample. Comparison of figure 41*a* and *b* shows that three (5×3) blocks, originally present, were eliminated in the first prolonged irradiation, and no subsequent block disproportionations resulted from the beam heating.

It may be concluded that a few A.W. displacements may unavoidably have been induced during the electron microscopy, but that the incidence of such artefacts during normal working was certainly too low to be misleading. The structures observed cannot have been significantly modified by beam damage, and the inferences drawn from them are valid.

References

Anderson, J. S., Bevan, D. J. M., Cheetham, A. K., von Dreele, R. B., Hutchison, J. L. & Strahle, J. 1975 *Proc. R. Soc. Lond.* A **346**, 139.

Andersson, S. & Wadsley, A. D. 1966 *Nature, Lond.* **211**, 581.

Andersson, S. & Wadsley, A. D. 1970 *Perspectives in structural chemistry* (ed. J. Dunitz), vol. III, p. 1. New York: Wiley.

Browne, J. M. & Anderson, J. S. 1974 *Proc. R. Soc. Lond.* A **339**, 463.

Browne, J. M. & Anderson, J. S. 1976 *Acta crystallogr.* A **32**, 670.

Bursill, L. A. & Hyde, B. G. 1972 *Prog. solid St. Chem.* **7**, 177.

Cahn, J. W. 1961 *Acta metall.* **9**, 795.

Cahn, J. W. 1962*a* *Acta metall.* **10**, 179.

Cahn, J. W. 1962*b* *Acta metall.* **10**, 907.

Chen, H., Comstock, R. J. & Cohen, J. B. 1979 *A. Rev. Mater. Sci.* **9**, 51.

De Fontaine, D. 1975 *Acta metall.* **23**, 553.

Fejes, P. L., Iijima, S. & Cowley, J. M. 1973 *Acta crystallogr.* A **29**, 710.

Hibst, H. & Gruehn, R. 1978 *Z. anorg. allg. Chem.* **442**, 49.

Hillert, M. 1961 *Acta metall.* **9**, 525.

Hutchison, J. L. & Lincoln, F. J. 1973 *Physica status solidi* a **17**, 169.
Hutchison, J. L., Lincoln, F. J. & Anderson, J. S. 1977 *Proc. R. Soc. Lond.* A **352**, 303.
Iijima, S. 1975 *Acta crystallogr.* A **31**, 784.
Kimura, S. 1973 *J. solid St. Chem.* **6**, 438.
McConnell, J. D. C. 1974 *Proc. 2nd NATO Advanced Study Institute, Feldspars*, p. 460.
McConnell, J. D. C. 1978 *Z. Kristallogr. Kristallogeom.* **147**, 45.
Norin, R., Carlsson, M. & Elgquist, B. 1966 *Acta chem. scand.* **20**, 2892.
Obayashi, H. & Anderson, J. S. 1976 *J. solid St. Chem.* **19**, 331.
Roth, R. S., Wadsley, A. D. & Andersson, S. 1965 *Acta crystallogr.* **19**, 643.
Schäfer, H., Gruehn, R. & Schulte, F. 1966 *Angew. Chem.* (Internatn edn) **5**, 40.
Skarnulis, A. J., Iijima, S. & Cowley, J. M. 1976 *Acta crystallogr.* A **32**, 799.

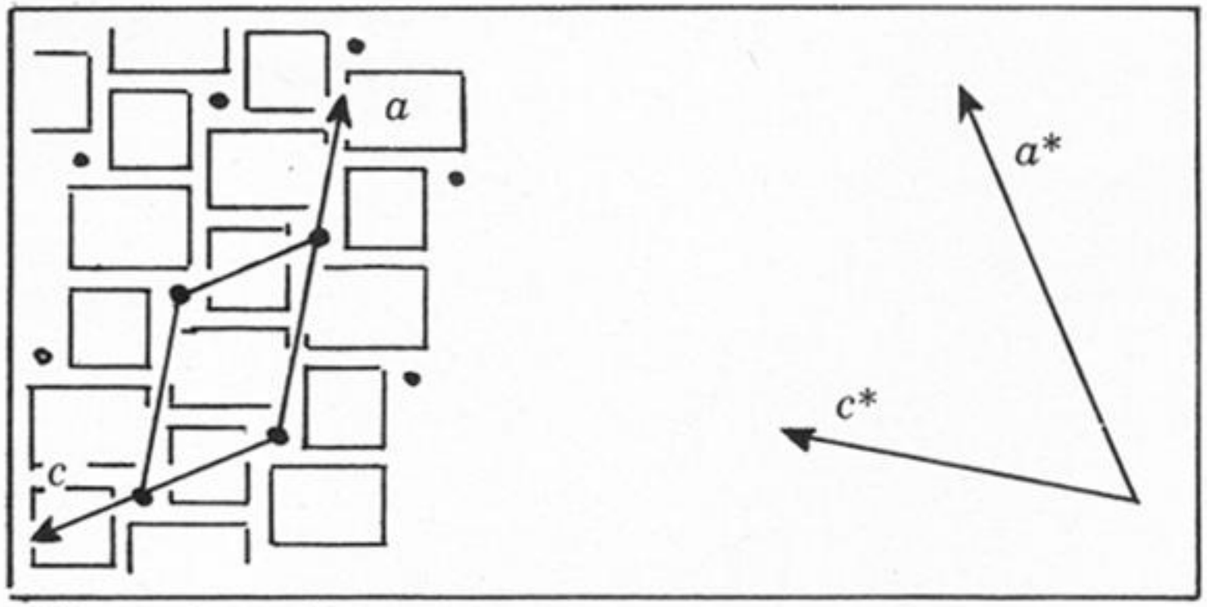

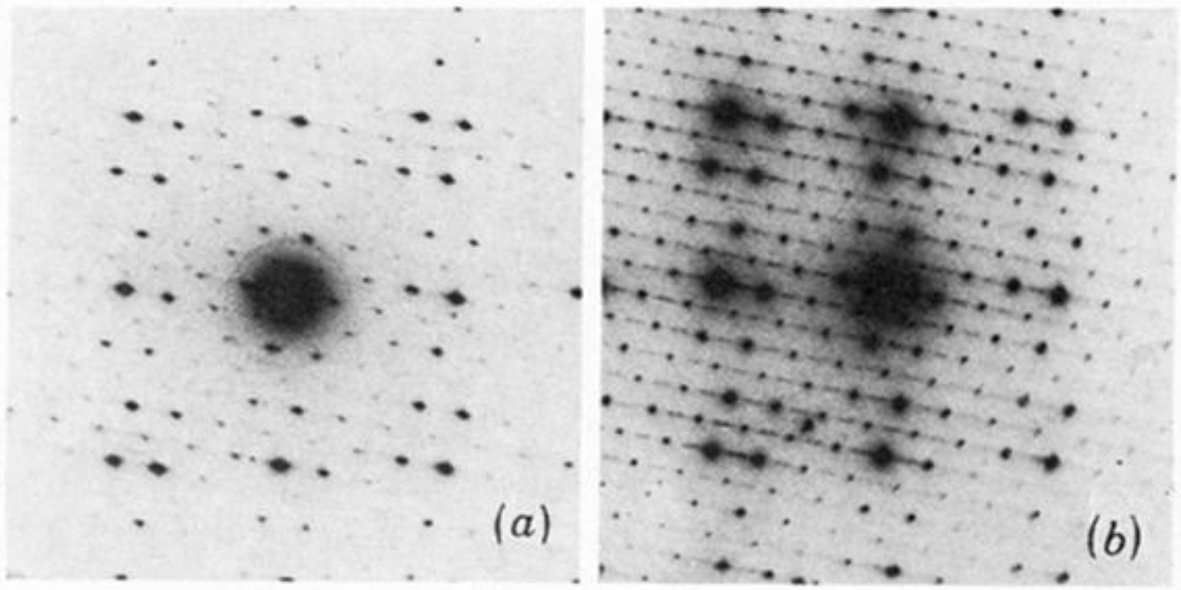

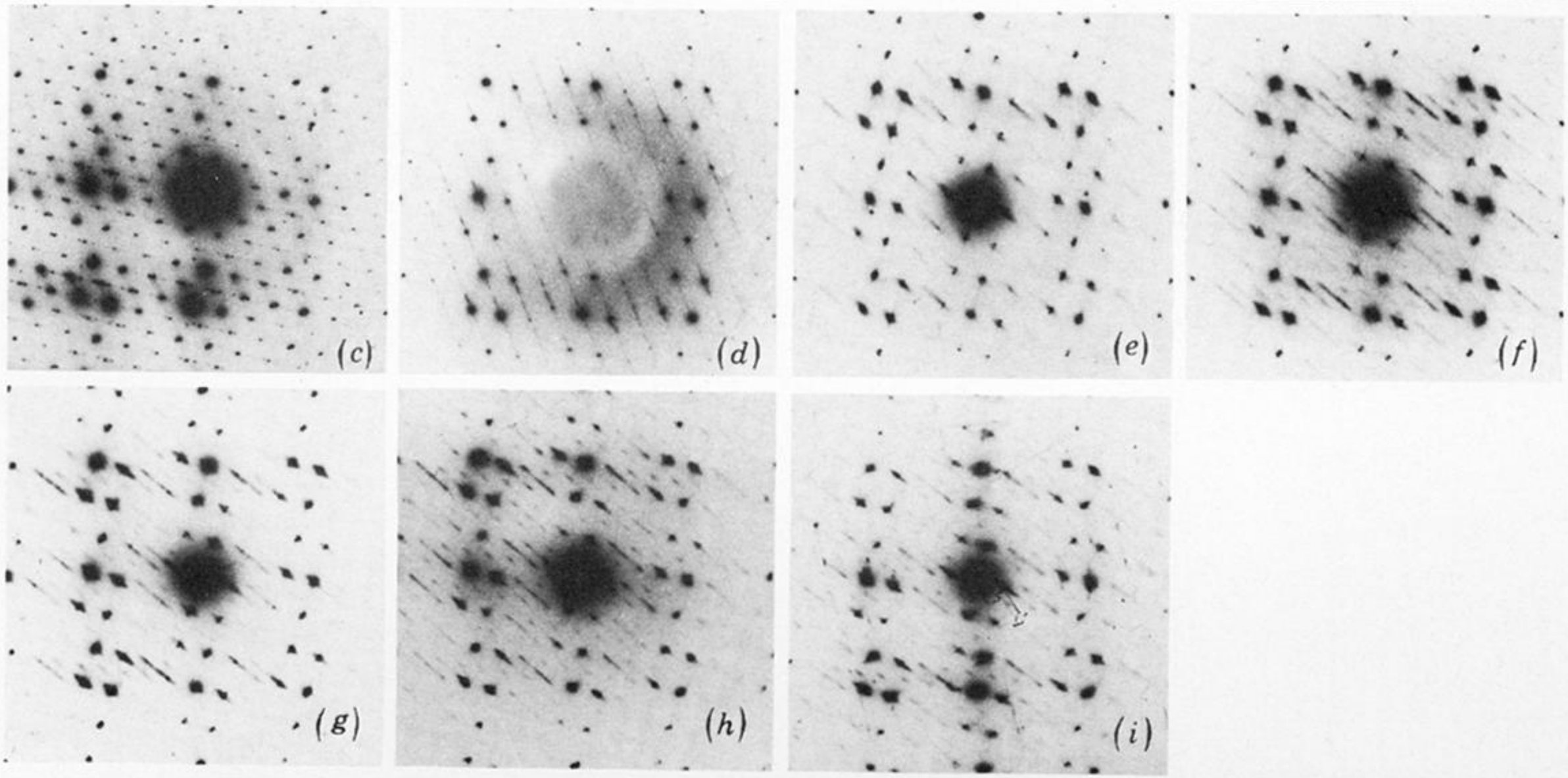

FIGURE 3. Selected area electron diffraction patterns at successive stages in the oxidation and transformation of $Nb_{22}O_{54}$ to OX4C.

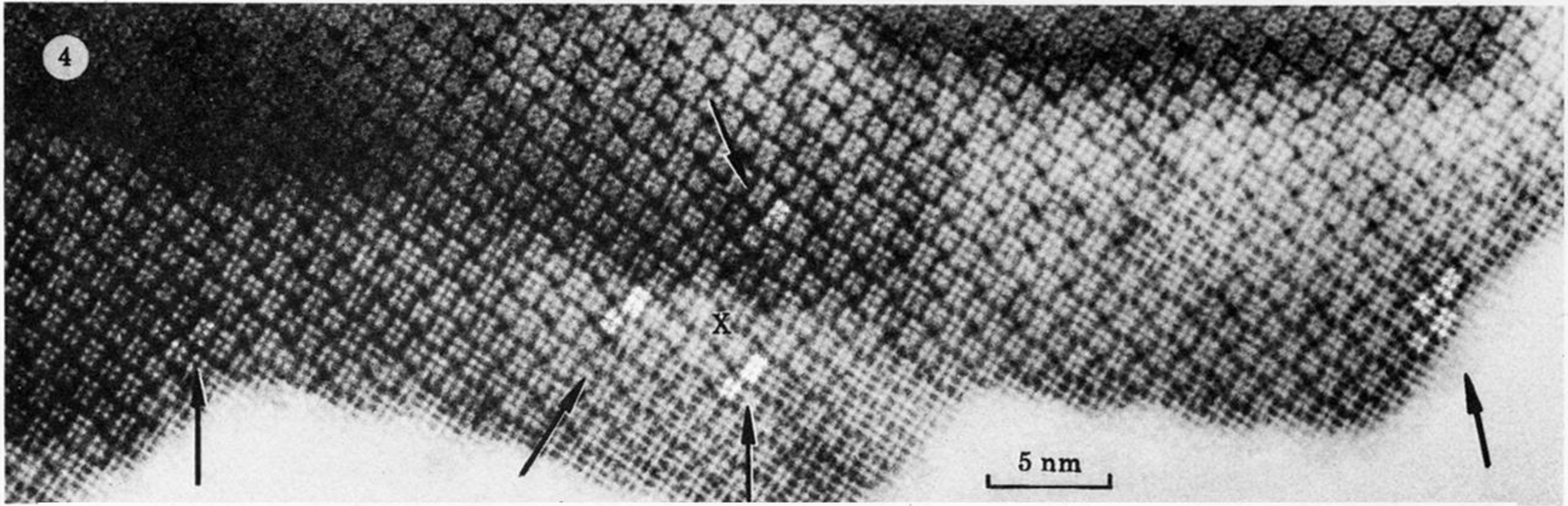

FIGURE 4. Structure image of oxidized $Nb_{22}O_{54}$, OX1C. Places where the positions of blocks have been interchanged are marked by arrows.

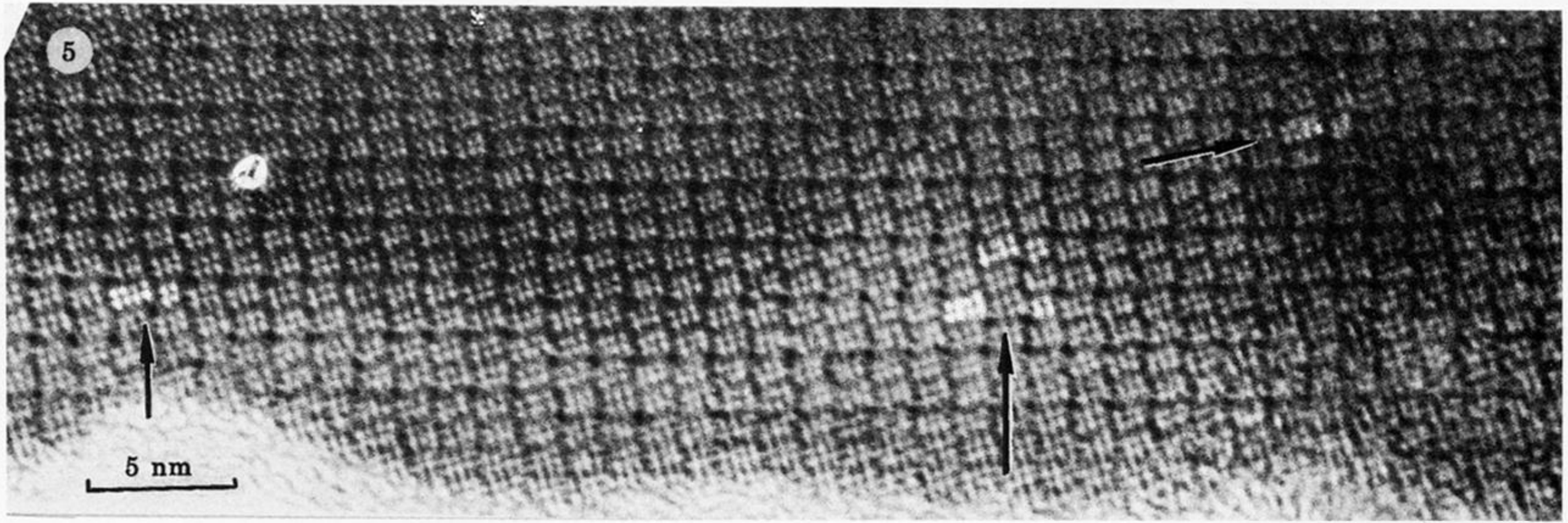

FIGURE 5. Structure image of oxidized $Nb_{25}O_{62}$, OX1E. Places where blocks have undergone disproportionation are marked by arrows.

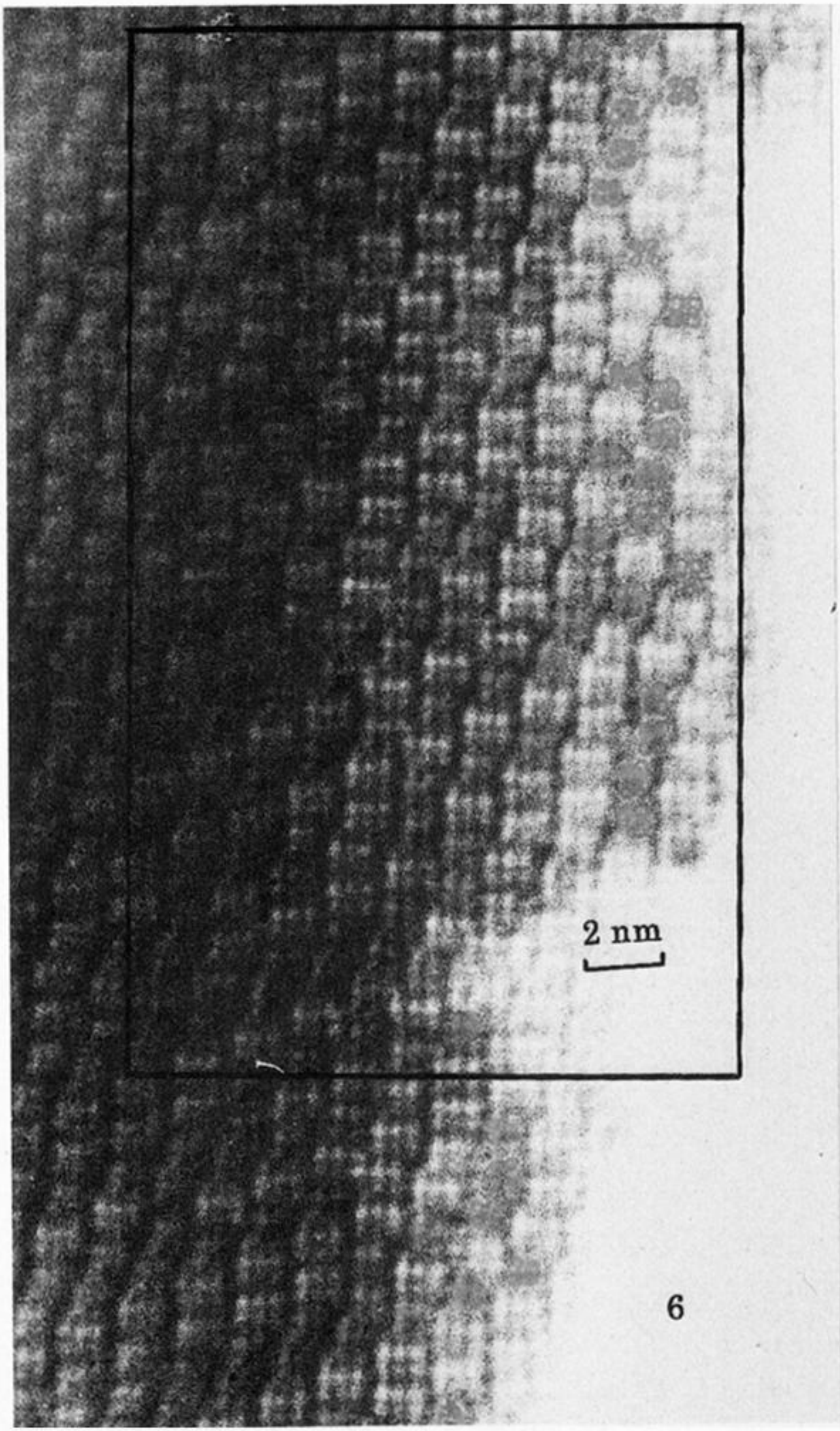

FIGURE 6. Earliest stage in the transformation of OX1C to OX2C.

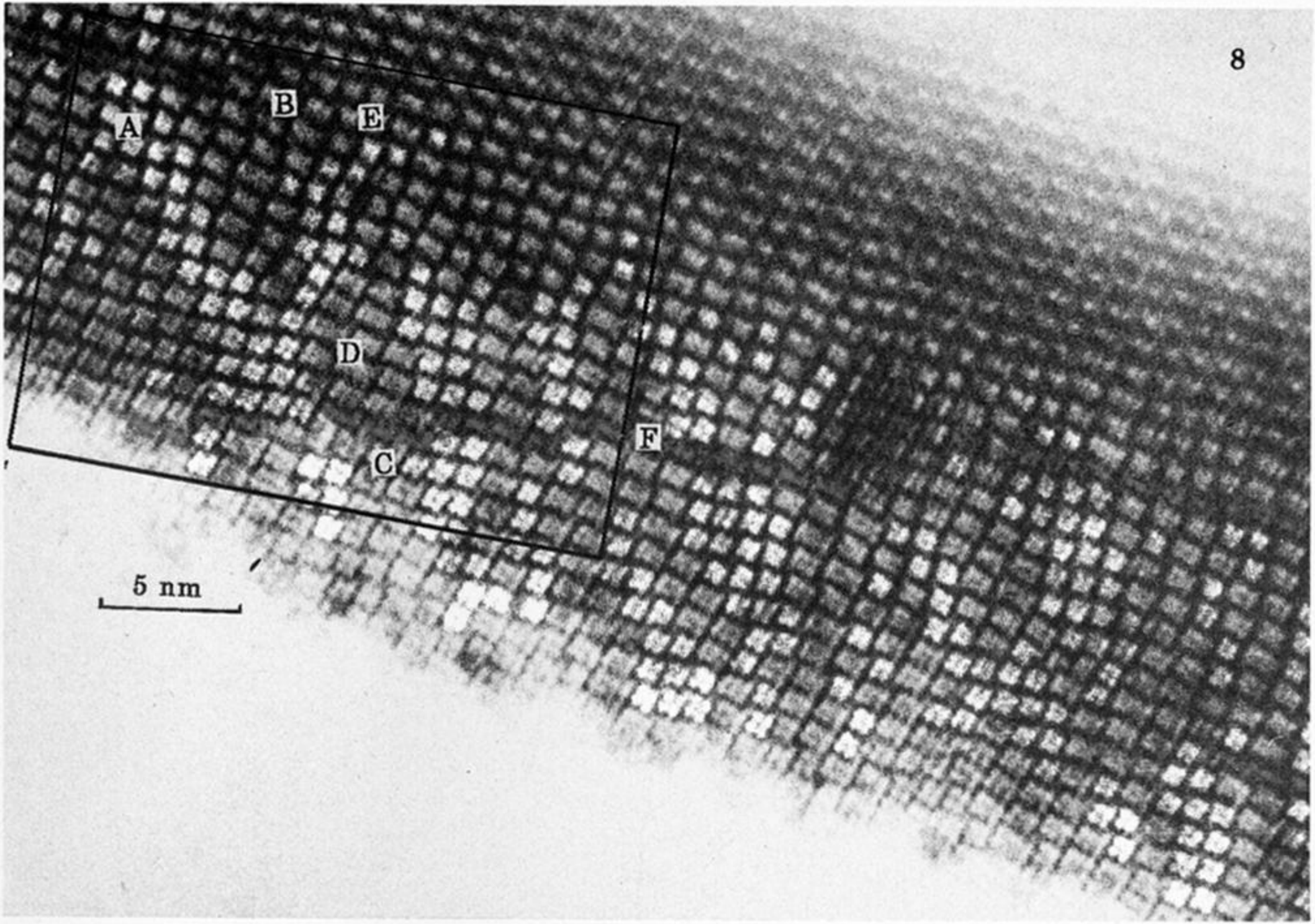

FIGURE 8. Rearrangement of OX1C to OX2C. (3 × 3) blocks are collected into irregular domains at A; there are incipient domains of *H*–Nb_2O_5, such as at D. F is a line of faulted structure.

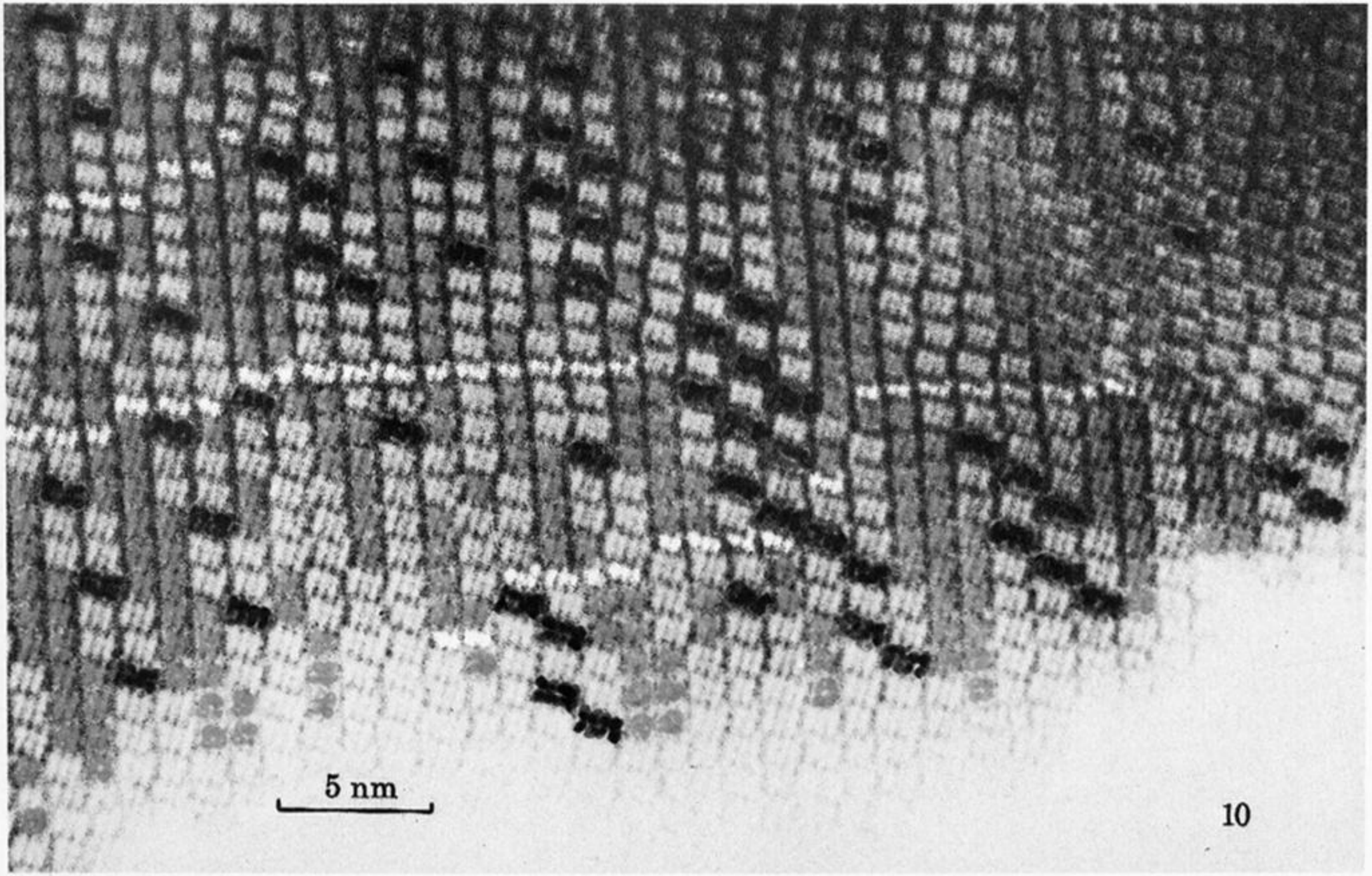

FIGURE 10. Fully developed OX2C structure. (3 × 3) blocks are almost completely segregated into regular, elongated arrays, in a matrix of, largely, *H*–Nb_5O_5 structure. Rows of fault structure cross these domains.

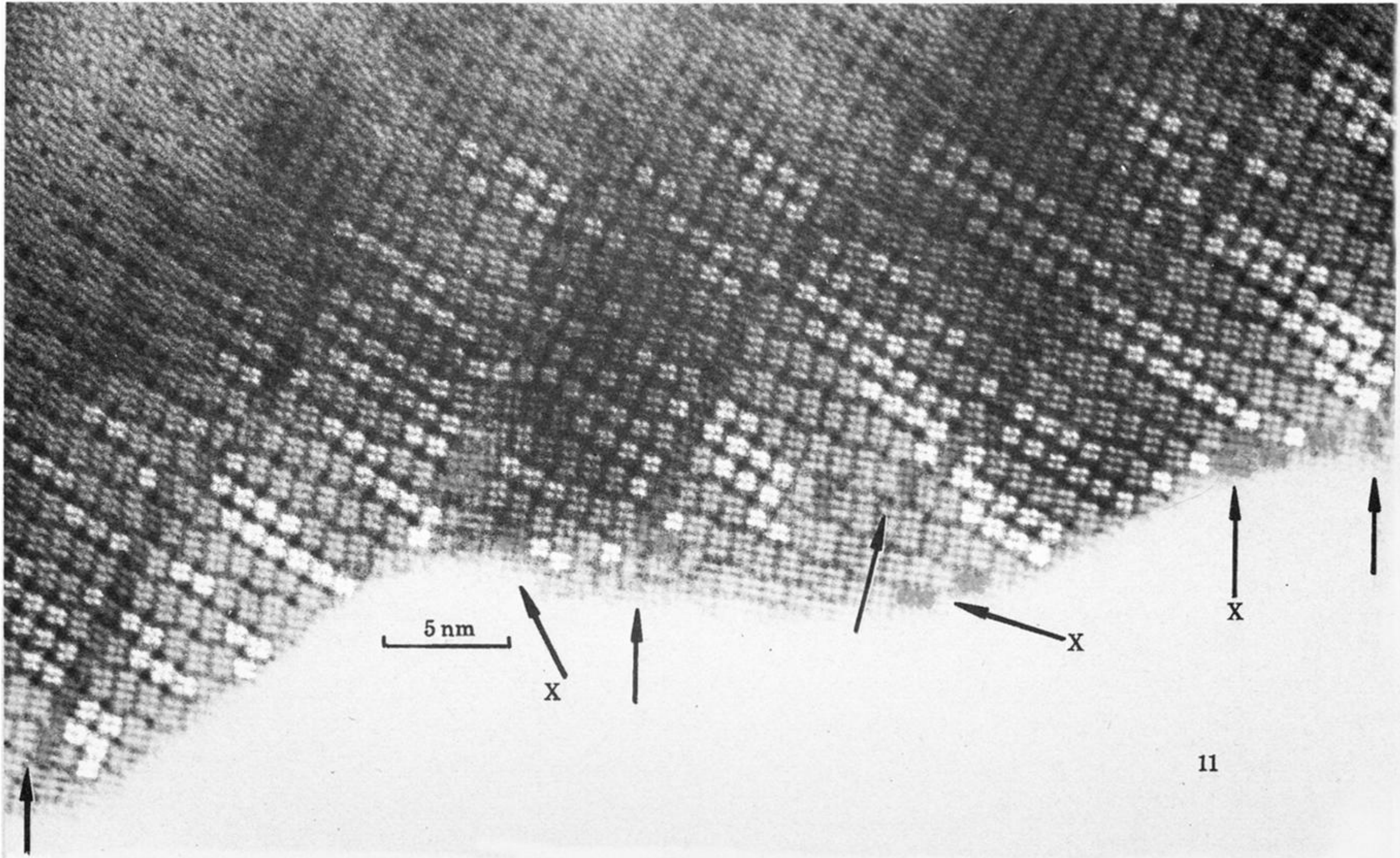

FIGURE 11. Fully developed OX2C structure, showing nearly regular recurrence of fault rows, with narrow blocks (arrowed). Occasional blocks are turned at right angles to the general configuration (X).

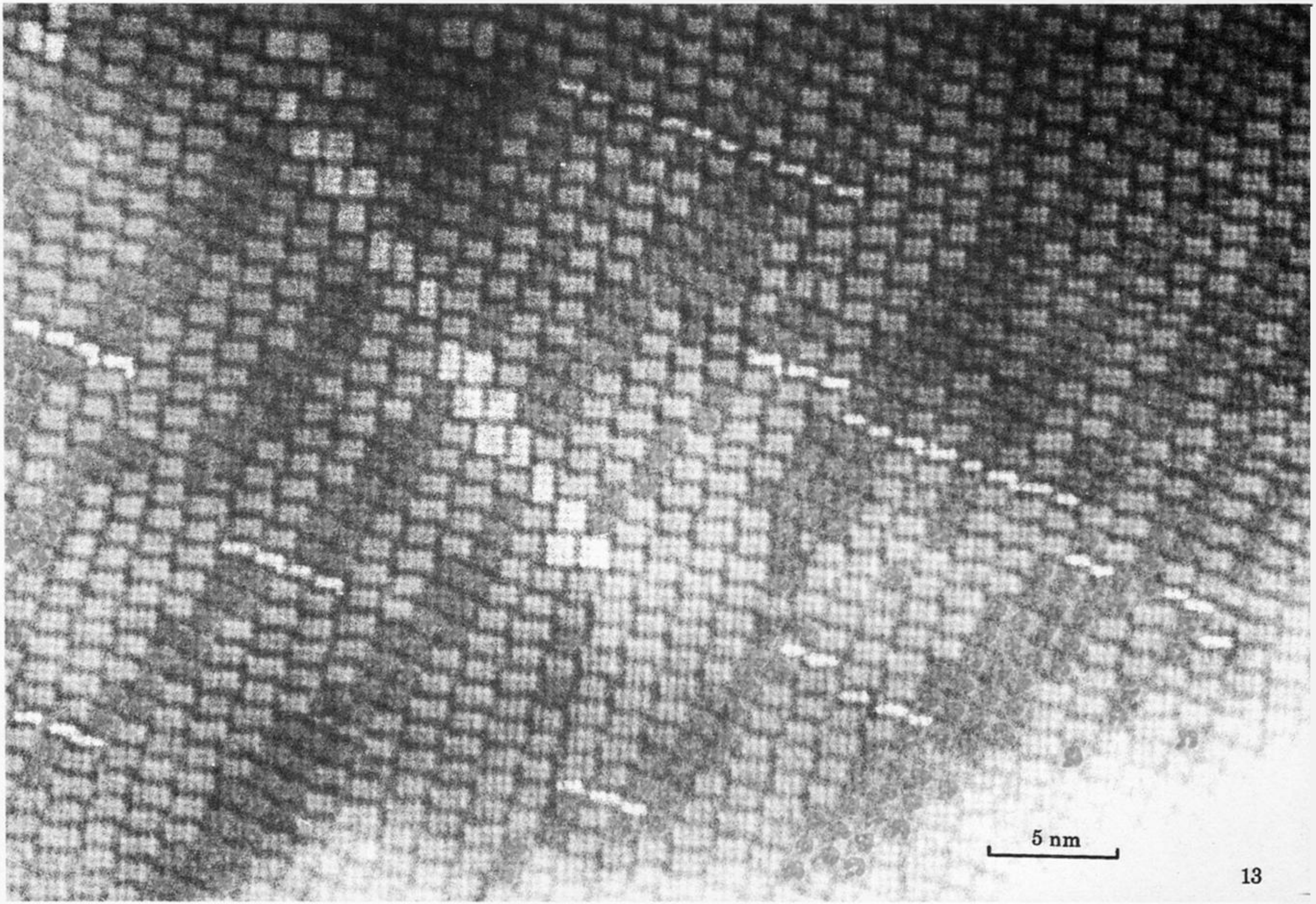

13

FIGURE 13. OX3C structure: long, regular arrays of (3×3) blocks ($Nb_{10}O_{25}$) and extensive domains of H–Nb_2O_5 structure. Fault rows, with narrow blocks, are undergoing replacement by walls of turned-around blocks.

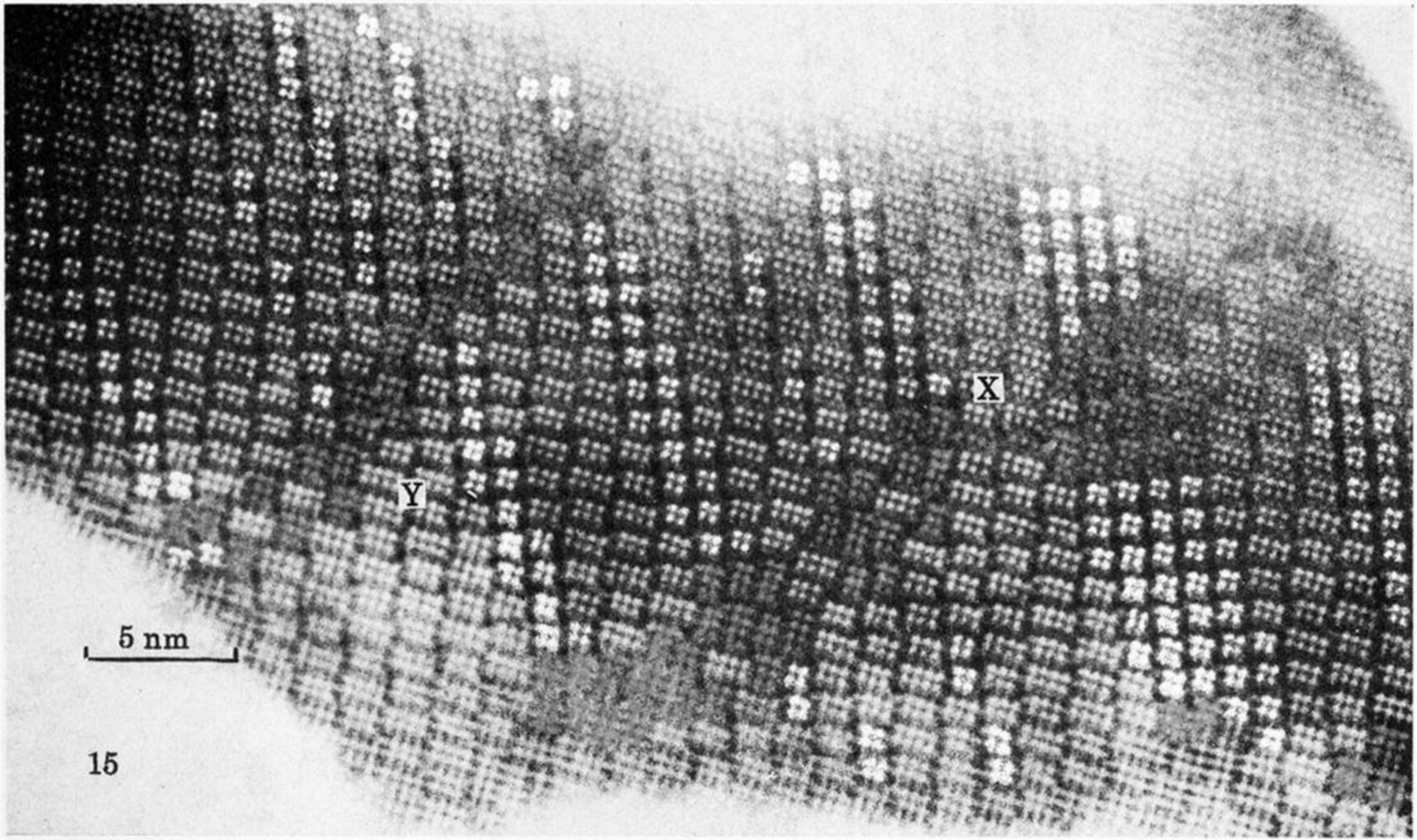

FIGURE 15. OX4C structure: arrays of $Nb_{10}O_{25}$ structure and of *H*–Nb_2O_5 structure, intersected by walls of turned blocks with occasional anomalous faults.

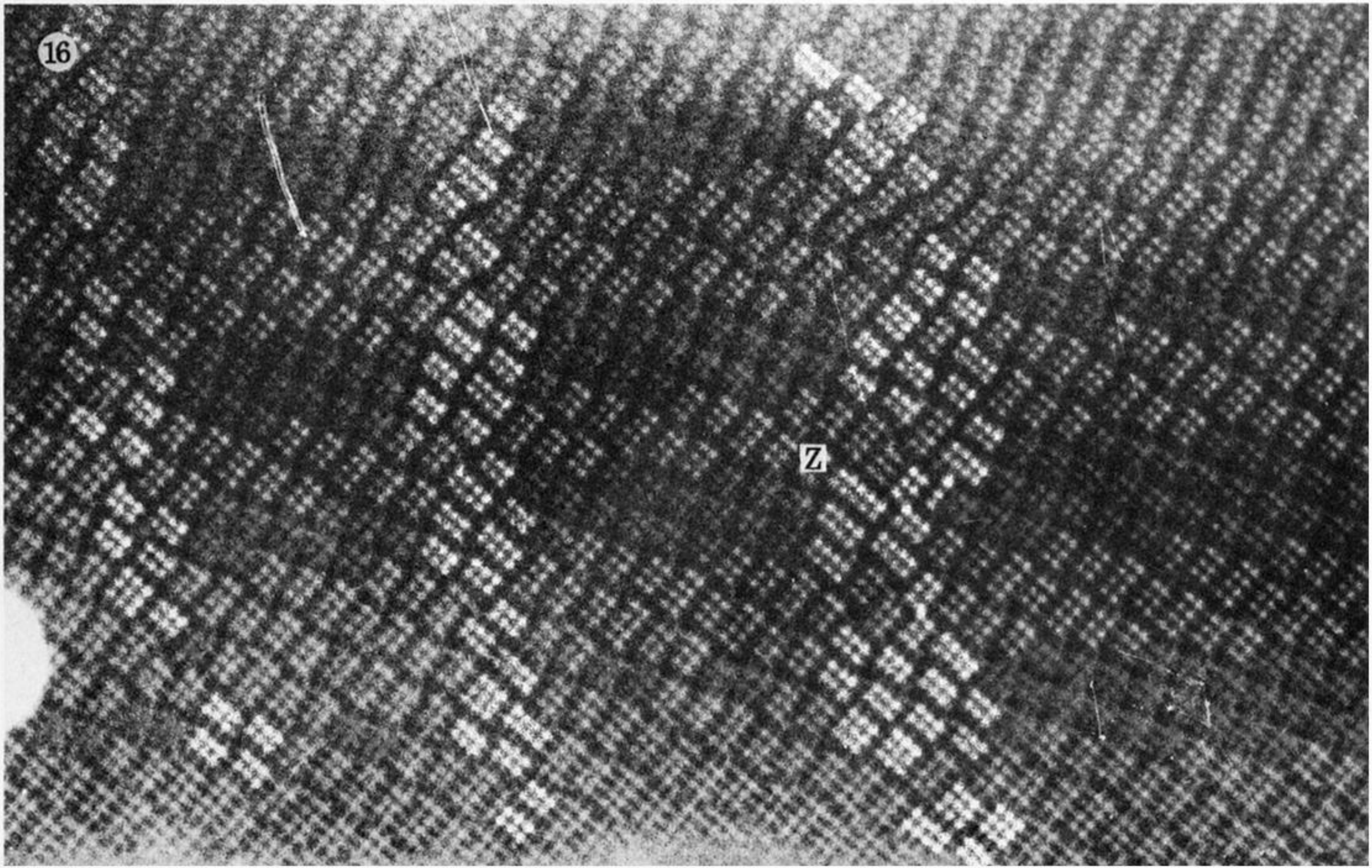

FIGURE 16. OX4C: detail of typical structure in the intersecting fault walls. At Z is a block (6 × 3) octahedra in cross section; to the right of, and below, Z are a block two octahedra wide and a 'spliced' pair of blocks. This is the location of a dislocation.

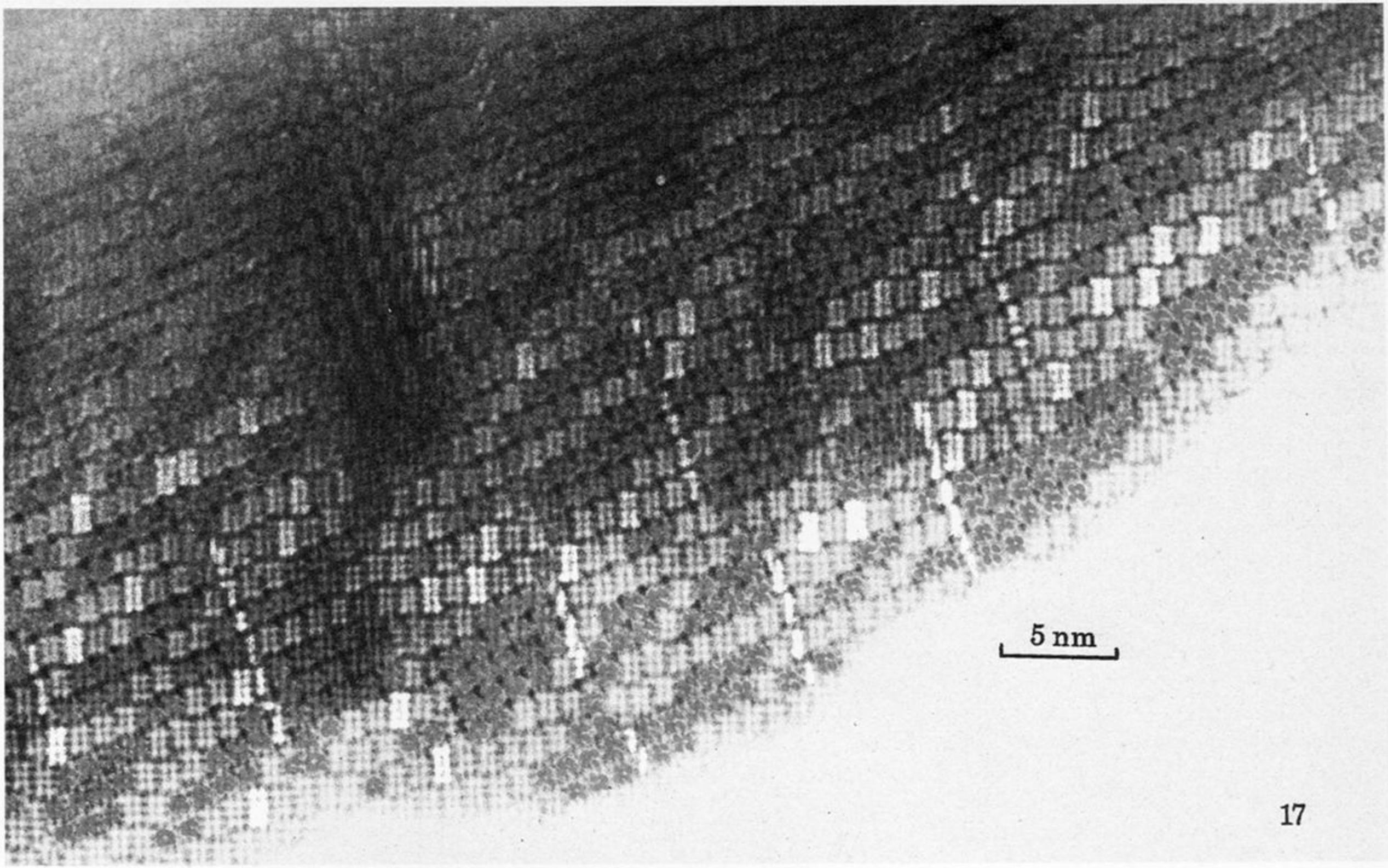

FIGURE 17. Oxidation of $Nb_{22}O_{54}$ at 500 °C, with no annealing. Immediate effect is extensive interchange of block positions, but relatively little disproportionation.

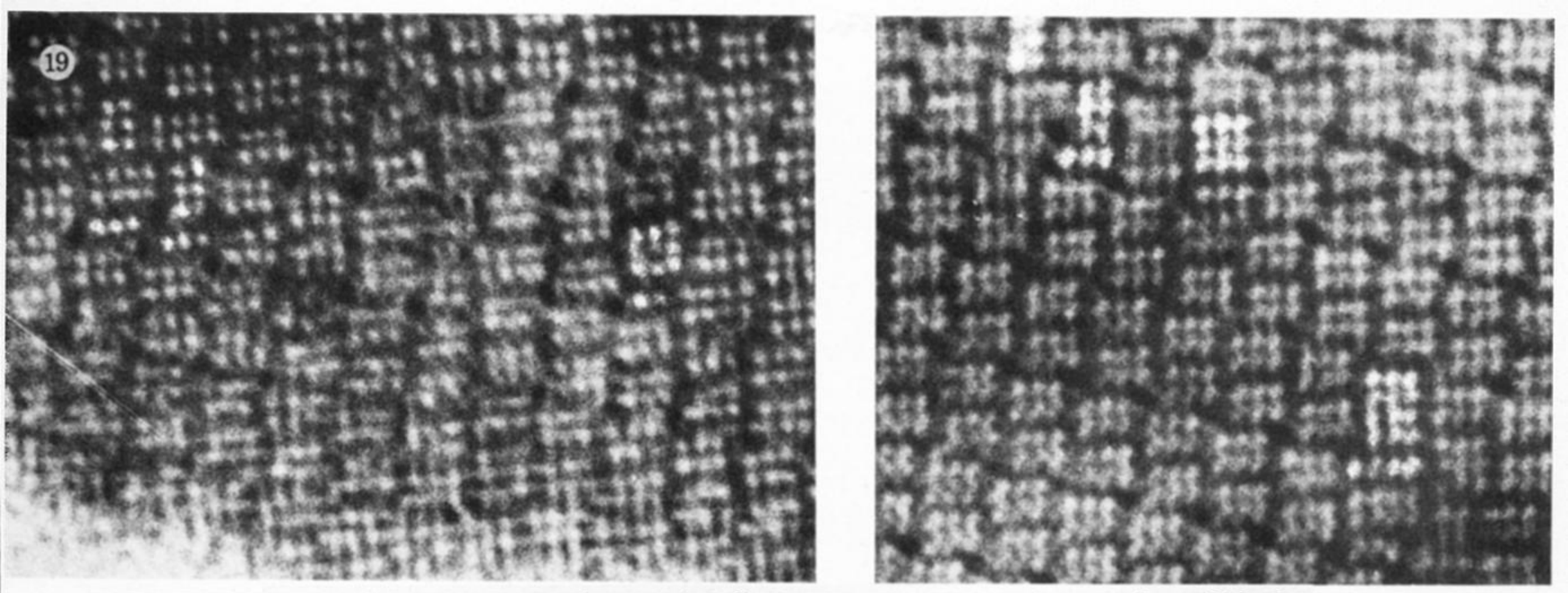

FIGURE 19. OX1E: occasional A.W. displacements across the longer edges of blocks.

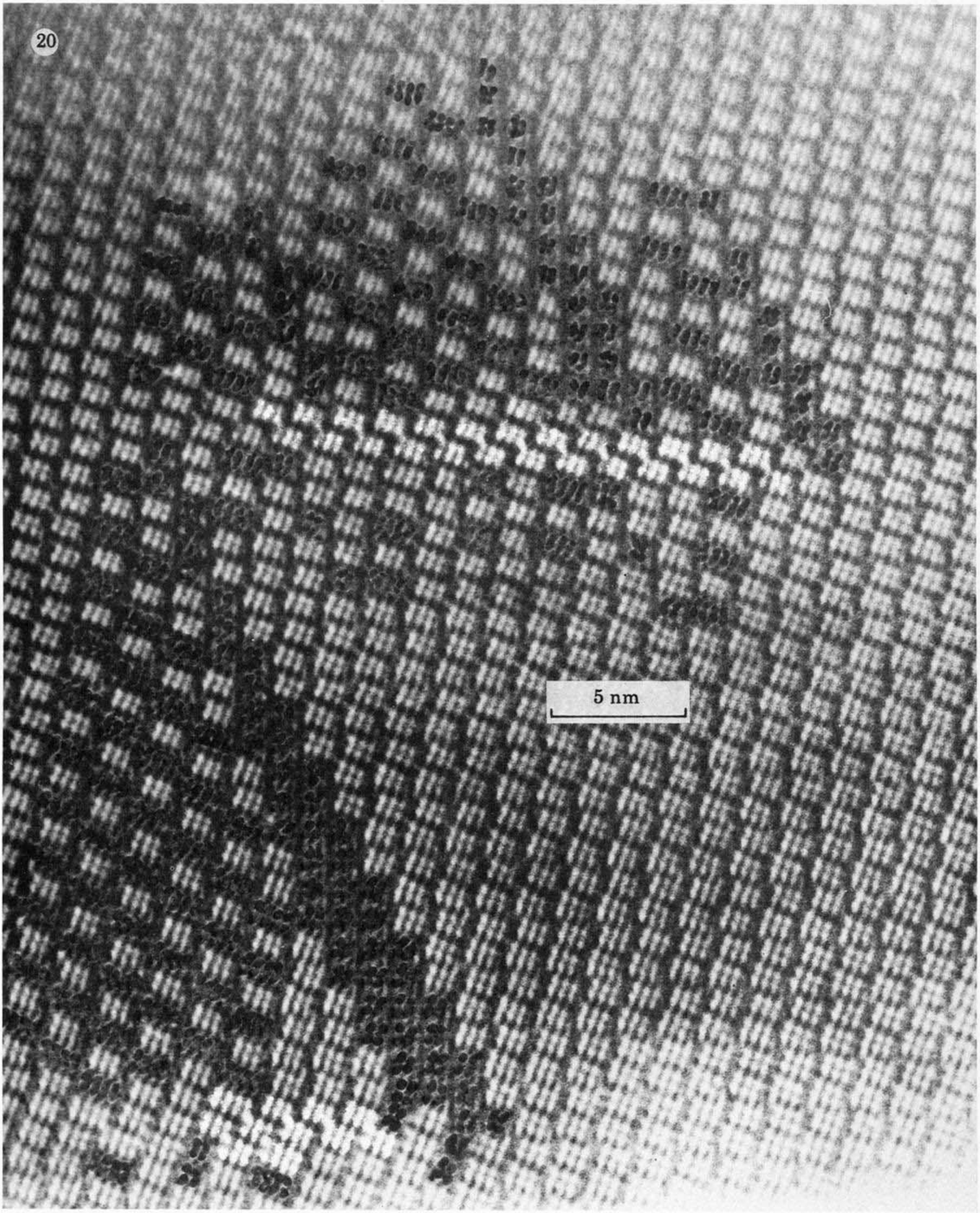

FIGURE 20. Nucleation in the conversion of OX1E to OX2E: two adjacent triangular nuclei. Note abrupt transition from unchanged $Nb_{25}O_{62}$ structure to $Nb_{10}O_{25}$ and *H*–Nb_2O_5 structures at the edges of the nuclei.

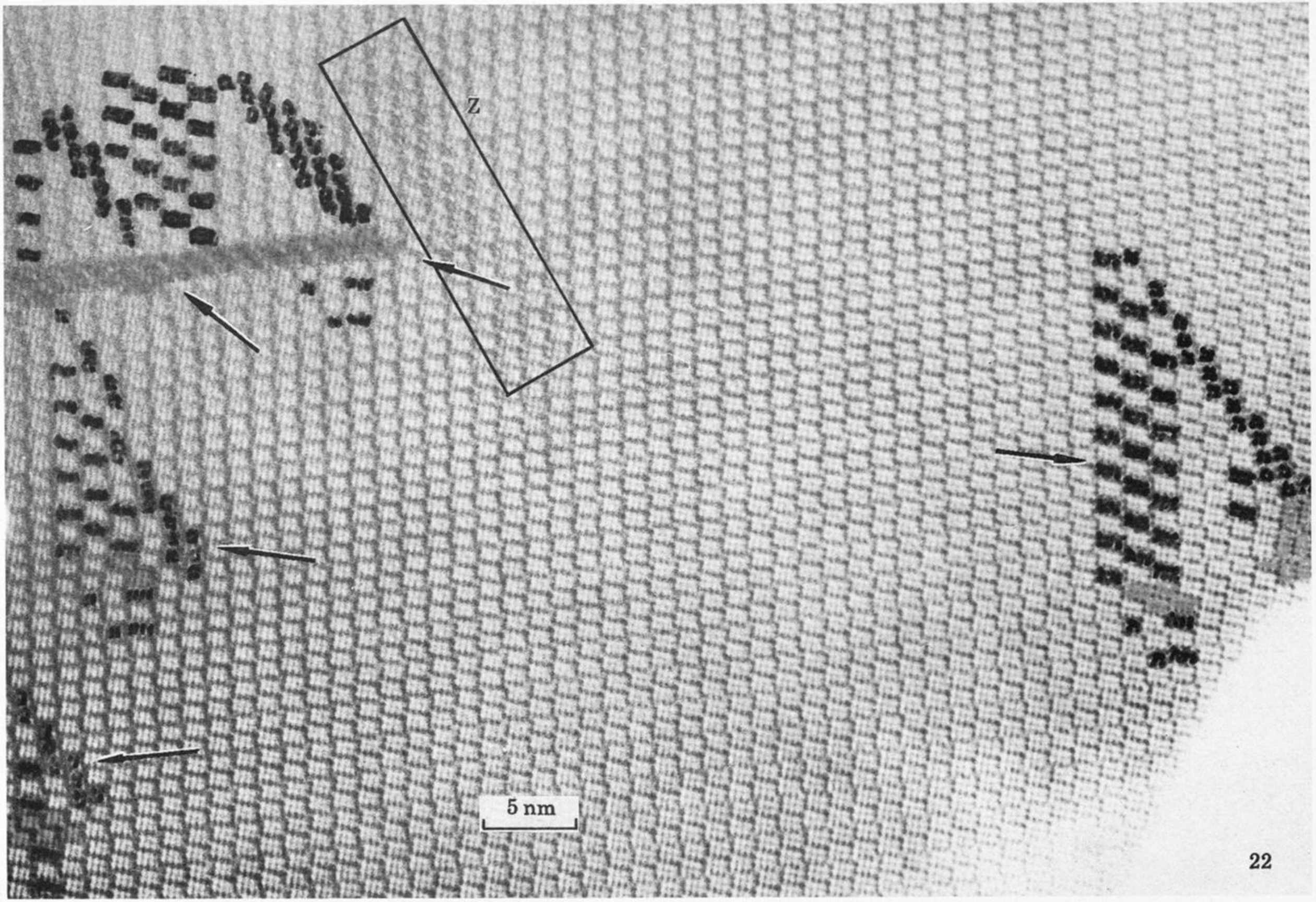

FIGURE 22. Nucleation in the conversion of OX1E to OX2E: five nucleation events marked by arrows. In the area Z, the distribution of overlap contrast indicates that another array of $Nb_{10}O_{25}$ is in process of formation.

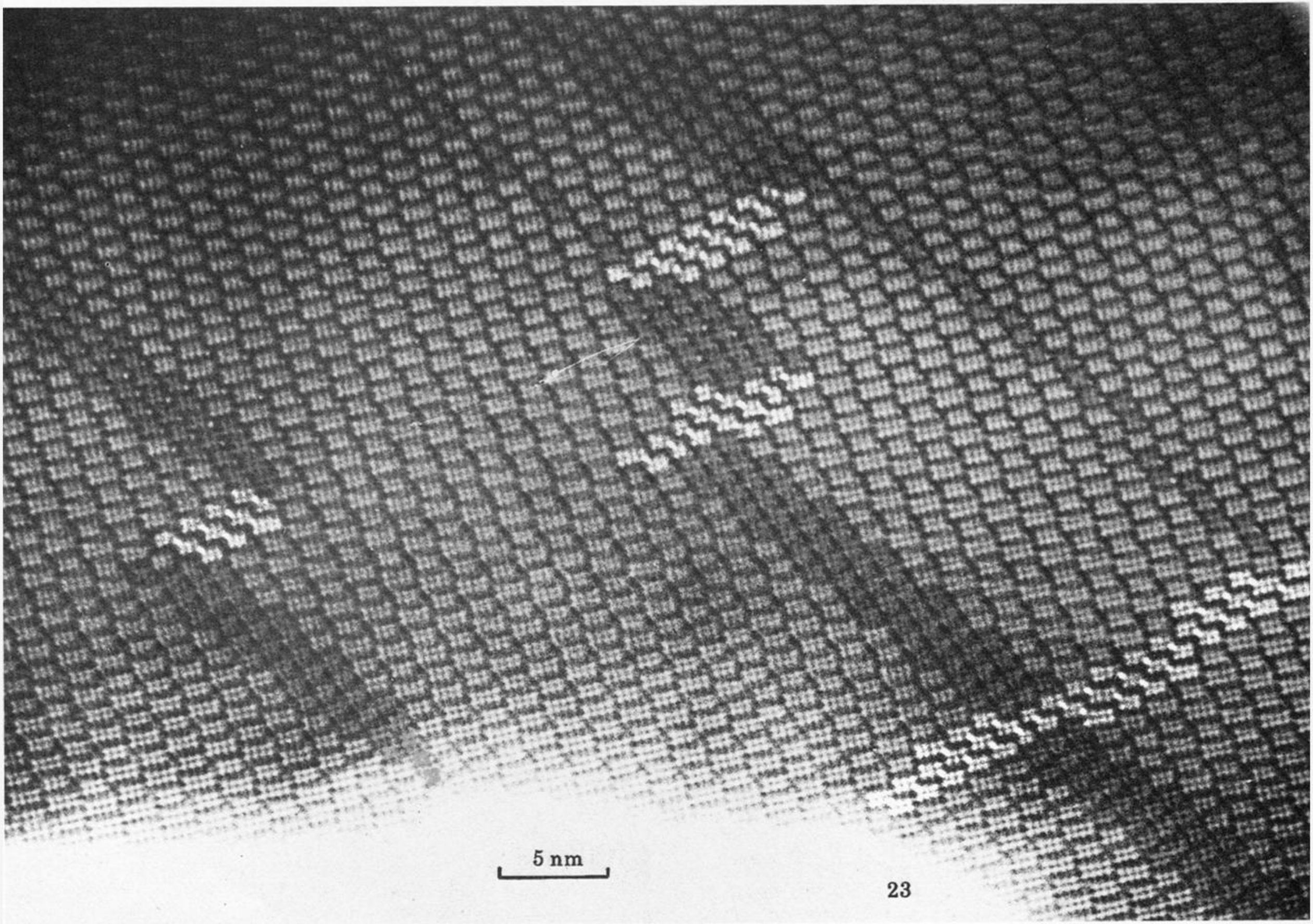

FIGURE 23. OX2E: merging of separate nucleation events creates large domains of H–Nb_2O_5 structure, long arrays of $Nb_{10}O_{25}$ and linking faults.

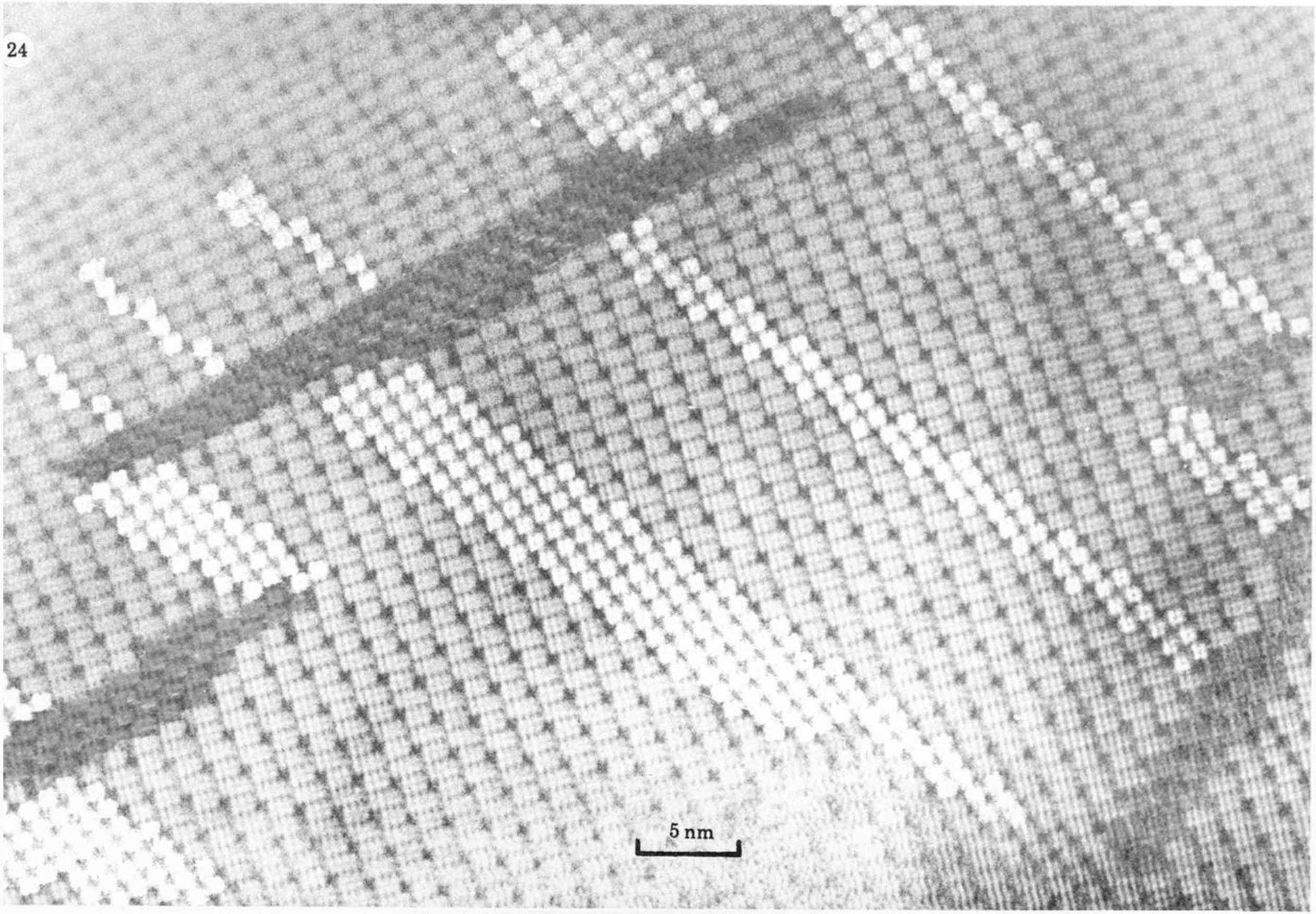

FIGURE 24. OX2E: two types of fault-bounding domains of H–Nb_2O_5. Upper left, lines of spliced or overlapping blocks; lower right, meandering arrays of turned blocks.

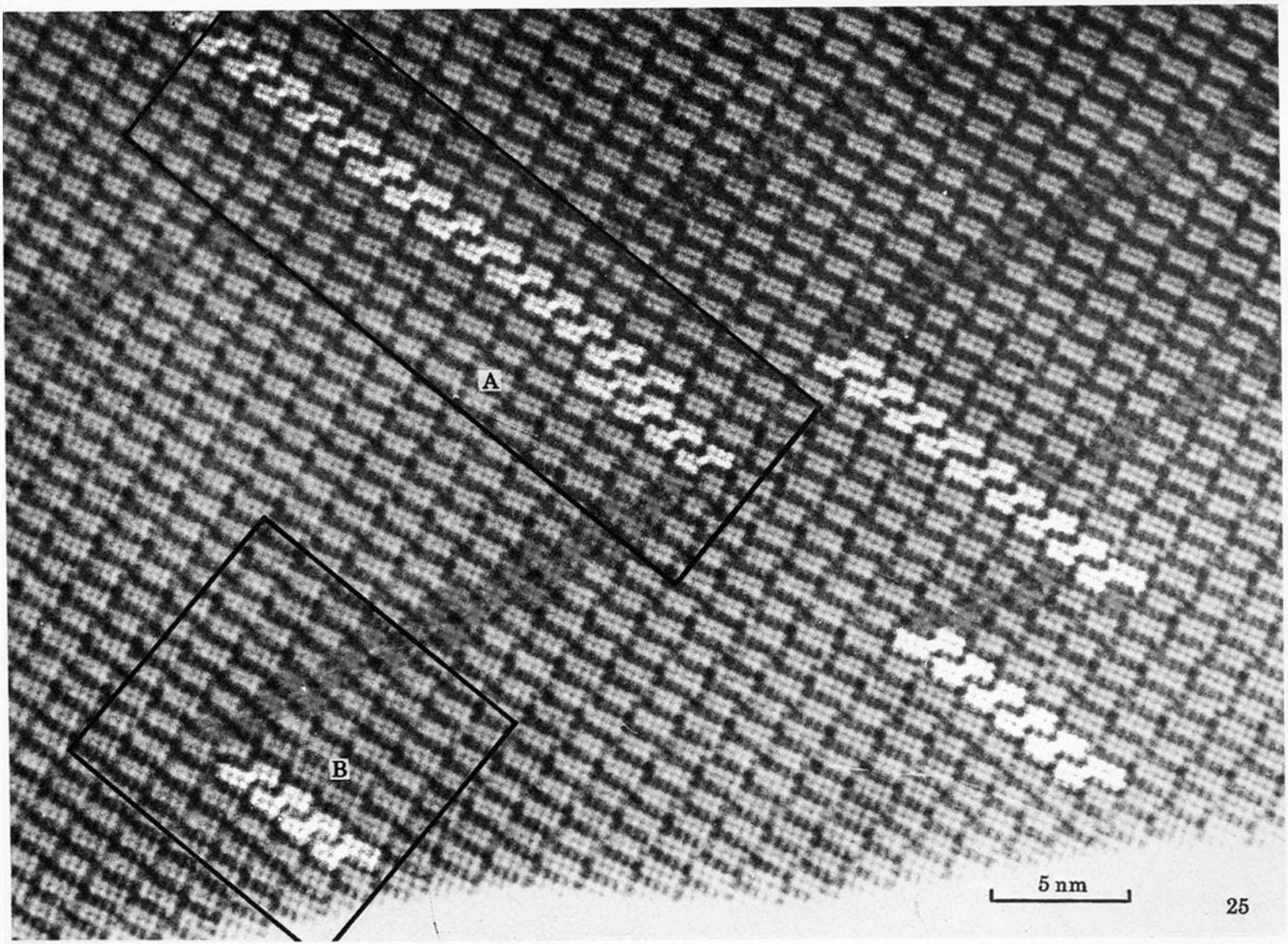

FIGURE 25. Oxidized $Nb_{53}O_{132}$: fully annealed OXF structure. Compare with figure 23.

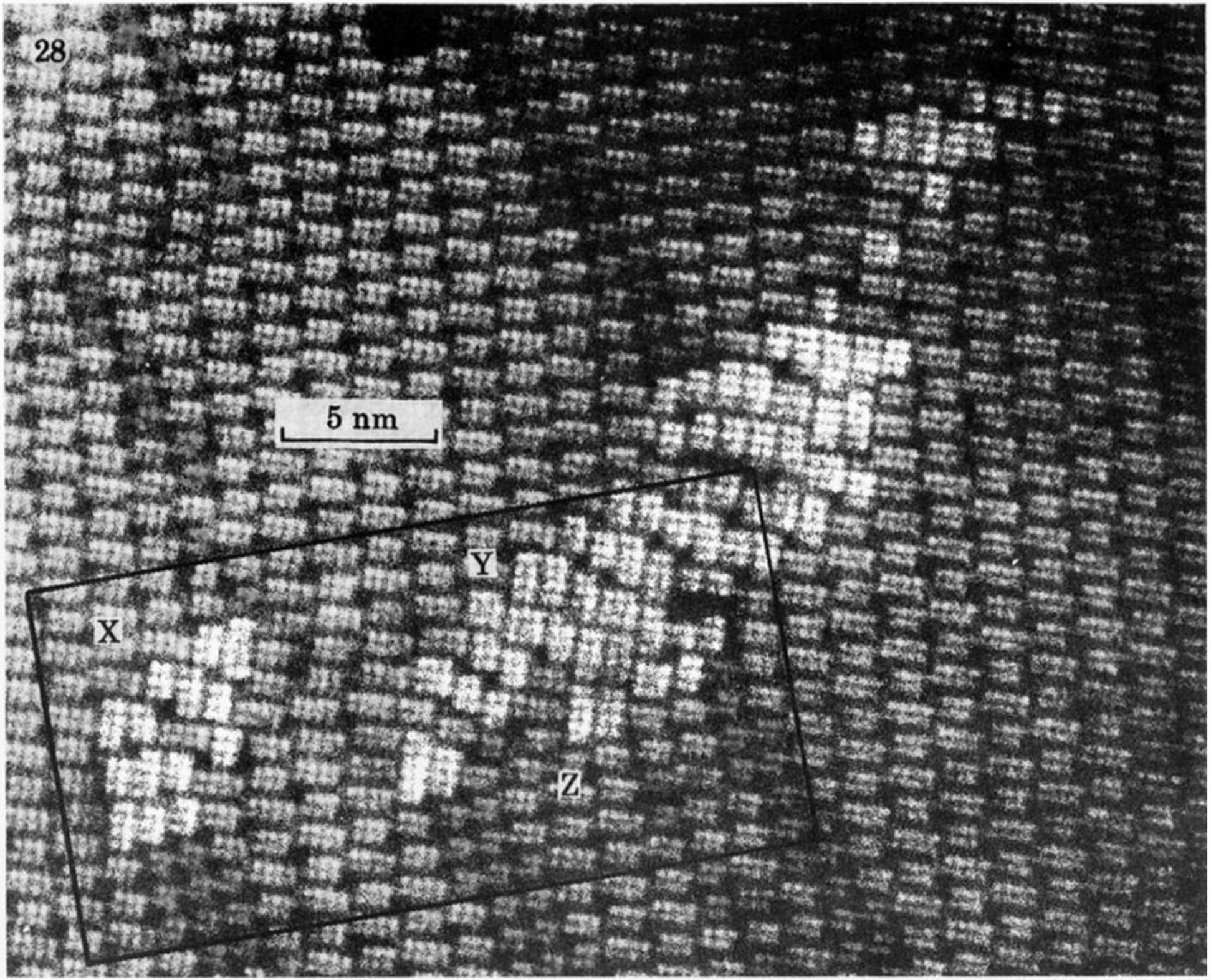

FIGURE 28. Faults: details of areas of turned blocks in OX2E. At X and Y, the turned blocks eliminate one row of cation sites; to the right of Z, two cation rows are eliminated.

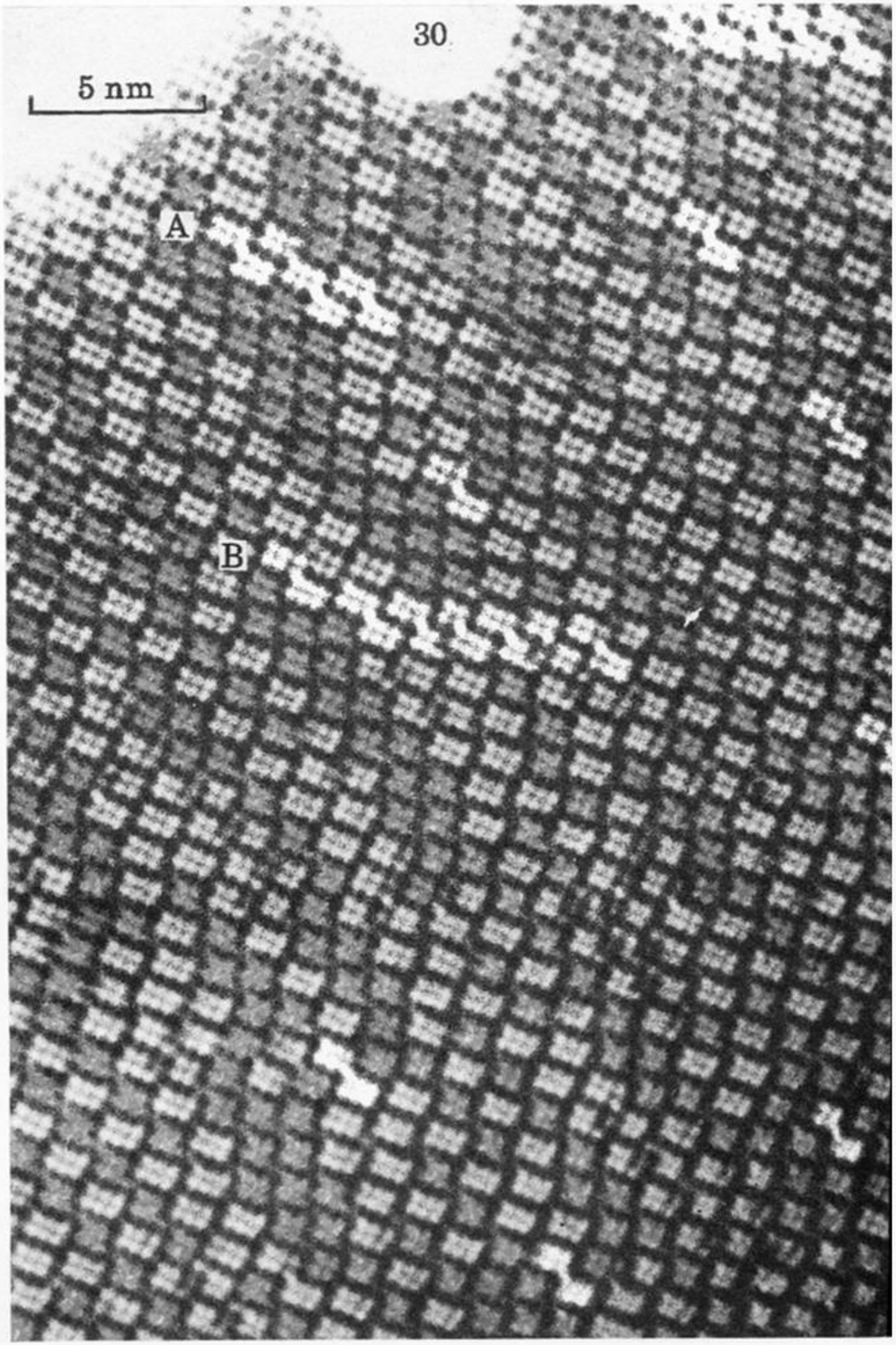

FIGURE 30. Faults: spliced blocks in the earliest stages of conversion of OX1C to OX2C.

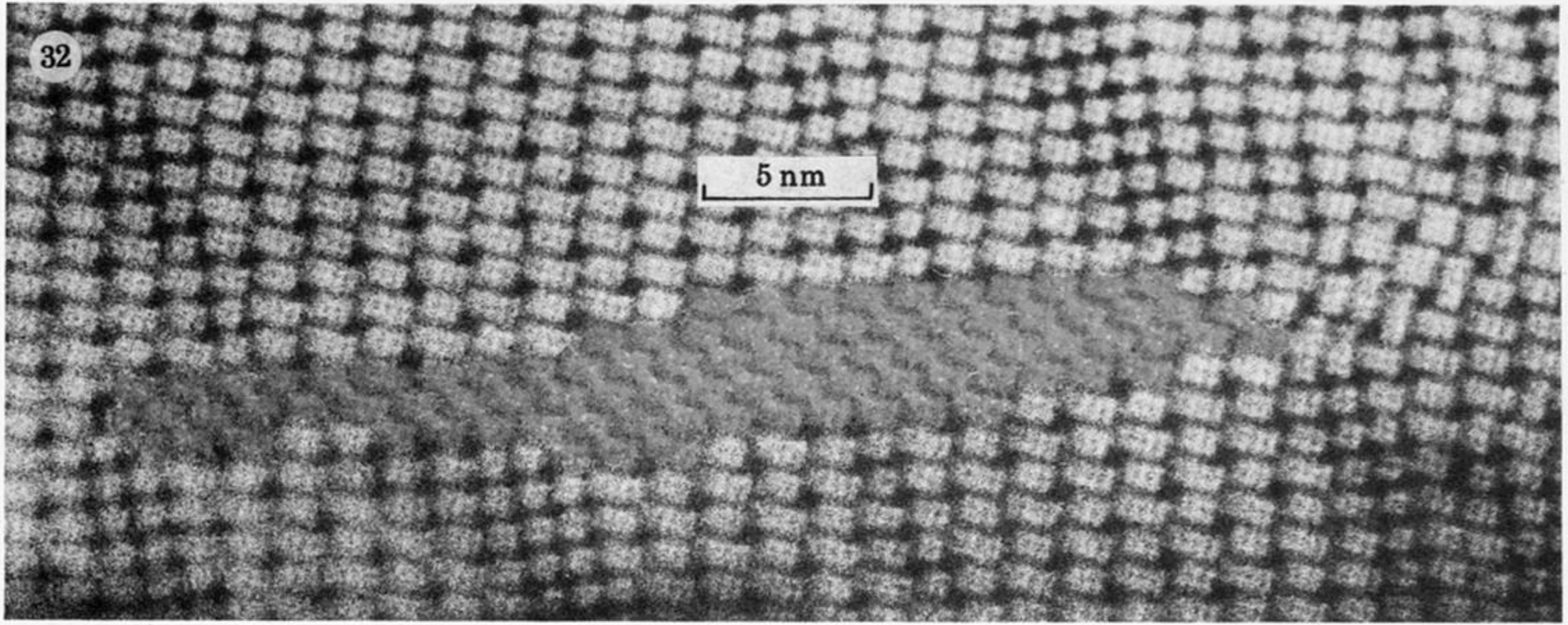

FIGURE 32. Broad bands of spliced blocks in OX2E, corresponding to a very large mutual displacement of the structure above and below the fault.

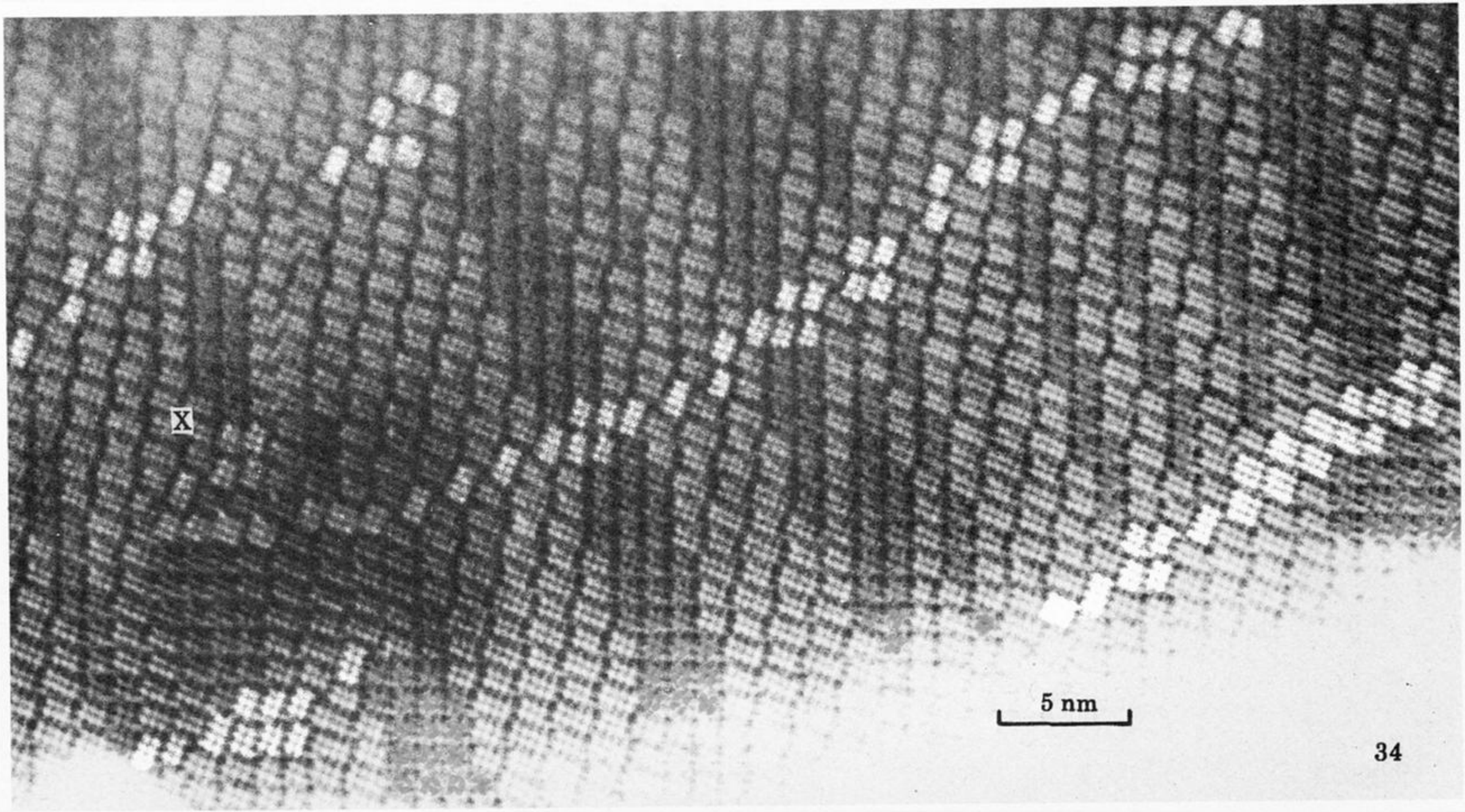

FIGURE 34. Structure of OX4C after annealing at a temperature (950 °C) above that at which direct conversion to *H*–Nb_2O_5 takes place.

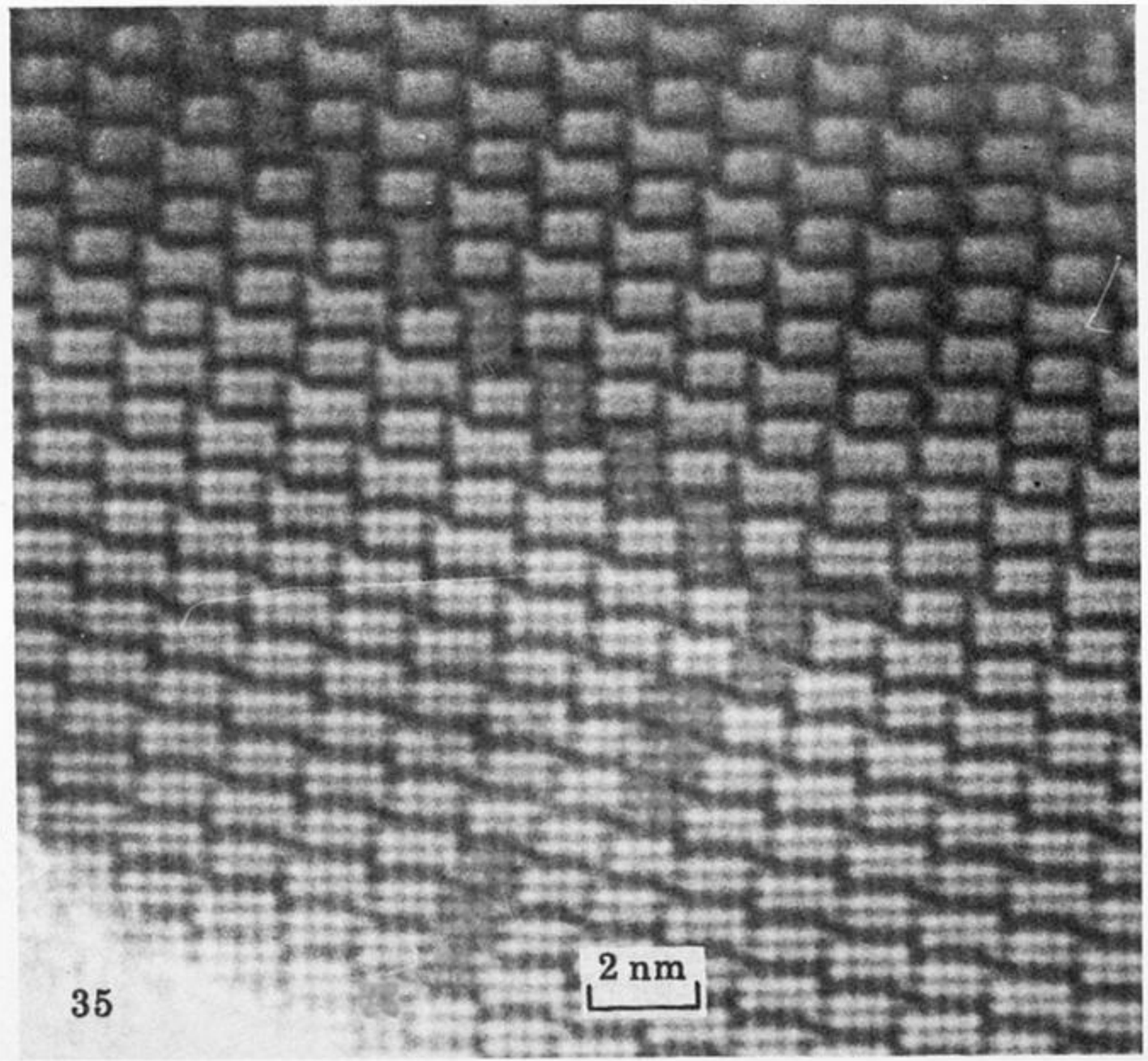

FIGURE 35. Final conversion of OX4C to *H*–Nb_2O_5: remaining relic array of $Nb_{10}O_{25}$ and an antiphase boundary with the formal stoichiometry $Nb_{25}O_{62}$.

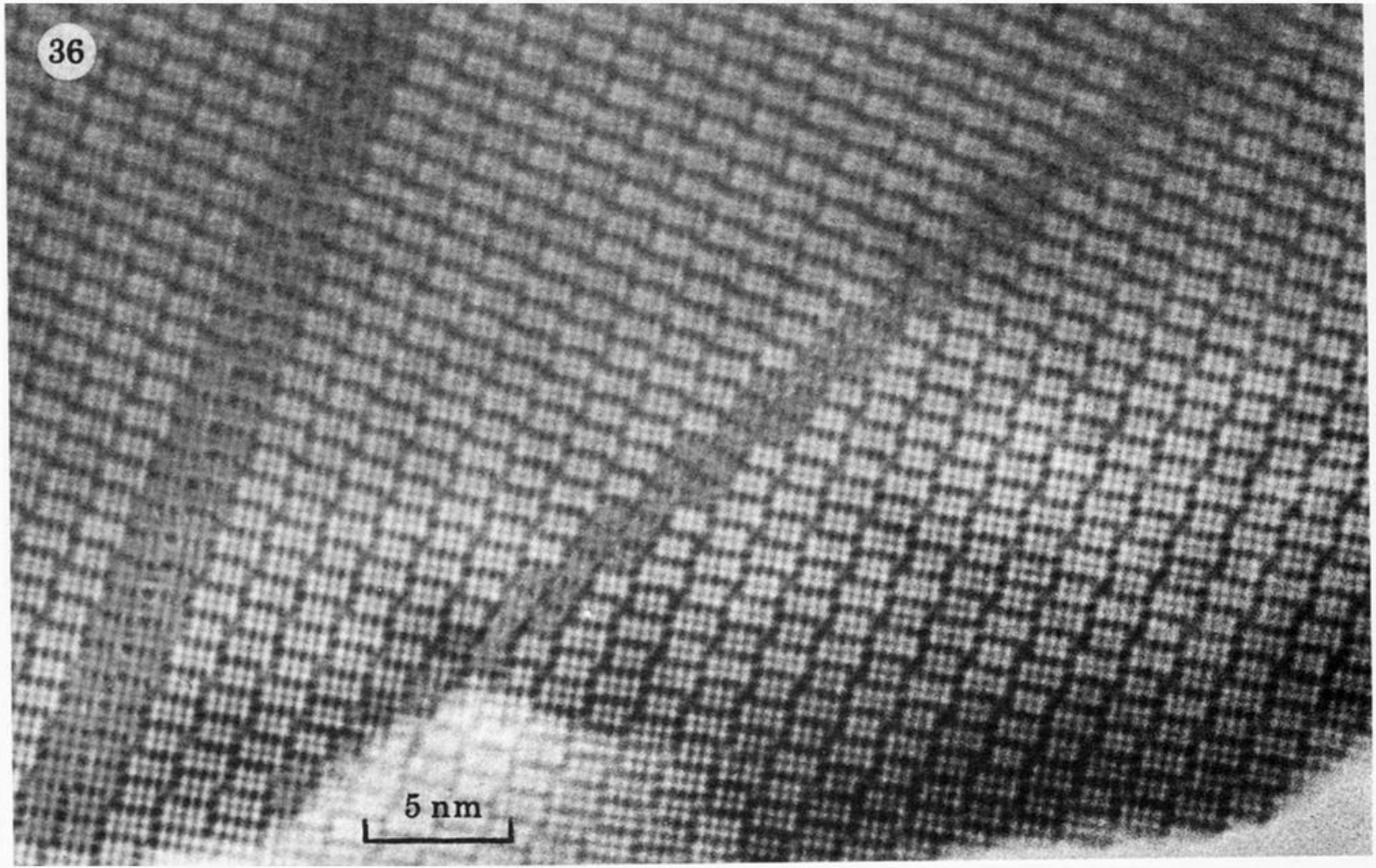

FIGURE 36. Final conversion of OX4C to H–Nb_2O_5: a relic array of $Nb_{10}O_{25}$ ending at a terminating twin band in the H–Nb_2O_5 structure. There is a dislocation at their junction.

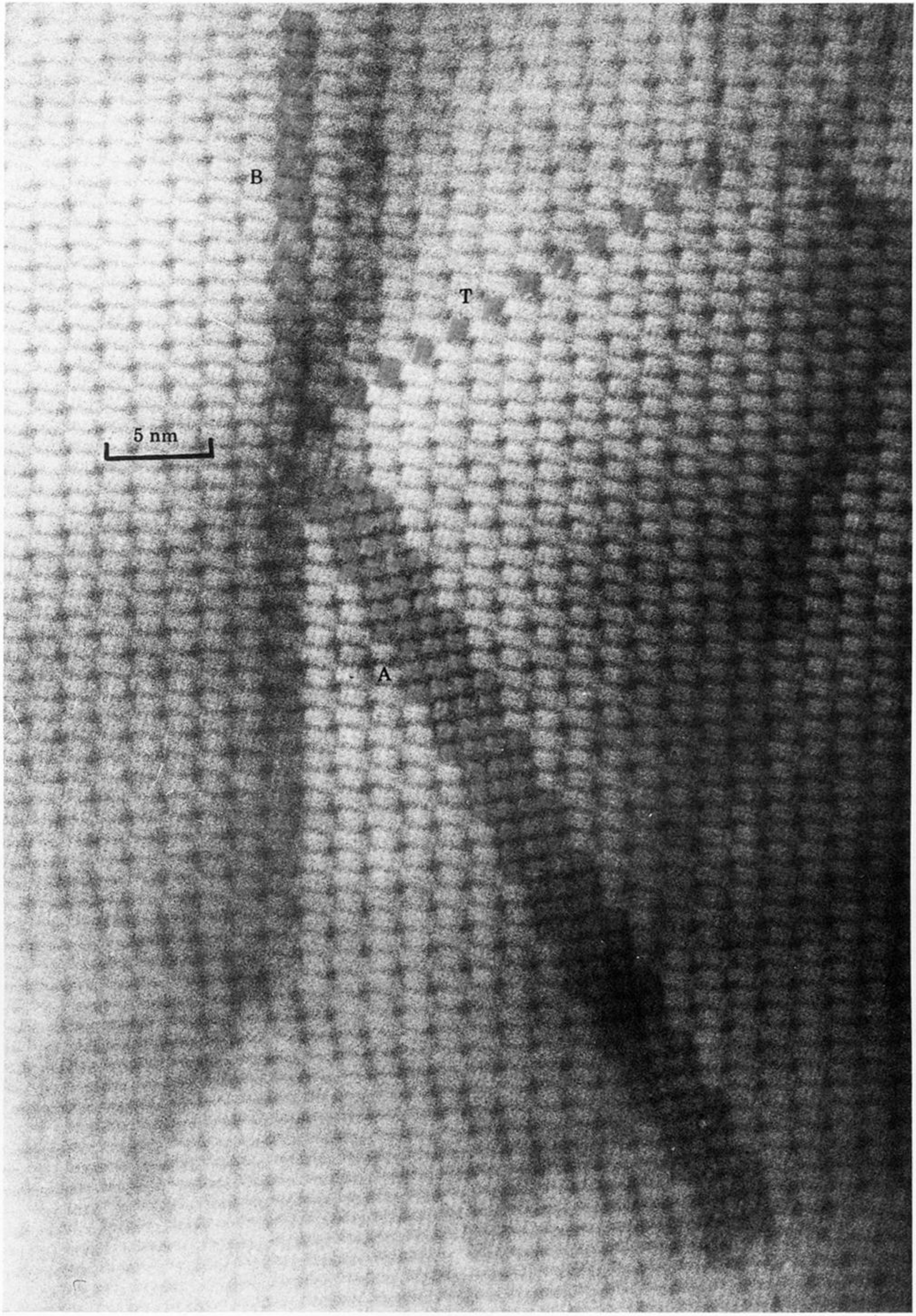

FIGURE 37. Final conversion of OX4C to *H*–Nb_2O_5: a residual domain of $Nb_{10}O_{25}$, A, ends at a line of twinned structure, T, and one file of a new structure for Nb_2O_5, B – a $(5 \times 3)_3$ block structure, $Nb_{46}O_{115}$.

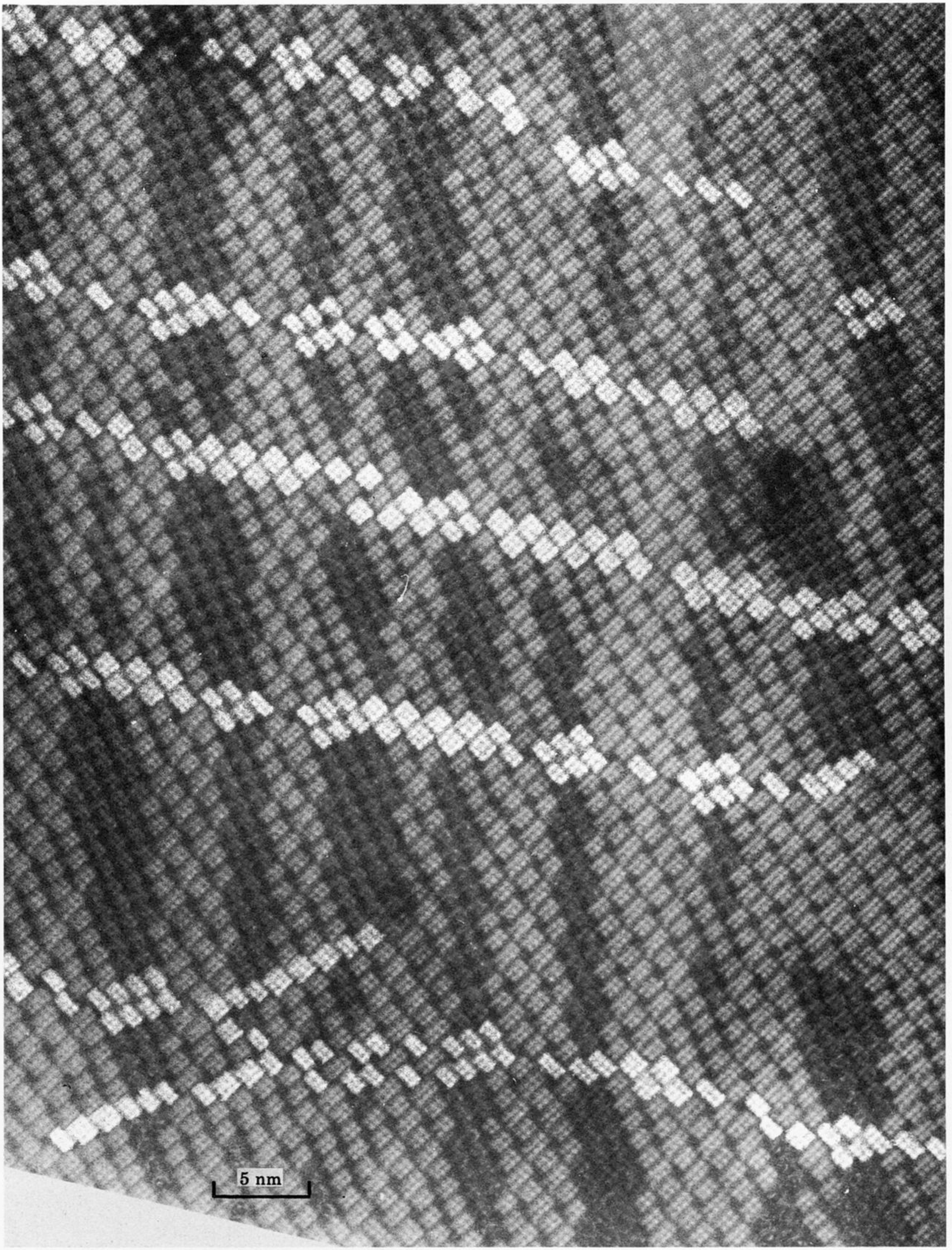

FIGURE 38. Heating above temperature of conversion to H–Nb_2O_5: OX4C after 90 s at 1000 °C. Fault walls largely transformed to N–Nb_2O_5 structure.

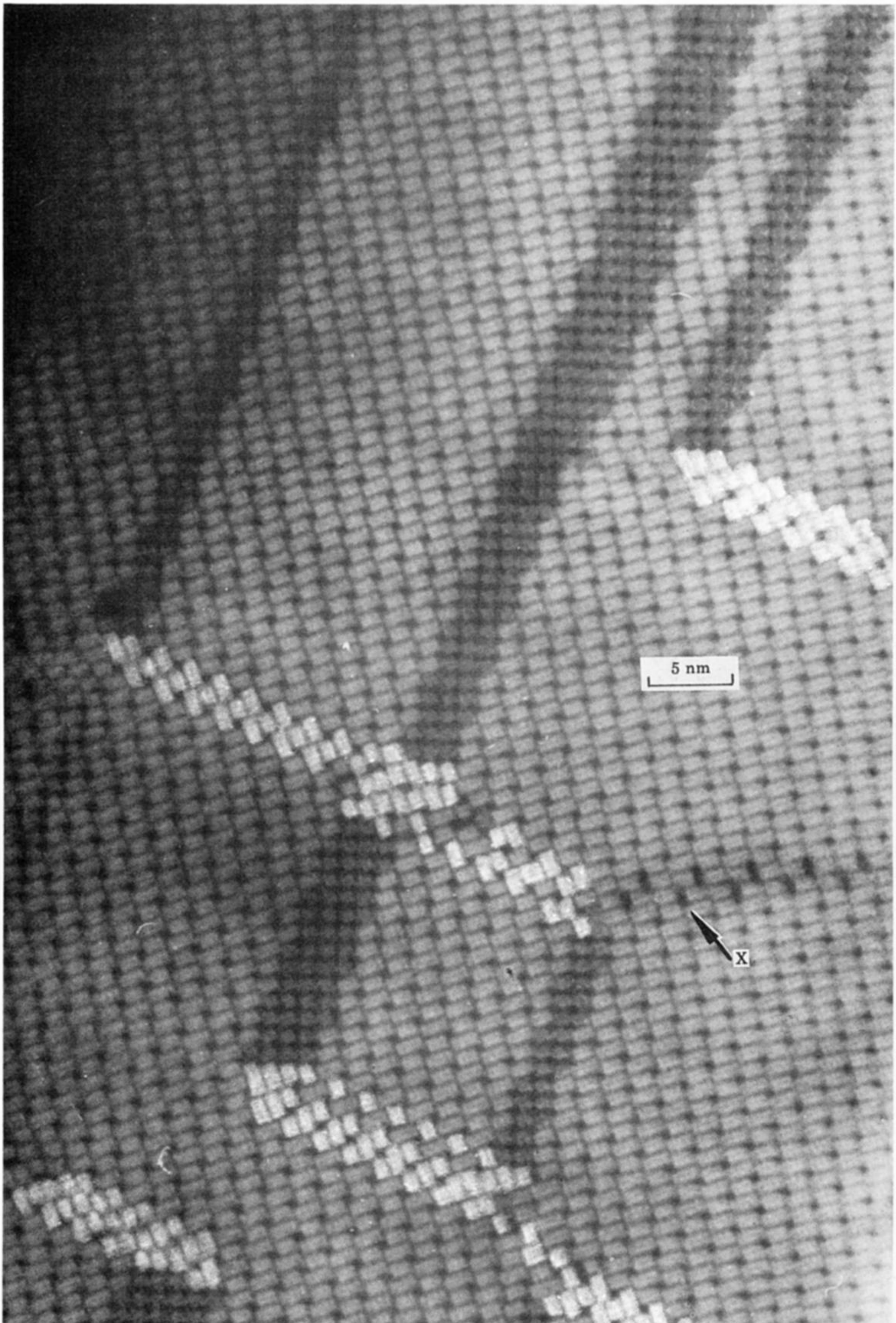

FIGURE 39. Heating above temperature of conversion to H–Nb_2O_5: OX2E after 205 s at 1000 °C.

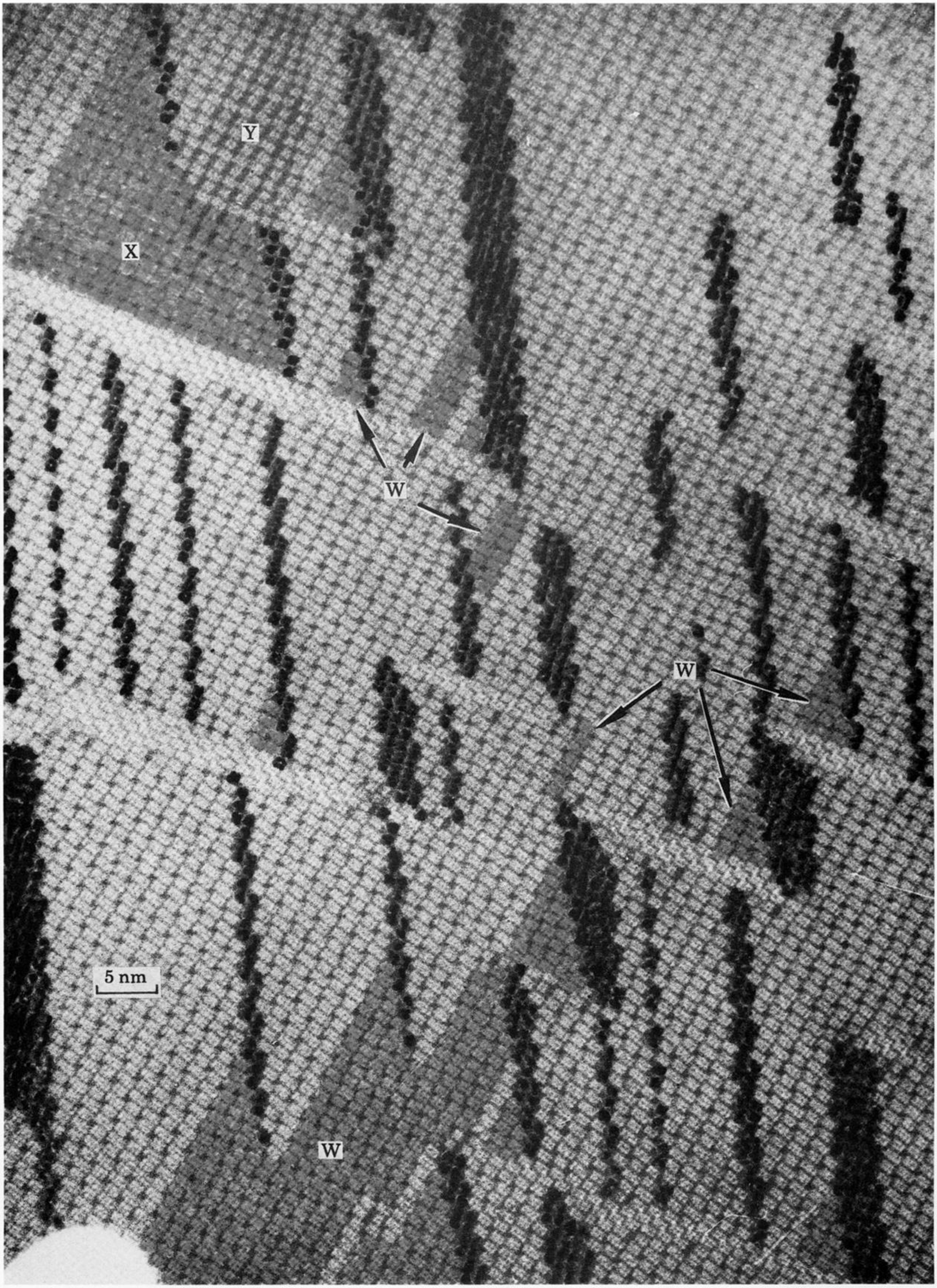

FIGURE 40. Heating above temperature of conversion to *H*–Nb_2O_5: OX2E after 180 s at 1120 °C. Areas marked W have retained or reverted to the $Nb_{25}O_{62}$ block structure. The similar area X abuts on a region Y where overlap contrast indicates frozen-in, uncompleted block rearrangements.

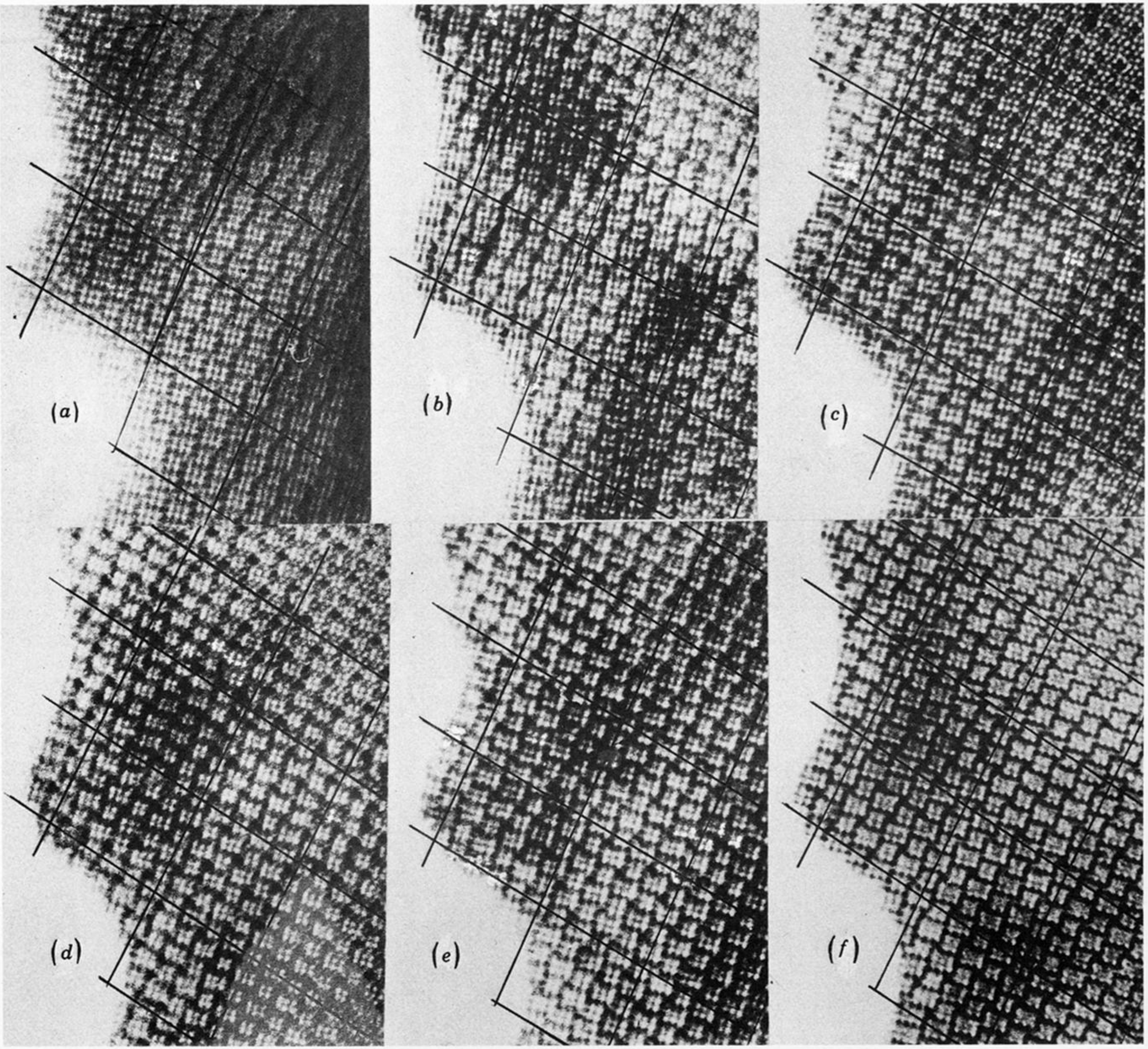

FIGURE 41. Beam stability: the same area of a crystal of OX1C after a series of intense irradiations in the electron microscope. Blocks found to undergo interchange of position at the next irradiation are enhanced in tone.